SUBSURFACE MAPPING AND 3D FLEXURAL MODELING OF THE PUTUMAYO FORELAND BASIN, COLOMBIA

A Thesis Presented to the
Department of Earth and Atmospheric Sciences
University of Houston

In Partial Fulfillment
of the Requirements for the Degree
Master of Science

---

by

Luis Fernando Pachón-Parra

August, 2013

SUBSURFACE MAPPING AND 3D FLEXURAL MODELING OF THE PUTUMAYO FORELAND BASIN, COLOMBIA

_____

Luis Fernando Pachón-Parra

APPROVED:

_____

Dr. Paul Mann, Chairman

_____

Dr. Jolante Van Wijk

_____

Dr. John Londoño

_____

Dean, College of Natural Sciences and Mathematics

Dedicated to the memory of Ruth Milena Pachón

ACKNOWLEDGEMENTS

My special thanks go to Dr. Paul Mann for his guidance throughout this project. Special thanks go to Dr. John Londoño and Dr. Jolante van Wijk for their constructive comments and their support. I would also like to thank the members of the Caribbean Basin, Tectonics, and Hydrocarbons (CBTH) group at the University of Houston and their support over the last two years, especially to Naila Dowla, Joan Marie Blanco, and Marie de los Santos for all their help. I would also like to thank the industry sponsors of the CBTH project for the financial support of my research assistantship at the University of Houston. I am also grateful with Carlos Lombo and all the work-team of La Cortez Energy for providing me the Putumayo data-set. I greatly appreciate the dedication and the keen interest of Dr. Nestor Cardozo and Dr. Alejandro Escalona. I would like to thank to my parents Ligia and Israel, and my sisters Saida, Paola, and Ruth for their love and prayers for the successfully completion of this project. Last, but not means least, I am very grateful with Catalina for her patience, her tireless love, and her encouragement to overcome these difficult times.

SUBSURFACE MAPPING AND 3D FLEXURAL MODELING OF THE PUTUMAYO FORELAND BASIN, COLOMBIA

An Abstract of a Thesis
Presented to the
Department of Earth and Atmospheric Sciences
University of Houston

In Partial Fulfillment
of the Requirements for the Degree
Master of Science

---

by

Luis Fernando Pachón-Parra

August, 2013

ABSTRACT

The Putumayo foreland basin (PFB) is located in southernmost Colombia and forms a 250-Km-long segment of the 7000-Km-long corridor of Late Cretaceous-Cenozoic foreland basins formed by the eastward thrusting of the Andean mountain chain over Precambrian rocks. The current daily production of the Putumayo basin is ~90K BOPD of 15-35° API oil and 300K BOPD of 20-35º API oil in the contiguous Maranon foreland basin to the south, in Ecuador. This study uses ~4000 Km of 2D seismic data tied to 28 exploratory wells to describe the structure and stratigraphy of the basin. The PFB is located adjacent to the NNE-trending Colombian Andes that have been influenced by the oblique and shallow subduction of the Carnegie Ridge starting 8 Ma. Based on mapping of the subsurface of the PFB and comparison with published works from the southward continuation of the PFB into Peru and Ecuador, three main across-strike, structural zones, and five tectonosequences of the PFB are described based on seismic interpretations. The structural zones of the PFB include: 1) the 20-Km-wide, Eastern structural zone closest to the Andean mountain front characterized by inversion of older, Jurassic half-grabens during the late Miocene; 2) the 45-Km-wide, Central structural zone characterized by moderately-inverted Jurassic half-grabens; and 3) the 120-Km-wide, Eastern zone characterized by the 90-Km-wide, N-S trending Caquetá arch with a few slightly inverted normal faults at its crest. The five, mainly clastic tectonosequences of the PFB include: 1) pre-foreland basin Early Cretaceous sedimentary rocks; 2) the Late Cretaceous-Paleocene foreland basin deposits; 3) the Eocene foreland basin deposits related to the early uplift of the Eastern Cordillera; 4) underfilled foreland basin deposits of the Oligocene-Miocene age; 5) overfilled foreland basin deposits of the Plio-Pleistocene age.

I used 3D flexural modeling to identify the present-day tectonic elastic thickness (T_e) values for the lithosphere below PFB, in order to model the location of the sedimentary-related and tectonically-related forebulges in PFB units from the Cretaceous to Oligocene. This analysis

shows two pulses of rapid, foreland-related subsidence during the Late Cretaceous-early Paleocene and the Oligocene-Miocene. Despite present-day oblique thrusting of the mountain front, the PFB basement flexure reveals a tectonic forebulge located in the Eastern structural zone that acts as the updip limit for most hydrocarbons found in the basin.

TABLE OF CONTENTS

ABSTRACT vi
TABLE OF CONTENTS viii
LIST OF FIGURES xii
LIST OF TABLES xv

CHAPTER 1: INTRODUCTION 2

1.1. OBJECTIVES 5
1.2. MOTIVATION 6

CHAPTER 2: STRUCTURAL AND EVOLUTION OF THE PUTUMAYO FORELAND BASIN, SOUTHERN COLOMBIA 10

2.1. INTRODUCTION 10
2.2. PREVIOUS WORKS 12
2.3. PRESENT-DAY TECTONIC SETTING OF THE PUTUMAYO FORELAND BASIN 15
2.3.1. Subducting Nazca plate 15
2.3.2. Carnegie ridge 17
2.3.3. Guayaquil-Caracas megashear 18
2.4. STRUCTURAL GEOLOGY OF THE PUTUMAYO FORELAND BASIN 20
2.4.1. Eastern Cordillera 20
2.4.2. Putumayo foreland basin 21
2.4.3. Basement structural highs 24
2.5. TECTONO- STRATIGRAPHIC FRAMEWORK 26
2.5.1. Basement: Guyana shield and Cambrian? metamorphism 26
2.5.2. Paleozoic 27

2.5.3. Triassic-Jurassic 27
2.5.4. Cretaceous 28
2.5.5. Cenozoic 29
2.6. DATA AND METHODOLOGY 32
2.6.1. Well data in this study 33
2.6.2. Seismic data in this study 33
2.6.3. Methodology 34
Loading of seismic and well data 34
Seismic interpretation and definition of stratigraphic units and structural styles 34
well-log cross section 35
2.7. TECTONOSEQUENCES AND STRUCTURAL OBSERVATIONS 37
2.7.1. Structural zones 37
Western structural zone 37
Central structural zone 38
Eastern structural zone 39
2.7.2. Structural thrust front 42
2.7.3. Tectonosequences 45
Pre-Cretaceous basement 45
Sequence I : Cretaceous 50
Sequence II : Paleocene 54
Sequence III: Eocene 57
Sequence IV: Oligocene 60
2.8. DISCUSSION 62
2.8.1. Main structural features in PFB 62
Right-lateral strike-slip deformation 62
Deformation of the PFB mountain front 63
Implication of north-south striking pre-Aptian structures 64
Caquetá arch: Eastern boundary 65
2.8.2. Summary of basin evolution and paleogeography 68
Early Cretaceous (Sequence I) 68
Late Cretaceous (Sequence I) 69

Paleocene (Sequence II) 69
Eocene (Sequence III) 70
Oligocene (Sequence IV) 70
Miocene-Pliocene (Sequence V) 71
2.8.3. Implications for hydrocarbon exploration 74
Reservoir rock 75
Trap 75
2.9. CONCLUSION 78

CHAPTER: 3D FLEXURAL MODELING OF THE PUTUMAYO FORELAND BASIN 81

3.1. INTRODUCTION 81
3.2. PREVIOUS WORKS 84
3.3. FLEXURAL MODEL AND SENSITIVITY PARAMETERS 87
3.4. CASE STUDY: PUTUMAYO FORELAND BASIN 90
Tectonic load: Colombian Andes 90
Foreland basin geometrical arrangement 90
3.5. METHODOLOGY 93
3.5.1. Flexure of the plate for present day: 93
Definition of main input modeling 94
3.5.2. Flexure of the lithosphere through the time in PFB 97
Prorosity-depth curves 97
Thickness maps of decompacted tectonosequences 100
Flexural deformation due to sedimentary load 101
Subsidence related to tectonic load 101
Load location through time 101
Flexural deformation related to tectonic load 102
3.6. 3D FLEXURAL MODELING OF THE PUTUMAYO FORELAND BASIN 106
3.6.1. Present-day lithosphere deformation: Profiles and deflection 106
3.6.2. Cretaceous-Oligocene lithosphere flexure 109

Cretaceous- Oligocene sedimentary load 109
Cretaceous- Oligocene tectonic load 112
3.7. DISCUSSION 115
3.7.1. Preexisting weaknesses in the foreland basin: Forebulge development at PFB 115
3.7.2. Evolutionary model 117
3.7.3. Model uncertainty and constraints 121
Uncertainty due to location and distribution of the tectonic load through the time 121
Te values for lithosphere under PFB 121
3.7.4. Implications for hydrocarbon exploration 122
3.7.5. Comparison between the Llanos and Putumayo forelands basin 123
3.8. CONCLUSION 126

REFERENCES 128

LIST OF FIGURES

Figure 1.1 Tectonic map of northern South America showing major tectonic features and global positioning system (GPS) vectors with respect to a fixed South American plate (from Trenkamp et al., 2002). WC = Western Cordillera, CC = Central Cordillera, EC = Eastern Cordillera, RC = Real Cordillera, MR = Macarena range, CR = Chibiriquete range. 8

Figure 2.1 Topographic map showing the main oil and gas fields, their infrastructure and pipelines, and the cumulative production of the Putumayo foreland basin of Colombia, the Oriente foreland basin of Ecuador, and the Marañon basin of Peru (modified from ANH, 2012). The locations of important previous studies in the area are shown as polygons. 14

Figure 2.2 A.) Map view of earthquakes occurring between 1990 and 2011 and locations of active volcanoes (yellow triangles) of southern Colombia (data taken from USGS, 2012). B.) AB profile shows the seismicity (hypocenters shown as dots) used to infer the position and angle of the subducted Nazca slab beneath Colombia. 19

Figure 2.3 Geological map modified from Gomez et al. (2007) showing the main structural features of the PFB and adjacent areas. 23

Figure 2.4 Bouguer GEOSAT gravity map of the southern part of Colombia, showing the basement highs and the three main structural zones described from the Oriente basin and extrapolated to the PFB. WSZ = Western structural zone. CSZ = Central structural zone. ESZ = Eastern structural zone. 25

Fig. 2.5 Generalized stratigraphic column of the PFB. The stratigraphic units are based on outcrop studies along the Andean mountain front and wells within the Putumayo basin. Section modified from Beicip-Ecopetrol (1998). 31

Figure 2.6 Location of seismic and well data in the Putumayo foreland basin outlined by white line. Transect shown by yellow line is shown in Figure 2. 36

Figure 2.7 Main tectonosequences and petroleum system elements (R= reservoir rock, S = seal rock and S = source rock), seismic expression, gamma ray log, resistivity log with time and depth reference, and interpreted five key horizons in well Evelyn-1. The main tectonosequences identified include sequence I, sequence II, sequence III, sequence IV, sequence II, sequence III 40

Figure 2.8 Regional 2D seismic profile showing the three main structural zones of the PFB. The seismic lines are migrated but the quality of the lines differs based on the parameters, age, and processing method; A) Un-interpreted regional seismic section in PFB; B) Interpreted regional seismic line. Note that the Pre-Cretaceous mega-sequence is unconformably overlain by upper Mesozoic formations. Older Triassic-Jurassic? normal faults in the present-day foredeep of the basin are reactivated during Cenozoic times. The Pre-Cretaceous basement seismic character is variable given its diversity of metamorphic, igneous and sedimentary rocks; C) Location map of seismic lines in A, B, and C. 41

Figure 2.9 Thrust belt front structures at different locations; A) Orito thrust front area; B) Central thrust front area; C) Costayaco thrust front area; D) Location map including the main geological units and surface faults. The seismic lines were all migrated but the quality of the lines differs according to the parameters, age and processing methods. 44

Figure 2.10 A) Well-log correlation at sequence tops in the PFB. Wedging can be seen in the PFB beginning in the Oligocene. The correlation is based on gamma-ray logs, resistivity, and sonic logs related to the asymmetrical foreland basin; B) Location map of wells. 48

Figure 2.11 A) Pre-Cretaceous basement structural depth maps. Depth is measured in ft. with the deeper values being the cooler colors and the shallower values being the warmer colors; B) Thickness map of sequence I (Cretaceous), from top pre-Cretaceous basement to top Cretaceous; C) Time vs. depth graph. Linear regression is applied to identify the relationship between both variables. 49

Fig. 2.12 A) Top Cretaceous tructural depth maps. Depth is measured in ft. with the deeper values being the cooler colors and the shallower values being the warmer colors; B) Thickness map of sequence II (Paleocene), from top Cretaceous (Villeta Fm.) to top Paleocene (Rumiyaco Fm.); C) Time vs. depth graph. Linear regression is applied to identify the relationship between both variables. 53

Fig. 2.13 A) Top Paleocene structural depth maps. Depth is measured in ft. with the deeper values being the cooler colors and the shallower values being the shallower values being the warmer colors; B) Thickness map of sequence III (Eocene), from top Paleocene (Rumiyaco Fm.) to top Eocene (Pepino Fm.); C) Time vs. depth graph. Linear regression is applied to identify the relationship between both variables. 56

Fig. 2.14 A) Top Eocene structural depth maps. Depth is measured in ft. with the deeper values being the cooler colors and the shallower values being the shallower values being the warmer colors; B) Thickness map of sequence IV (Oligocene), from top Eocene (Pepino Fm.) to top Oligocene (Oteguaza Fm.); C) Time vs. depth graph. Linear regression is applied to identify the relationship between both variables. 59

Fig. 2.15 A) Top Oligocene structural depth maps. Depth is measured in ft. with the deeper values being the cooler colors and the shallower values being the shallower values being the warmer colors; B) Time vs. depth graph. Linear regression is applied to identify the relationship between both variables..... 61

Figure 2.16 A) The mountain front is interpreted as two left-stepping restraining bends produced by right-lateral shear along the mountain front fault (Velandia et al., 2005). The oil fields at the foreland area are mainly controlled by pre-Cretaceous, N-S-striking normal faults (F1) and by inversion structures related to oblique compression during Cenozoic times; B) Restraining bend model and the infinitesimal strain ellipse associated with a strike-slip showing areas of compression and extension (modified from Wilcox et al., 1981). 67

Fig. 2.17 Paleogeographic maps overlain on tectonic reconstructions of basement blocks and showing paleo-flow directions, and hinge-lines for: A) Early Cretaceous (Sequence I); B) Late Cretaceous (Sequence I); C) Paleocene (Sequence II); D) Eocene (Sequence III). White

spaces represent areas of future shortening related with the uplift of the Andes mountain (tectonic reconstructions are taken from Mann et al., 2010). Paleogeography in the Upper Magdalena valley (UMV) is taken from Villamil, (1985) 72

Fig. 2.18 Synthesis of the geological evolution of sedimentary sequences in Putumayo foreland basin. Each tectonosequence is thought to be developed in a similar process because Nazca plate has been subducting since Precambrian. Modified from Cordoba et al., (1997). 73

Figure 2.19 Play concept map for the PFB; A) map view of all play concepts showing major trap types; B) plays associated with Eastern Cordillera uplift; C) plays associated with inverted rift structures; D) plays associated with stratigraphic traps. 77

Figure 3.1 Map of northern South America showing the location of the Oriente-Putumayo-Llanos foreland basins of Colombia and major arches and basement highs separating these basins. GPS data are from Trenkamp et al. (2002). 83

Figure 3.2 Model of the deflection of a continuous plate under a distributed sedimentary load from foreland basin sediments and tectonic load from an orogenic belt (modified from Allen and Allen, 2005). The arrows show the buoyancy effect of the lower mantle beneath the lithosphere..... 86

Fig. 3.3: Squematic cross-section of the foreland basin systems and fold and fold-thrust belt showing the wedge-top, foredeep, forebulge, and back-bulge depozones shown at approximately true scale (DeCelles and Giles, 1996)..... 92

Fig. 3.4 The Andean mountain range is identified as the tectonic load of the PFB; A) topographic surface with contours every 500-m between the Andean trust front and the Romeral fault system; B) Tectonic load modeled as rectangular blocks of average height,and density; C) 3D grid from Matlab script (Cardozo, 2009). 103

Fig. 3.5: Work-flow summary for the 3D modeling, after Londoño et al., (2012) 104

Fig. 3.6 Porosity trends, showing the mathematical regression and the values for porosity at surface and the constant C. A) Early Cretaceous; B) Late Cretaceous; C) Paleocene; D) Eocene; E) Oligocene; F) Mio-Pliocene 105

Fig. 3.7: 3D flexure of the lithosphere under the PFB and the Andean Mountain range as the tectonic load, for different Te (Te= 15 Km, Te=20 Km, Te=25 Km, Te=30 Km, Te=35Km, and Te= Tassara,(2007). A) 3D Model; B) Location map of regional sections; C) Comparison of different regional section. 107

Fig. 3.8 Map view of the present-day forebulge location for different values of EET 108

Fig. 3.9: 3D flexure of the lithosphere under the PFB for 4 main tectonosequences as main sedimentary load using Te=30 Km. A) 3D Model, examples of lateral and above view of the tectonic load and the deflected plate for Cretaceous period; B) Location map of regional sections; C) Comparison of different regional section. 110

Fig. 3.10 Map view of the sedimentary forebulge location for different epochs. 111

Fig. 3.11: 3D flexure of the lithosphere under the tectonic load for 3 main tectonosequences as main load using Te =30 Km. A) 2D model examples of the residual deflection for positive and negative values; B) Location map of regional sections; C) Comparison of different regional section. 113

Fig. 3.12 Map view of the tectonic forebulge location for different epochs……114

Figure 3.13: Present-day forebulge interpretation. A) 3D flexural modeling result. The model predicts that the modern forebulge does not coincide with the Caquetá arch; B) Geological interpretation; C) Regional structural profile. The zone of maximum flexure has been located along the western area of the central structural zone since Oligocene. I interpret the forebulge of the PFB to be fault-bounded along its eastern edge and to include a half-graben represented by the Caguán-Yarí basin. 116

Figure 3.14 Simplified geologic evolution since the Late Cretaceous of the PFB (modified from Londoño, 2012). Two main foreland stages related with the uplift of the paleo-Cordillera Central and the Eastern Cordillera were identified. The thicker part of the PFB is adjacent to the thrust belt and contains up to 3 Km of Paleocene to recent clastic sedimentary rocks of non-marine origin, which can be interpreted as overburden rocks overlying Cretaceous source rocks. 119

Figure 3.15 Burial history for Putumayo-1 well located in the foredeep of the PFB. The subsidence curve, shows two main tectonic pulses at Late Cretaceous-Paleocene and Eocene times..... 120

Figure 3.16 Comparison between the Llanos basin and the Putumayo basin, Colombia: A) Regional 2D seismic profile showing the geometrical arrangement of Llanos basin, and interpreted location of the tectonic load and forebulge of the basin (from Campos, 2011); B) Regional 2D seismic profile showing the geometrical arrangement of Putumayo basin and interpreted location of the tectonic load and forebulge of the basin; C) Summary of the basinal sizes, size of tectonic loads, and main characteristics of the forebulge for both basins; D) Location map of both foreland basins. 125

LIST OF TABLES

Table. 3.1 General mathematical parameters used in this study for modeling 96

CHAPTER 1: INTRODUCTION

1. INTRODUCTION

The Putumayo foreland basin (PFB) is located in the southern part of Colombia and forms one segment of the 7000-Km-long corridor of Late Cretaceous-Cenozoic foreland basins formed by the continuous eastward thrusting of the Andean mountain chain over Precambrian cratonic rocks of South America (Jacques, 2003) (Fig. 1.1). The major foreland basins in the area include the Putumayo basin of southern Colombia which continues to the south as the Oriente basin of Ecuador and the Marañon basin of Peru (Fig. 1.1).

Colombia is becoming a major oil producer in South America with a daily hydrocarbon production of about one million barrels (ANH, 2012). The PFB contributes around 400,000 thousand barrels of oil to this total that is transported to terminals on the Pacific margin of Colombia along the Trans-Andean pipeline (Fig. 2.1). Discoveries over the last decades in the PFB are mainly located in the foothills of the Andean Cordillera and include the Orito field with an average production of 380 MMBO (ANH, 2012) and the Sucumbíos field with 26 MMBO (ANH, 2012). Discoveries located to the east in the foreland are relatively small and their production is relatively low related with the giant fields located in the Oriente foreland basin in Ecuador, which includes giant fields as Sushufindi- Aguarico that have produced about one billion barrels of oil (Petroecuador, 2010) (Fig. 2.1). The

large differences in production in the different parts of the PFB are not well understood.

Northern South America has long been affected by eastward subduction of oceanic crust that began following the breakup of Rodinia in the Late Proterozoic (Ramos, 2009) (Fig. 2.2). After several episodes of rifting and terrane collisions during the Paleozoic, an important period of rifting caused by the Triassic breakup of Pangea along with the opening of the Thetian Ocean in the Early Jurassic (Ramos 2009) established the structural framework of southern Colombia (Fig. 2.3).

The first foreland basin stage experienced by the PFB occurred during the Cretaceous. A second foreland basin stage occurred as a result of the collision of the Cordillera Central during the Late Cretaceous to Paleocene (Gomez et al., 2001). This second foreland basin stage begins in the Paleocene and continues to the present, recording periods of quiescence and basin rebounding during the Eocene, and mountain building during the Miocene – Pliocene. As a result, the PFB experienced a major transition from underfilled to overfilled stage (Londoño et al., 2012).

Previous work in the PFB includes thesis work done through the University of South Carolina (Portilla, 1991), the University of Texas (Jimenez, 1997), Louisiana State University (Londoño, 2004), and through petroleum companies. For example, Ecopetrol conducted extensive research in the area during the 1990's focusing on geological and structural evaluation of the Western complex area of PFB.

This study is focused on defining the structural style, basin geometry through time, and evolution of the Putumayo foreland basin. Analysis of previous studies, well logs, and seismic reflection 2D data were integrated to build a 3D flexural modeling in following the methodology of Londoño et al., (2012) and Cardozo and Jordan (2001). The model suggests that the present-day PFB configuration is a combined result of successive tectonic and sedimentary loading events, producing a resultant lithospheric flexural deflection. This proposed tectonostratigraphic evolution has implications for hydrocarbon exploration, and represents an important contribution in the understanding o for the play concept in the area.

1.1. OBJECTIVES

The main objective of this work is to describe and analyze the geological and structural configuration and to quantify the lithospheric flexural deflection and possible variations north to south along the PFB. In order to accomplish these objectives the following tasks were conducted:

- Defining the structural framework, evolution, and depositional history of the basin.
- Constructing structure maps of major sequence boundaries to better define structural traps.
- Establishing the depositional environments and their aerial distribution of the main sequences identified.
- Defining the major pulses of foreland basin subsidence, and compare with adjacent areas using well subsidence history.
- Constructing thickness maps to better define basin filling history and growth periods on major faults.
- Creating a flexure model and compare model predictions to observed structures in the foreland basin.
- Use data and flexural model to identify potential stratigraphic traps in the less deformed, external parts of the foreland basin fill.

1.2. MOTIVATION

The aim of this thesis is to understand the structural and stratigraphic evolution of the PFB. An extensive well-log and 2D seismic dataset were provided by National Hydrocarbon Agency Colombia (ANH), Instituto Colombiano del Petróleo (ICP), and La Cortez Energy (LCTZ), and are now being used within the Caribbean Basins, Tectonics, and Hydrocarbons (CBTH) consortium at the University of Houston to address this topic.

The CBTH is an academic consortium that specializes in the tectonics and petroleum geology of northern South America, and in which I enrolled as a master's student with the geological evaluation and flexural model of the Putumayo foreland basin as my main thesis project. Previous to entering my master's studies, I completed my bachelor's degree at the Universidad Nacional de Colombia (UN) in 2007. Following my undergraduate degree, I worked four years as geophysicist at Ariana LTDA and La Cortez Energy in several basins of Colombia. Working in these areas brought to my attention the inequality between the small oil field in the Putumayo foreland basin and the adjacent giant field in Oriente basin. Dr. Paul Mann gave me the opportunity to develop this research together supervised with Dr. Jolante Van Wijk (University of Houston), Dr. John Londoño (Shell US E&P), and Dr. Nestor. Cardozo (University of Stavanger).

This thesis is structured in the following manner:

- *Chapter 2* provides a description and analysis of the regional configuration, structural, and stratigraphy of the PFB. This evaluation is based on

available literature, previous plate tectonic reconstructions, gravimetric data, interpretation of seismic information and recently acquired geophysical information in the area. The results include two regional seismic interpretation transects, structural subsurface maps of 5 key horizons, well-log cross correlations, and paleogeographic maps.

- *Chapter 3* discusses a three-dimensional flexural model for the Putumayo foreland basin through time based on the interpreted mapped surfaces and the maps generated in the previous chapter. The model helps to clarify the effects of vertical sedimentary and tectonic loads in subsidence and sedimentary geometry.

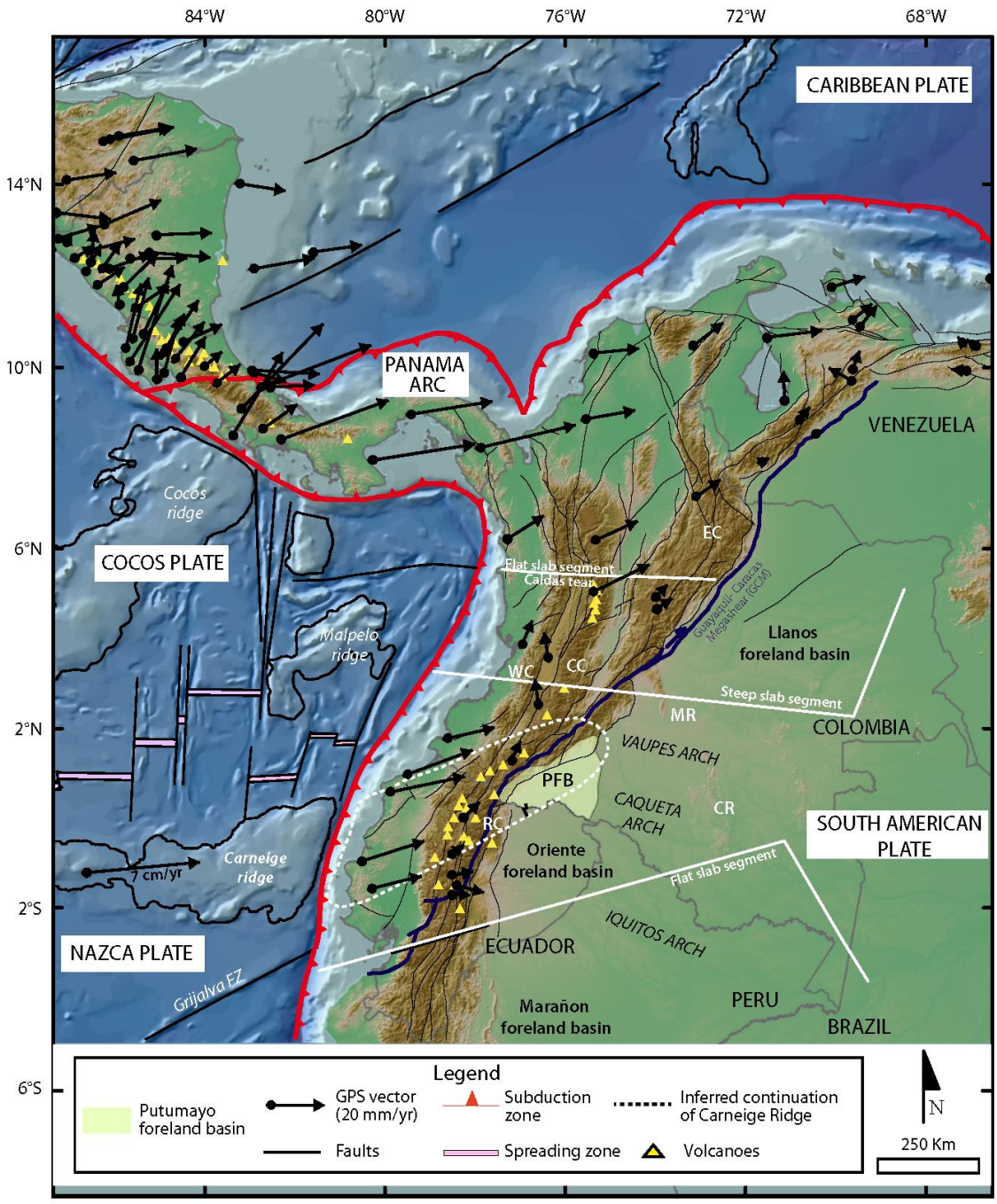

Figure 1.1 Tectonic map of northern South America showing major tectonic features and global positioning system (GPS) vectors with respect to a fixed South American plate (from Trenkamp et al., 2002). WC = Western Cordillera, CC = Central Cordillera, EC = Eastern Cordillera, RC = Real Cordillera, MR = Macarena range, CR = Chibiriquete range.

CHAPTER 2: STRUCTURAL AND EVOLUTION OF THE PUTUMAYO FORELAND BASIN, SOUTHERN COLOMBIA

2. STRUCTURAL AND EVOLUTION OF THE PUTUMAYO FORELAND BASIN, SOUTHERN COLOMBIA

2.1. INTRODUCTION

The Putumayo foreland basin (PFB), covering 50,000 Km^2, is located in the southern part of Colombia (Fig. 1.1). The PFB is bounded on the west by the Colombian Andes, a Cenozoic fold- thrust belt of mainly Mesozoic sedimentary rocks (Fig. 2.1). The Guyana shield forms the eastern and northern borders of the PFB and consists of the Caquetá basement arch, a topographic mountain range which separates the PFB from Caguán-Yarí sedimentary basin. Finally, the Vaupes subsurface arch separates the PFB from the Llanos basin to the north (Fig 1.1). To the south, the PFB is continuous with the Marañon foreland basin of Ecuador and the Oriente basin of Peru. Together, these cratonic basement, and pre-foreland structural features delineate the triangular-shaped of the PFB (Fig. 2.1).

Most of the PFB is a flat, low-lying area covered by dense rainforest of the upper Amazon River drainage. The location, the vegetation, and the thick Cenozoic sequence of the PFB make it necessary to use seismic and well data to understand the structure and stratigraphy of the PFB. It is also possible to use outcrops of Mesozoic and Paleozoic rocks located in folded and thrusted area along the Andean mountain front of the Oriental Cordillera to interpret and analyze the basin history (Jimenez, 1997). This chapter summarizes the tectonostratigraphic evolution of the Putumayo basin by integrating well, seismic, and potential field data along with and previous

work in the area. Data in this compilation constrain the timing of different tectonic pulses and stratigraphic arrangements through time in the PFB, which may aid future oil exploration in the basin (Fig. 2.1).

2.2. PREVIOUS WORKS

Geological studies of the PFB have been carried out by both industry and academic geoscientists over the past 30 years. A recent study on the sediment and tectonic-induced flexure of the basin was carried out by Londono (2004) and Londono et al. (2012). They used a computer routine developed in Matlab 6.5 and several seismic transects in the central area of Putumayo basin to calculate the effective elastic thickness of the continental lithosphere in the area, and to determine the role of tectonic and sediment load through the time (Fig. 2.1)

The most extensive and integrated structural interpretations of the southern area of the Putumayo basin were carried out by Portilla, (1991), Jimenez (1997), and Velandia et al., (2005) (their map areas are shown in Fig. 2.1). These studies were comprehensive, and provided an important starting point for my own study. Portilla (1991) interprets the structural style of the PFB as a combined effect of "thick-skinned" crustal deformation and consequent, shallow "thin-skinned" deformation in the Mesozoic and Cenozoic sedimentary cover. Using radar images, kinematic analysis of historical, earthquake fault-plane solutions, and interpretation of seismic profiles, Jimenez (1997) concluded that strike-slip faulting is the major control on the structural style in eastern Andean mountain front portion of the PFB (Fig. 2.2). Furthermore, Velandia et al., (2005) proposes that right-lateral transpressional deformation occurs along the Algeciras fault system striking parallel to the mountain front (Fig. 2.3).

In the Oriente foreland basin of Ecuador, regional studies have been done by Baby et al., (1997), and Dumont et al., (2005) (Fig. 2.4). The first study describes

three main tectonic corridors or zones in the foreland basin that are also visible on gravity data (Fig. 2.4): 1) the Western structural zone which represents the area of the Andean mountain front characterized by folding and thrusting; 2) the Central structural zone characterized by moderately inverted Triassic-Jurassic half-grabens overlain by a less-tilted post-rift section; and 3) the Eastern structural zone characterized by three, weakly-inverted rifts controlled by fabrics within Paleozoic basement rocks (Baby et al., 1997) (Fig. 2.4).

The study by Dumont et al. (2005) analyzes the right-lateral motion in the Ecuadorian Andean Cordillera along the Guayaquil-Caracas megashear. The results of both previous studies can be integrated and extrapolated to the Putumayo basin to the north in Colombia given that the Oriente basin is the direct, northward continuation of the Oriente and Marañon basins from the south (Fig. 2.4).

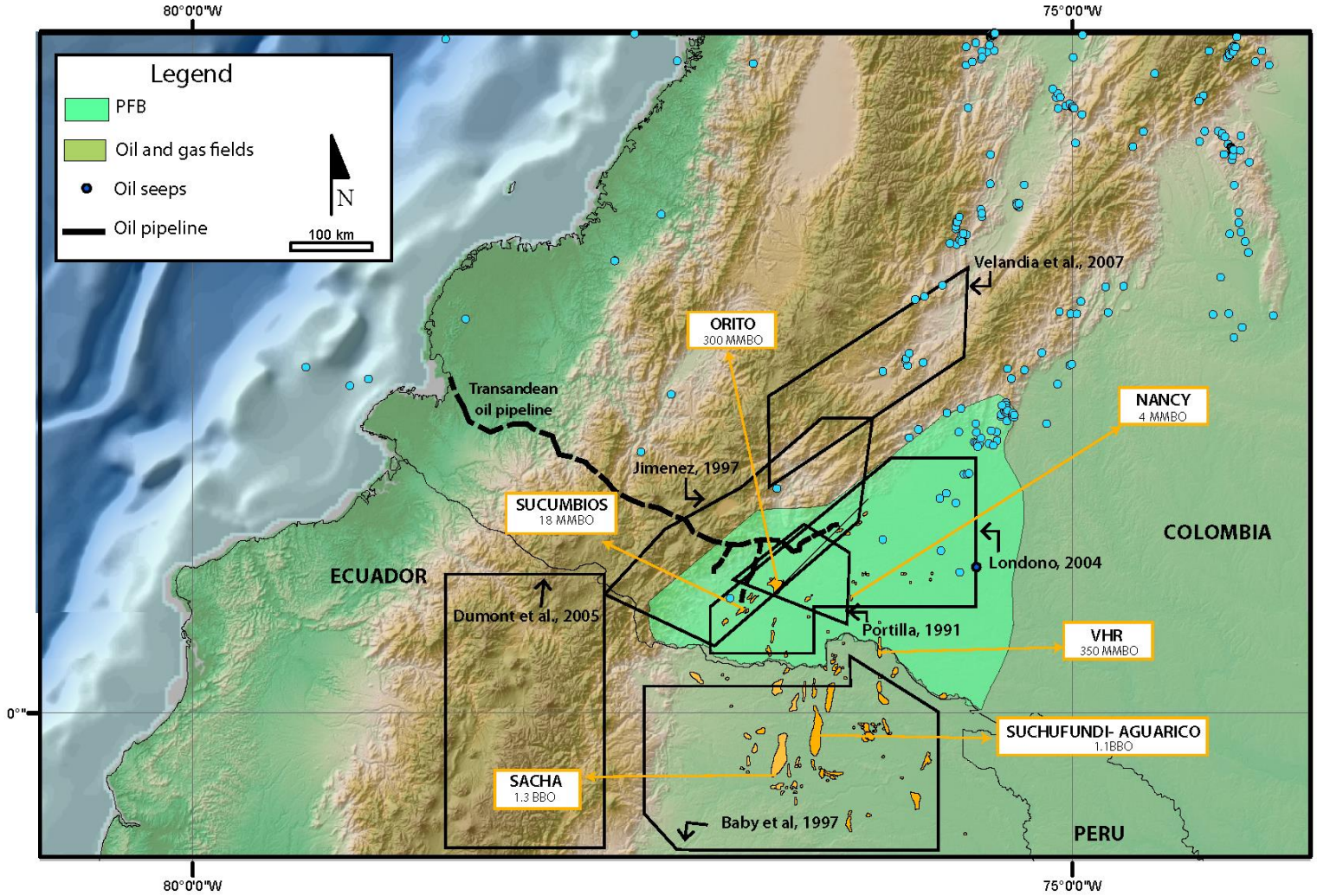

Figure 2.1 Topographic map showing the main oil and gas fields, their infrastructure and pipelines, and the cumulative production of the Putumayo foreland basin of Colombia, the Oriente foreland basin of Ecuador, and the Marañon basin of Peru (modified from ANH, 2012). The locations of important previous studies in the area are shown as polygons.

2.3. PRESENT-DAY TECTONIC SETTING OF THE PUTUMAYO FORELAND BASIN

The present-day tectonic setting of southern Colombia is controlled by the subduction of the Nazca plate beneath the South American plate, the Panama Arc-indenter in the north (Vargas and Mann, 2013), and the oblique subduction of the Carnegie ridge in the south (Gutscher et al., 1999) (Fig. 1.1). The resulting physiographic features in the southern part of Colombia include: 1) the Western Cordillera, aligned parallel to the subduction zone of the Pacific coast, and consisting of mafic igneous rocks associated with oceanic accreted terranes (Duque-Caro, 1990); 2) the Central Cordillera, interpreted to be an active continental magmatic arc, and forming a pre-Oligocene eastern boundary for sub-Andean basins (Cooper et al., 1995); 3) the Upper Magdalena Cretaceous foreland basin along which the Magdalena River flows northwards into the Caribbean (Gomez et al., 2005); 4) the Eastern Cordillera diverging progressively from the Central Cordillera in a north-northeast direction as a doubly-vergent, fold-thrust belt related to the Cenozoic inversion of Mesozoic rifts (Schmitz, 1994); and 5) the Putumayo foreland basin located parallel to the fold and thrust belt (Portilla, 1991) (Fig. 1.1).

2.3.1. Subducting Nazca plate

The Nazca plate is subducting eastward beneath South America at a rate of 7 cm/year (Trenkamp et al., 2002) (Fig. 2.2). The boundary between both plates is a convergent margin defined by the Ecuador–Colombia trench, and the Andean magmatic arc (Fig. 2.2). This convergence began soon after the breakup of Rodinia in

the Late Proterozoic, and since that time, the more dense oceanic crust has continued to subduct under the lighter continental crust of the South American craton (Ramos, 2009). Present-day seismicity reflects the geometry of the active convergent boundary between the plates in which the subduction zone or Benioff zone geometry is defined by shallow earthquakes zone located along the shallow part of the subduction zone along the Pacific coastline (Pennington, 1981), and deeper earthquakes beneath the Andean Cordillera (Chinn and Isacks, 1983) (Fig. 2.2).

Three distinct areas of seismicity and volcanic activity are present in the Colombian Andes. The northernmost region (western Colombia) shows a steeply-dipping slab segment (45° dip) with a narrow and active, andesitic volcanic arc (Bourdon, 2003). In contrast, the Ecuadorian region shows shallow seismicity with an adiakitic volcanic arc that is interpreted as a "flat slab" expression of the shallow subducting of the Carnegie ridge (Gutscher et al., 1999). The Putumayo area, which has an anomalous northeast trend, is defined as a transition zone between the two well-defined seismicity regions (Fig. 1.1).

Figure 2.2 shows a map view of earthquakes occurring between 1990 and 2011, from the U.S. Geological Survey (2012) database along with a >1000-Km-long transect from the Colombian trench on the Pacific margin to the continental crust of the PFB. The earthquake data define the subducted oceanic slab of the Nazca plate with a crustal thickness < 30 Km. The subduction angle is <15° extends over a distance of >100 Km that extends from the Colombian trench to the Central Cordillera of Colombia. Beneath the Central Cordillera, the dip on the subducted Nazca slab steepens to >30°, perhaps related to its interaction with the base of the

South American continental crust. Large earthquakes along this transect in the Colombian trench may be produced by the shallow subduction of the Carnegie ridge (Gutscher et al., 1999). Crustal thickness beneath the Cordillera Central in the southern region of the Galeras volcano is about 40-50 Km (James, 1984) (Fig. 2.2).

2.3.2. Carnegie ridge

The Carnegie ridge is a 250-Km-wide area of thickened oceanic crust on the Nazca plate that is subducting obliquely beneath the South American plate. Gutscher et al. (1999) used earthquake depths and focal mechanisms to show that the subducted Carnegie Ridge may extend downdip for as far as 500 Km in an east-northeasterly direction beneath Ecuador and southern Colombia (yellow outline shown in Figure 1.1). The down-dip area of the Carnegie ridge is characterized by a lack of intermediate depth seismicity, complex shallow depth seismicity, and a broader and more geochemically complex zone of active, arc-related volcanoes strongly influenced by slab melts (Bourdon et al., 2003) (Fig. 1.1).

The Andean foreland basin varies across this region from a very small or absent basin in the PFB of southern Colombia to two to three times wider in the south Marañon and Oriente foreland basins of Peru and Ecuador, respectively (Fig. 1.1). The thinner part of the foreland in the PFB in the north along with adjacent arches in the craton was produced as the result of far-field convergence that accompanies the subduction of the Carnegie ridge over the past 8 Ma (Gutscher et al., 1999).

In the area overlying and adjacent to the subducted Carnegie ridge, structural basement highs in the cratonic area are more prominently expressed,

including the Macarena range, and Caquetá arch of the Eastern structural zone (Fig. 2.4). It is possible that these broad arches in the craton were partially reactivated during the late Miocene to recent history of Carnegie ridge subduction as the Carnegie ridge is inferred to extend to the western limit of the PFB (Fig. 2.2).

2.3.3. Guayaquil-Caracas megashear

The Guayaquil-Caracas megashear is a continental, right-lateral fault zone that bounds the mountain front of the Andes and the eastern edge of the North Andean block in northwestern South America. According to GPS measurements by Trenkamp et al., (2002) this transpressive regime is the result of the northeastward motion of the North Andean block at a rate of 1 cm/year (Fig. 2.3). This produces extension, and extends the Gulf of Guayaquil, Ecuador and some pull-apart structures on the northern part of the block (Dumont et al., 2005) (Fig. 1.1). In the Putumayo mountain front this regional feature is observed as linked right-lateral strike-slip faults called "Algeciras fault system" by Velandia et al., (2005) (Fig. 2.3).

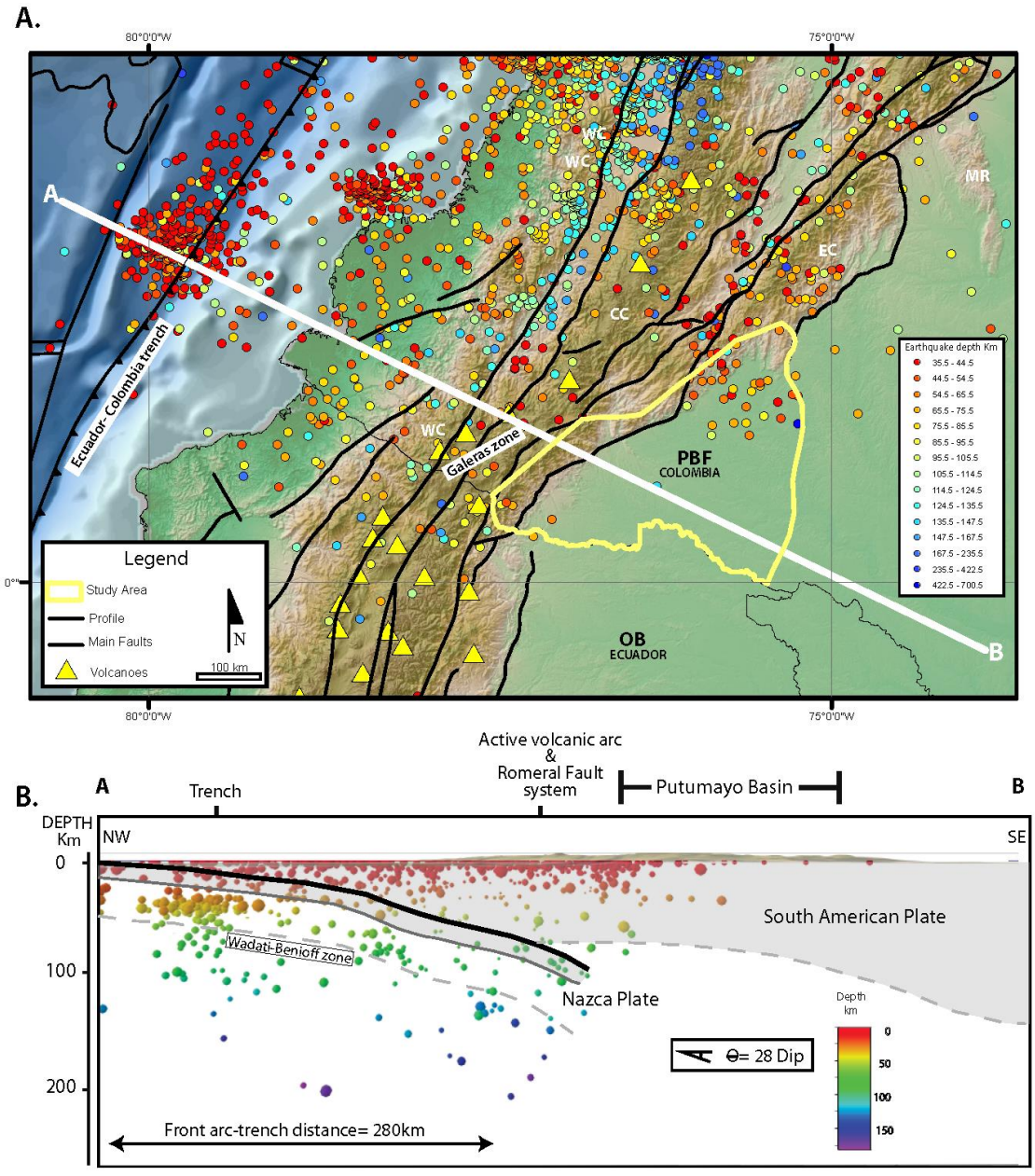

Figure 2.2 A.) Map view of earthquakes occurring between 1990 and 2011, and locations of active volcanoes (yellow triangles) of southern Colombia (data taken from USGS, 2012). B.) AB profile shows the seismicity (hypocenters shown as dots) used to infer the position and angle of the subducted Nazca slab beneath Colombia.

2.4. STRUCTURAL GEOLOGY OF THE PUTUMAYO FORELAND BASIN

The geometry of the PFB consists of an asymmetrical sedimentary wedge typical to that of other foreland basins. Its western boundary is the Eastern Cordillera thrust and fault belt followed by the PFB foothill region where thrusting, and transpressional structures indicate strong shortening in the mountain front area. The foreland area is characterized by relatively planar topography that extends for more than 150 Km where the sediments are deposited on top of the Precambrian basement (Fig. 2.3). The western boundary of the PFB is a subsurface structural basement high that divides the Putumayo basin from the Caguán-Yarí basin (Fig. 2.4).

2.4.1. Eastern Cordillera

Compressive episodes produced by the convergence between the Nazca and South American plates have been proposed as the mechanism for uplifting the Andean Cordillera (Pardo-Casas and Molnar, 1987). The southward continuation of the compressive uplift can be followed into Ecuador, where the Real Cordillera uplift may be also considered a vestige of a regional Eastern Cordillera fault system (Campbell, 1965) (Fig. 2.3).

The Eastern Cordillera system is a southwest-striking, doubly-vergent thrust belt that places the Cretaceous and Paleogene rocks over a thick Cenozoic rocks succession. Paleozoic and Neo-Proterozoic basement rocks are exposed in its axial area (Bayona et al., 2008). The basement rock outcrops in the southern part of Colombia are related with the north-northwest-trending Garzón (Fig. 2.3). This northwest orientation is also present in the Macarena range, which differs

significantly from the overall trend of the Eastern Cordillera, implying a previous NS tectonic event that formed the regional structural highs in the south of the study area (Moreno-Lopez, 2012).

2.4.2. Putumayo foreland basin

The structural geology of the Putumayo foreland basin, including its timing and deformation styles have been described by Portilla, (1991) and Jimenez (1997); I have integrated information from all three of the main structural zones described on the Ecuadorian Oriente basin with the PFB (Fig. 2.4).

- *Structural zones*

The structural zones in the PFB can be extrapolated from the Oriente foreland basin because both basins are genetically related, and they are part of the same foreland basins trend (Fig. 2.4). Three fault zones were identified in Ecuador based on seismic interpretation, well-log data, and outcrops by Baby et al, (2013). The structural zones are identified on Figure 2.4.

Western structural zone: The western zone includes the foothills area deformed by fold and thrust faults along the Andean mountain front, and forming the first major area of topographic relief in the PFB (Fig. 2.3). This structural zone was uplifted and deformed during the Miocene-Pliocene along the frontal thrust fault system of the Andean range. This deformation is associated with a positive flower structure developed in a transpressional tectonic environment which remains seismically and volcanically active (Baby et al., 2013) (Fig. 2.4).

Central structural zone: The center of the basin is a result of the moderate inversion of north-northeast-trending, half-grabens. The inverted faults are thick-skinned and dipping vertically with depth. This fault system has been active since the Upper Triassic to Lower Jurassic and was last reactivated during a Cenozoic inversion. Inversion effects decrease to the east as shown by progressively smaller displacements of associated, antithetic normal faults (Baby et al., 2013) (Fig. 2.4).

Eastern structural zone: The eastern zone is a reactivated thick-skinned fault system which is likely rooted in Paleozoic rocks that are shallowly buried by the thin sedimentary fill of the eastern PFB (Fig. 2.3B). These high-angle faults have been proposed such as single a basal detachment in the Paleozoic basement rocks; these high-angle faults are thought to have produced uplifted structural highs (Baby et al., 2013) (Fig. 2.3B).

The structural configuration of the Putumayo foreland basin, including timing, and deformation styles have been defined by Portilla, (1991) and Jimenez (1997); however, three main structural zones described on the Ecuadorian Oriente basin might be integrated into the study area.

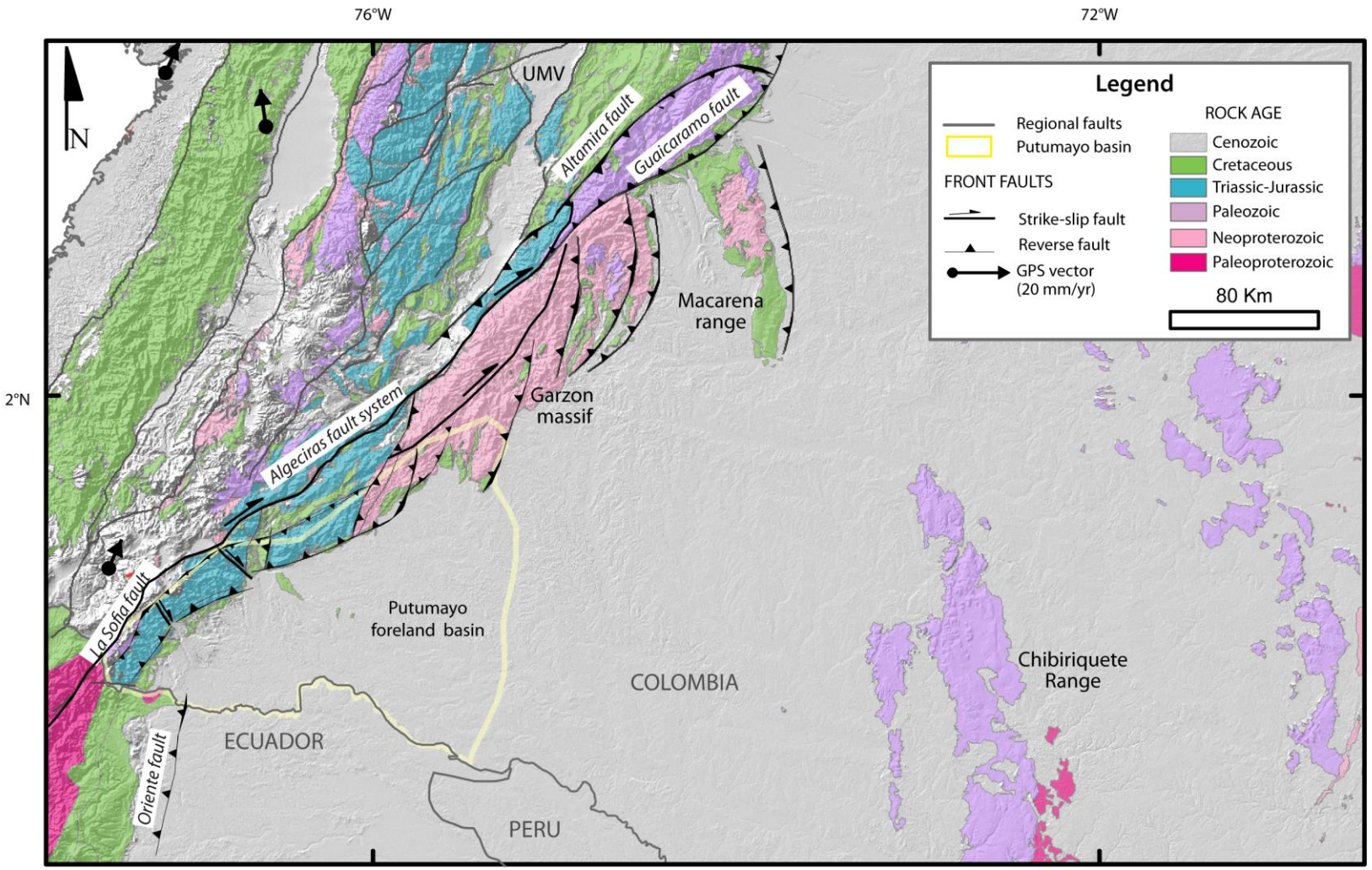

Figure 2.3 Geological map modified from Gomez et al. (2007) showing the main structural features of the PFB and adjacent areas

2.4.3. Basement structural highs

Southeastern Colombia is dominated by a series of north-south-oriented basement structures that plunge northwards that are well illustrated on the gravity map shown in Figure 2.4. On this map, the positive anomalies, ranging from 10 to 50 mgal, are associated with Paleozoic crystalline basement due to its high density compared to the low values, ranging from 232-292 mgal.

Located to the east of the Putumayo basin, the Caquetá, the Viento-Melon, and the Macarena basement highs, plays an important influence on the basinal structure to the east and northeast of the PFB (Fig. 2.4). The presence of basement structures in the eastern area of the PFB are the result of a the lower Paleozoic shortening event that also affected the older Precambrian rocks (De Righi and Bloomer, 1975), and is marked by the presence of major, north-south-striking thrust faults to the east (Fig. 2.3B).

The Caquetá arch is the westernmost structural high and represents the eastern boundary of the PFB (Fig. 2.4). This structure controls the deposition of the PFB sedimentary sequences and has acted as a paleogeographic barrier since the Paleozoic (De Righi and Bloomer, 1975) (Fig. 2.3B).

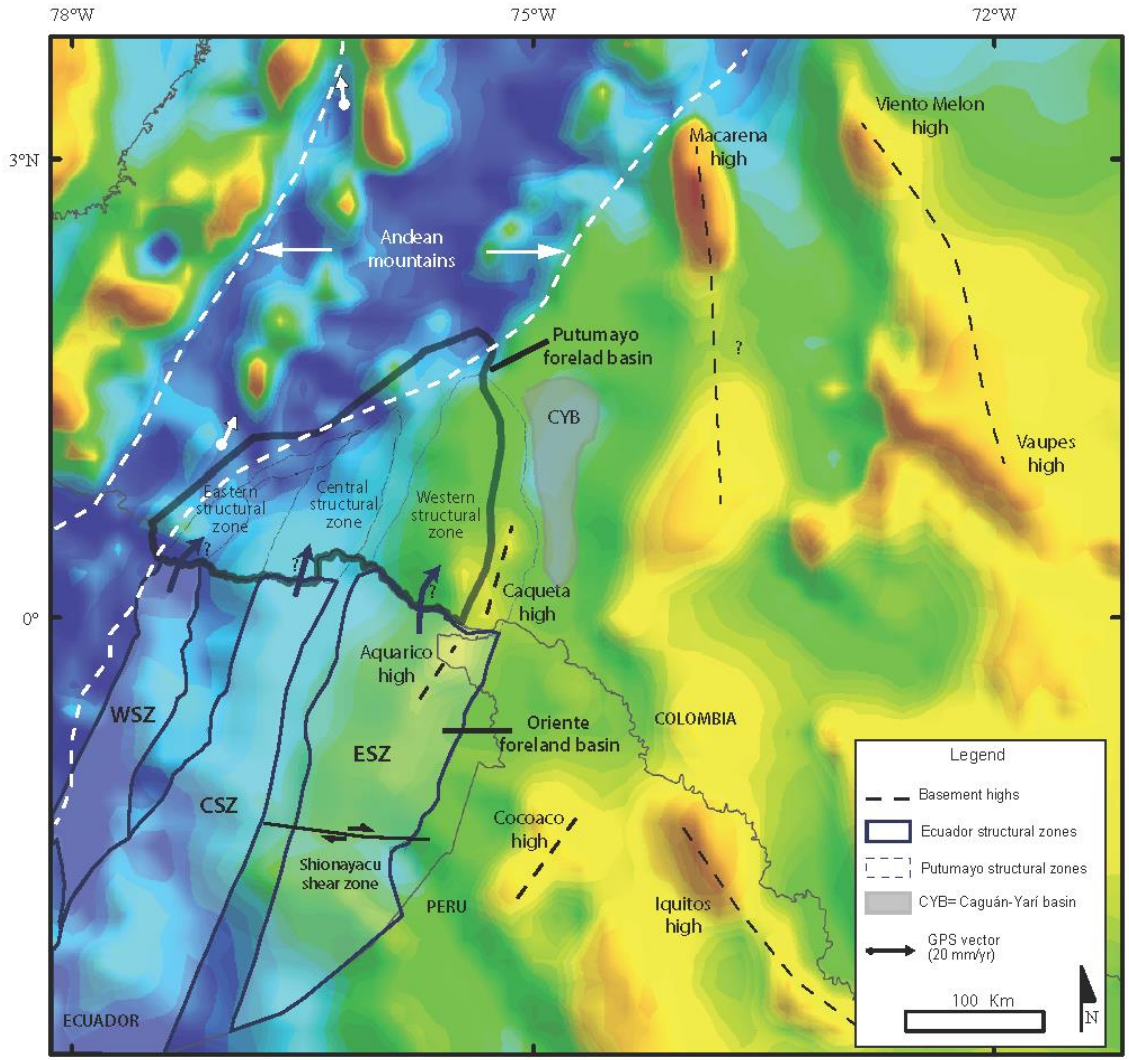

Figure 2.4 Bouguer GEOSAT gravity map of the southern part of Colombia, showing the basement highs and the three main structural zones described from the Oriente basin and extrapolated to the PFB. WSZ = Western structural zone. CSZ = Central structural zone. ESZ = Eastern structural zone.

2.5. TECTONO- STRATIGRAPHIC FRAMEWORK

Southern Colombia has experienced several major tectonic events since the Upper Paleozoic that influenced both its sedimentary history, and also affected its present-day structural configuration (Portilla, 2001). Figure 2.5 shows a generalized stratigraphic column ranging from Pre-cambrian to Quaternary. These sedimentary rocks record the evolution of the PFB associated with four tectonic events: 1) Pre-cambrian to Cambrian metamorphism (Ibanez-Mejia et al., 2011); 2) transgressive Paleozoic period (Rosello et al., 2006); 3) Jurassic-Triassic to Early Cretaceous back-arc rifting (Cooper et al., 1995); and 4) middle Cretaceous to Cenozoic foreland basin phase (Gomez et al., 2005).

2.5.1. Basement: Guyana shield and Cambrian? metamorphism

The Guyana shield which is outcropping towards the east of the PFB, is composed of granites, granodiorites, and syenites with Paleo-Proterozoic ages (Cordani et al., 2010). Recent studies have identified a younger basement beneath the sedimentary sequence of the PFB. Well samples contain migmatitic gneisses with an absolute ages ranging from ~950 Ma to 1100 Ma (Ibanez-Mejia et al., 2011). These rocks were affected by fringing-arc terrane collisions in which the latest stage of metamorphism is constrained by felsic leucogranites sampled from the Caiman-3 well (Ibanez-Mejia et al., 2011) (Fig. 2.5).

2.5.2. Paleozoic

The Paleozoic has been defined mainly from the sedimentary record observed in the Oriente and Marañon basins south of the PFB. The lower Paleozoic is characterized by dark marine shale and quartzitic sandstones deposited during the Silurian?-Devonian; these form include the Pumbuiza Formation (Barret and Isaacson, 1988), and the Cabanillas Formation in Peru (Isaacson and Sablock, 1988). Intra-formational disconformities are present showing that this sequence was affected by several compressional events (Rosello et al., 2006).

The upper Paleozoic (Carboniferous to Permian) is composed by marine carbonate and shale of the Macuma Formation in Ecuador (Rosello et al., 2006), Copacabana-Tarma-Ambo and the Mitu Groups of Peru (Isaacson and Sablock, 1988) supporting a regional transgressive setting (Fig. 2.5). A significant period of non-deposition or erosion is recorded between the Paleozoic sequence and the Triassic-Jurassic (Rosello et al., 2006). This period may be related to the Pangea assemblage during the Late Triassic (Williams, 1995).

2.5.3. Triassic-Jurassic

A Triassic-Jurassic sedimentary section is represented by the Motema Formation in the Putumayo basin (Beicip and Ecopetrol, 1988). This unit consists of red arkosic sandstones, shales, and volcano-clastic debris, located mainly in the eastern area of the basin (Beicip and Ecopetrol, 1988). It can be correlated with the Santiago – Chapiza Formation in Ecuador, and the Pucara –Sarayaquillo Group in

Peru (Rosello et al., 2006). The tectonic setting interpreted is a rift phase; where the sedimentary units (red beds) are the syn-extensional sediments (Portilla, 1991) (Fig. 2.5).

2.5.4. Cretaceous

Cretaceous shallow marine deposits of transitional to inner platform facies are represented by the Caballos and Villeta Formations (Higley et al., 2001). These sedimentary rocks comprise most of the Cretaceous sedimentary record in the basin, and represent the main petroleum system in PFB (Beicip and Ecopetrol, 1988). The Caballos Formation (Aptian to Albian) sandstones were deposited on a continental and shallow-marine environment, and are the main reservoir of the PFB with more than 290 million of produced barrels (Gonçalves et al., 2002). The Villeta Formation overlies the Caballos Formation that includes marls, limestone, and few sandstones embedded in dark gray to black shale, and represent several rises and falls of sea level (Fig. 2.5). The upper Villeta strata mark the transition from marine to continental conditions of the basin in the Late Cretaceous (Beicip and Ecopetrol, 1988).

During the Santonian- Campanian (120 My), a contractional event produced deformation in the Central Cordillera (Colleta et al., 1990) with the Putumayo Province as the foreland basin (Gomez et al, 2005). As a result of this new cycle of sedimentation an extensive deposition of reddish siltstones and mudstones of the Rumiyaco Formation occurred (Beicip and Ecopetrol, 1988) (Fig. 2.5).

2.5.5. Cenozoic

The region experienced significant tectonic events including: an increasing convergence rate between the Nazca and South American plates during Paleocene-middle Eocene (Daly, 1989); the convergence of the Panama block with South America (Mann and Burke, 1984); and the collision terrain between the Andes and the Choco Terrene during the middle Eocene to the middle Miocene (Sarmiento, 2001) (Fig. 2.5).

The middle Eocene sediments are represented by the Pepino Formation, which is composed of three units. The upper and lower units consist of coarse conglomerates, principally comprising fragments of igneous rocks and sandstones, and are separated by a middle sequence of shale, siltstone, and sandstone (Ecopetrol and Beicip, 1988). These depositional environments were interpreted as alluvial fans and braided rivers (Portilla, 1991). The middle unit is constituted by limestone, and siltstones that have been interpreted as alluvial plains and outer alluvial fans (Portilla, 1993) (Fig. 2.5). This unit records two events during the Central Cordillera uplift, identified as the sediment source area, corresponding to each conglomeratic unit (Portilla, 1993).

The upper Eocene-Oligocene-middle Miocene sediments in the Putumayo comprise the Orito Group, which consists of the Oligocene Orteguaza Formation and the lower-middle Miocene Belen Formation. The Orito Group consists of argillaceous sandstone, siltstone, and clay (Ecopetrol and Beicip, 1988). These sequences were deposited in fluvial environment with some lacustrine layers (Portilla, 1991) (Fig. 2.5)

The upper Miocene section is represented by the Ospina Formation, which is made up of poorly sorted, fine-to-coarse-grained, main carbonaceous sandstones and claystones deposited in lacustrine conditions. Plio-Pleistocene sediments comprise the Guamuez-Caiman Formations. These clastics were deposited in an alluvial fans and braided environments recording the last tectonic pulse of the Andean Orogeny (Cordoba et al, 1997) (Fig. 2.5).

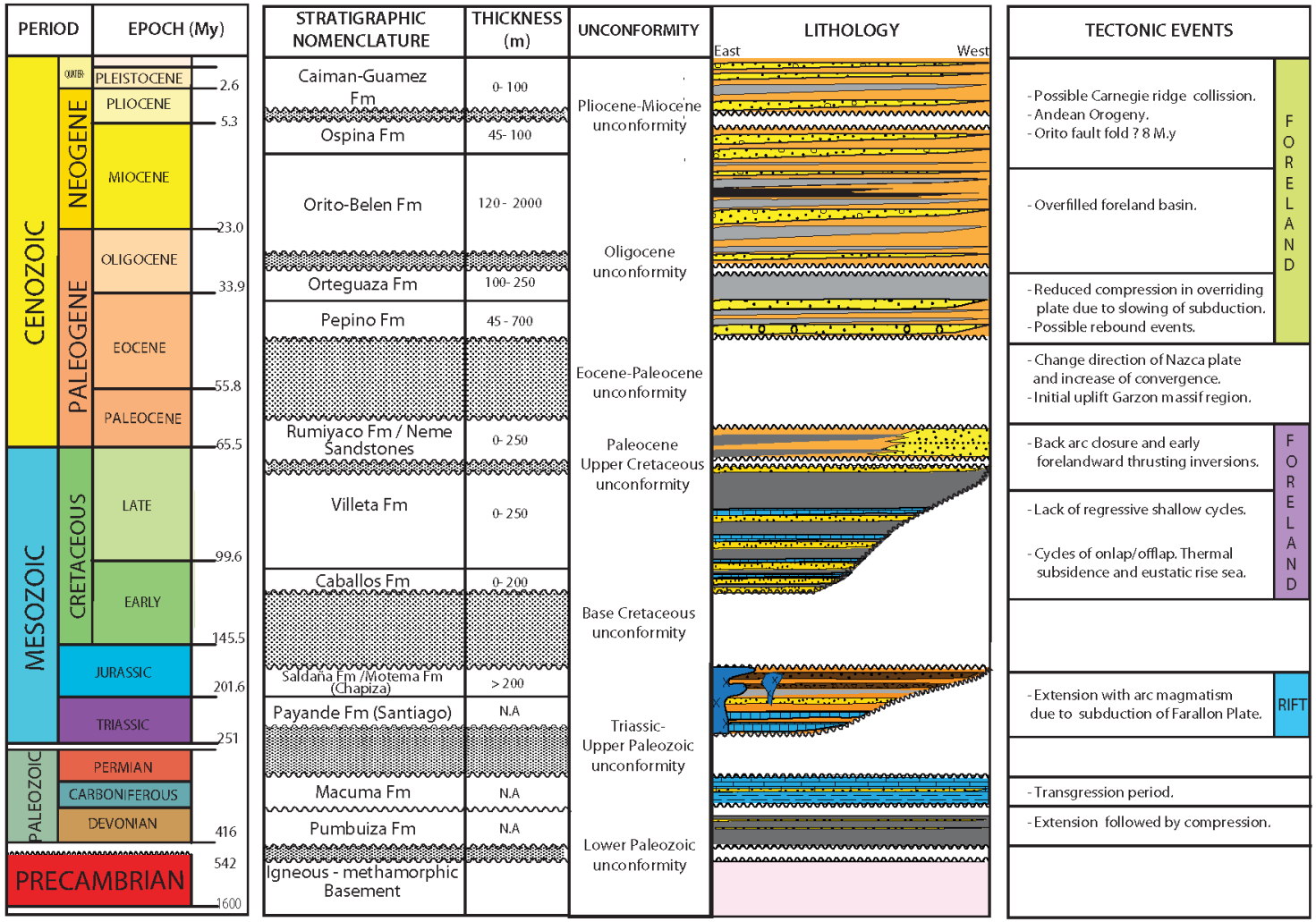

Figure 2.5 Generalized stratigraphic column of the PFB. The stratigraphic units are based on outcrop studies along the Andean mountain front and wells within the Putumayo basin. Section modified from Beicip-Ecopetrol (1998).

2.6. DATA AND METHODOLOGY

Several datasets were integrated in order to describe the PFB. They include: 1) bathymetric and topographic data from a SRTM 30m digital elevation model; 2) satellite GEOSAT free air gravity data; 3) well data; 4) 2D seismic lines with different acquisition parameters; 5) surface geologic data the Colombian Geological Service (Gomez et al., 2007); 6) GPS plate velocities from Trenkamp et al., (2002); and 7) the compilation of published lithological description, age data, academic studies, and industry reports.

Figure 2.6 shows well data and 2D seismic coverage used for the project, and illustrates areas in the east in which seismic data and well data are not available. It was in these areas lacking seismic and well data where Bouguer gravity data provided an important tool for defining the structural configuration and areal extent of the basin (Fig. 2.4). Figure 2.6 also shows the location of a regional seismic profile (Fig. 2.8), a well cross section in the southern part of the study (Fig. 2.10), and three mountain-front examples used to explain the main tectonosequences, timing of deformation and the structural style of the study area (Fig. 2.9).

The Fig. 2.6 shows well data and 2D seismic coverage used for the project, and illustrates areas in the east in which seismic data and well data are nonexistent. It was in these areas where potential fields method, such as the Bouguer map, were the most important tool in defining the structural configuration and areal extent of the basin. It also shows the location of a regional seismic profile, a well cross section in the southern part of the study, and three mountain-front examples used to explain the

main tectonosequences, timing of deformation, and the structural style of the study area.

2.6.1. Well-log data in this study

A total of 32 exploration wells were used for time-depth reference, and to correlate main tectonosequences throughout the basin. 27 wells have a complete set of log curves, while the remaining 5 wells included only images of the composite log and reports.

A set of log curves, including gamma ray, sonic and resistivity, geological information (including formational tops, and rock descriptions), and geophysical information (check-shot, and velocity seismic profile VSP) were used to constrain the synthetic seismogram, determine the geophysical properties of keys reflectors, and to correlate the logs with the seismic character.

2.6.2. Seismic data in this study

A total of 3000 Km of 2D seismic kindly provided to me by the ANH, the ICP and La Cortez Energy for use in this MS thesis were loaded into the workstation and interpreted (Fig. 2.6). The seismic information used in this study represent a significant amount data of the total existing 2D seismic available in the PFB and were acquired between the years of 1969 and 2005. Seismic data quality varies because of differences in acquisition parameters, sampling time, coordinate systems, seismic processing sequence, and target unit of different seismic surveys.

2.6.3. Methodology

- *Loading of seismic and well data*

The database consists of approximately ~3000 Km of 2D multi-channel seismic data and 32 wells (Fig. 2.6). The raw data for the construction of this seismic dataset consist of SEG-Y, UKOOA, LAS files, time-depth tables, and technical reports. Due to non-standardization of seismic data, the loading process included: re-projection of coordinates at UTM Bogota Bogotá zone, creation of a seismic datum at 1,312 ft. (400 m), and establishment of a replacement velocity of 7,874 ft. (2400 m/s) used to calculate appropriate TWT static shifts between 50-500 ms for each seismic program. Also, several post-stack geophysical processing techniques were used to correct for acquisition differences, balance amplitudes, and frequencies.

- *Seismic interpretation and definition of stratigraphic units and structural styles*

Several seismic sequences were interpreted in order to define the main tectonostratigraphic units or tectonosequences of the PFB. Using physical characteristics of the reflector horizons (amplitude, frequency, and continuity), formation evaluation logs of several wells, technical reports, and criteria of reflection terminations, the following tops formations were identified and mapped: the Basement, the Caballos and Villeta Formations, the Rumiyaco Formation, the Pepino

Formation, the Orteguaza-Belen-Orito Formations, and the Ospina-Caiman Formations (Fig. 2.5).

Calibration of seismic to well control using synthetic seismogram, and interval velocities for each formation was calculated from check-shot logs in order to convert time values into depth values. Finally, thickness maps in depth of major sequence boundaries were constructed to better define basin depocenters, structural control filling history, and growth periods on major faults.

- *Well-log cross section*

A well-log cross section in the southern part of the study area was built to understand the spatial and temporal distribution of the mapped sequences. The methodology and terminology followed to describe and analyze stacking patterns from well data is based on Escalona and Mann (2006).

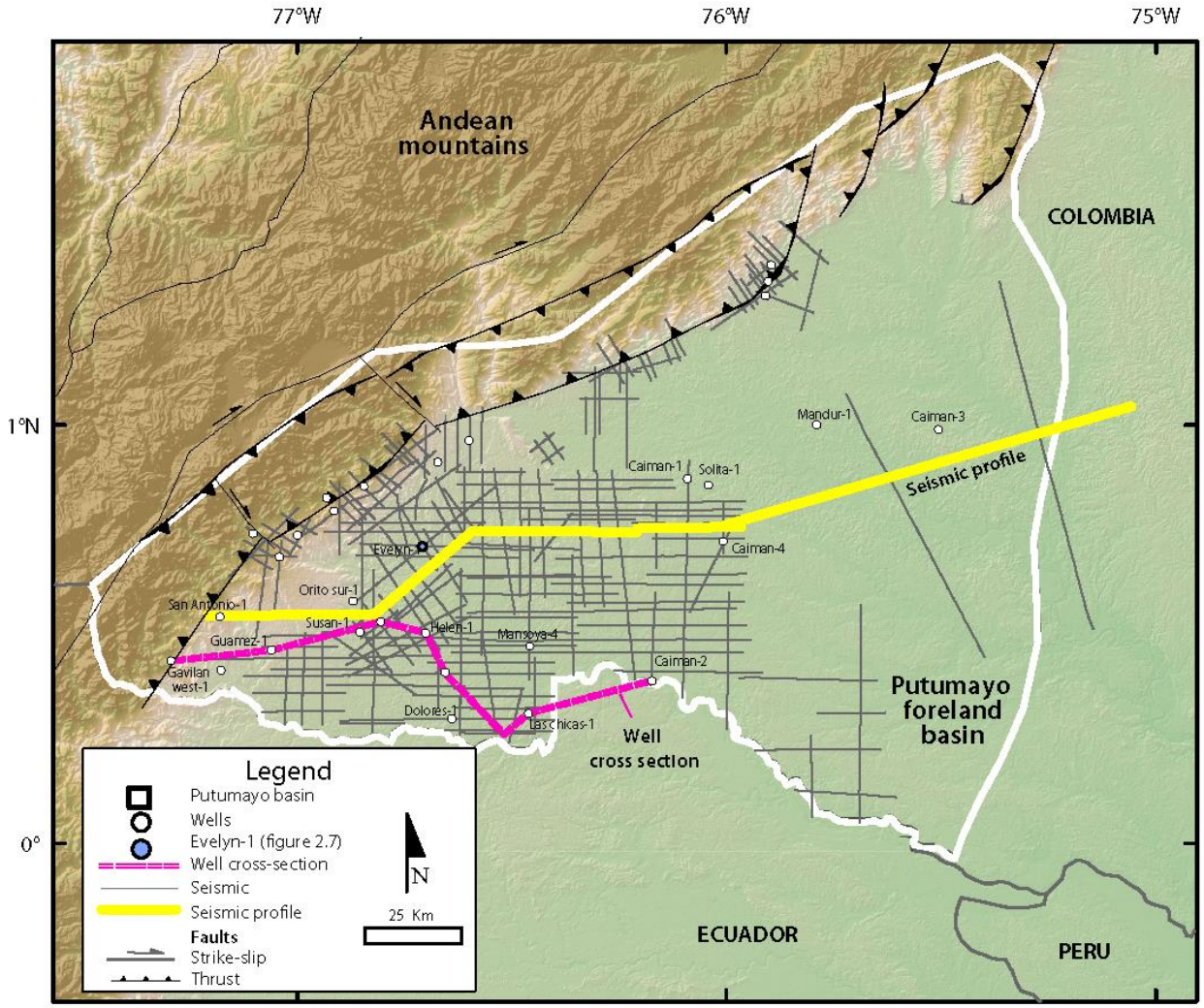

Figure 2.6 Location of seismic and well data in the Putumayo foreland basin outlined by white line. Transect shown by yellow line, and the well cross-section is shown in pink.

2.7. TECTONOSEQUENCES AND STRUCTURAL OBSERVATIONS

The Putumayo basin has a relatively thick sequence about 3.5 Km in thickness composed of the Cretaceous and Cenozoic rocks (Fig. 2.7); in which stratigraphic and structural observations together with important unconformities surfaces, seismic character, and reflectors relationship were used to identify three (3) structural zones, shown in a regional 2D seismic profile (Fig. 2.8); and five (5) main sequences, including: sequence I - Cretaceous; sequence II - Paleocene; sequence III - Eocene; sequence IV - Oligocene; and sequence V-Miocene. These sequences with their key interpreted horizons in relationship with the seismic expression, well-log response, lithostratigraphic units, and petroleum system are shown in Fig. 2.7.

2.7.1. Structural zones

Three different structural zones are identified in the study area. The structural zones with decreasing deformation from west to east include: 1) Western structural zone to the west near the Andean mountain front; 2) the Central structural zone, and 3) the Eastern structural zone (Fig. 2.8).

- *Western structural zone*

This zone is interpreted as a thick-skinned, north-south-striking fold-thrust belt that is called here “fault family 3”. The Western zone is observed on the regional seismic section (Fig. 2.8). Faults are steeply dipping, and do not show detachment in the basement (Fig. 2.8). Moreover, east-dipping backthrusts found near the Andean

mountain front also involve basement and are here called “fault family 4”. The continuation of fault family 4 southward in Ecuador has been mapped as an east-dipping frontal thrust fault system developed during Pliocene to Quaternary, and it is produced by transpressional inversion of a north-northeast-trending Triassic-Jurassic rift (Baby et al., 1997)

- *Central structural zone*

Located in the central area of PFB, this structural zone is characterized by NNE-SSW-trending faults (fault family 2). This fault family has average throw of 50 ms affecting the Cretaceous and Paleocene sediments (Fig. 2.8). It is bounded to the east by remarkable west-vergent inverted graben where the Caiman-1 well is located. The Central structural zone includes asymmetrical graben bounded by two planar faults (Fig. 2.8). An angular unconformity is observed between the sediment deposited in the half-graben structure and the overlying and less deformed Late Cretaceous sediment (Fig. 2.8).

The smooth anticlines in this structural zone were developed in the Late Cretaceous (Turonian-Maastrichtian) and the lower Paleocene as seen in the seismic expression of the Sequences I and III. Those structures exhibit low relief, and small areas of extension which differs from the Ecuadorian broad anticlines located south of the Central structure zone of the PFB. In Ecuador the Central structural zone is characterized by a vertical strike-slip faults that may develop flower structures at the surface (Baby et al., 1997).

- *Eastern structural zone*

The Caquetá arch, located in the Eastern zone of the PFB, is the most visible feature of this structural zone (Fig. 2.8). It is characterized by presence of acoustic basement composed by low intensity reflections with poor lateral continuity and homogeneous and chaotic seismic facies. In addition, strongly dipping reflections are interpreted as basement fabric discontinuities or igneous intrusions. Limited to the south by the Shinayacu shear zone, and to the north as a plunging structure, the Caquetá arch represents an important structure of the Eastern structural zone along the Putumayo-Oriente basin (Fig. 2.4).

The Caquetá arch has geomorphologic expression at the surface, especially at its eastern end, where it is marked by observable surface lineaments that control the direction of important rivers such as the Caquetá and Putumayo (Fig. 2.3 A). The lack of seismic coverage east of the basement high does not allow the identification of the expected inverted structure as observed in the Ecuadorian sector of the Eastern structural zone. The Ecuadorian continuation of the Eastern structural zone is characterized by three extensional depocenters heavily influenced by underlying Paleozoic basement fabrics (Belotti et al., 2003) that were reactivated both by the Jurassic rifting event along with the Early Cretaceous uplift period (Balkwill et al., 1995)

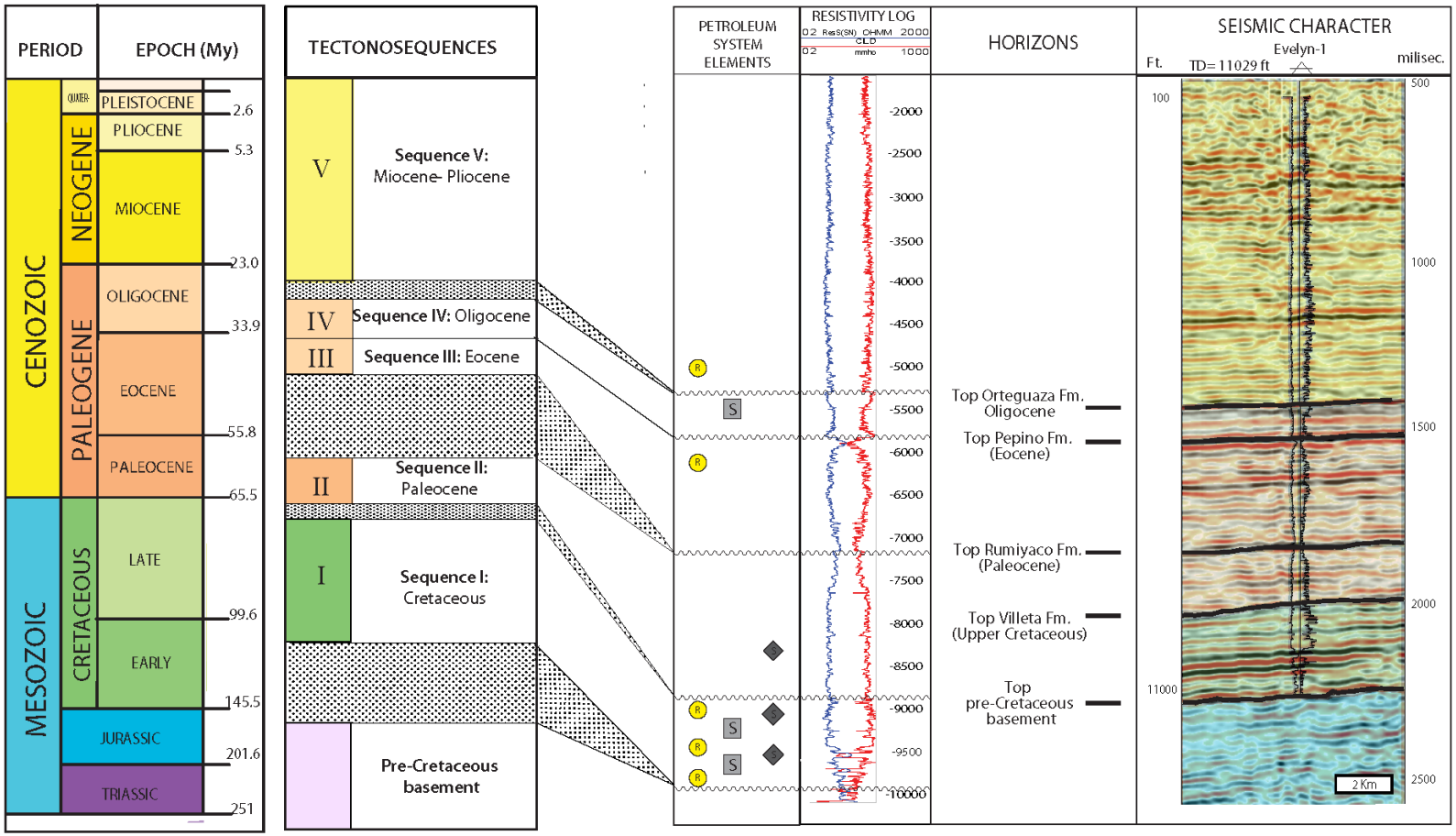

Figure 2.7 Main tectonosequences and petroleum system elements (R= reservoir rock, S = seal rock and s = source rock), seismic expression, gamma ray log, resistivity log with time and depth reference, and interpreted five key horizons in well Evelyn-1. Main tectono secquences identified: Cretaceous, Paleocene, Eocene, Oligocene and Mio-Pliocene.

A.

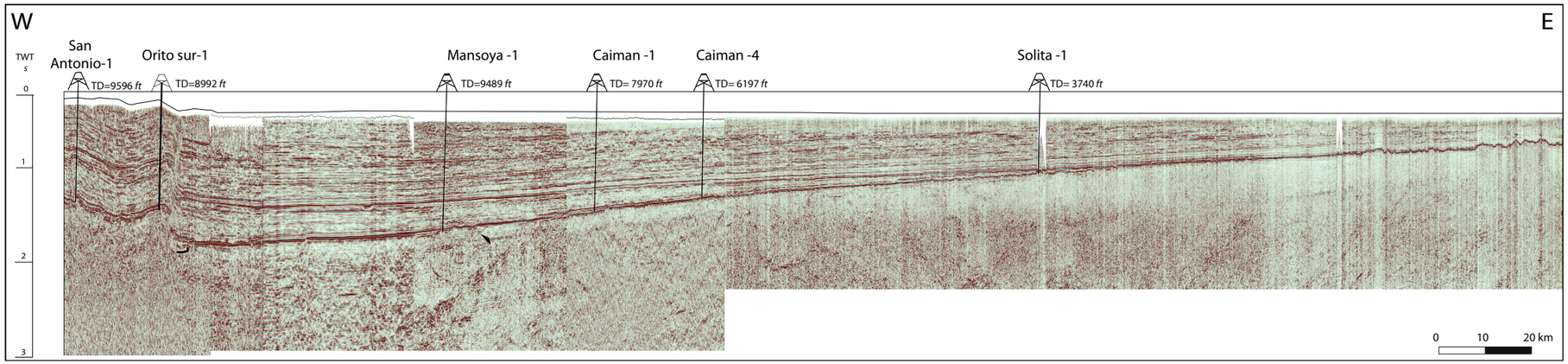

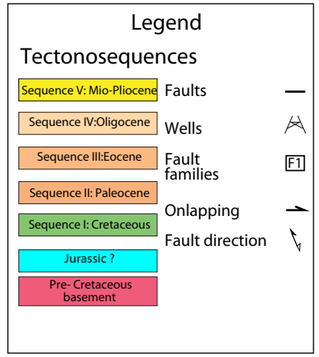

B.

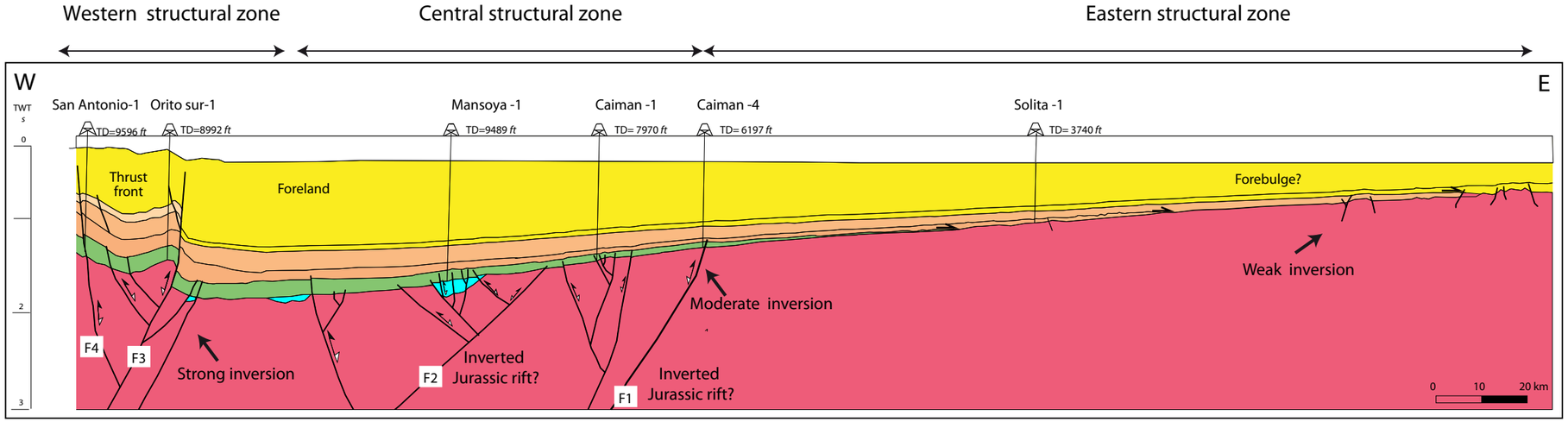

C.

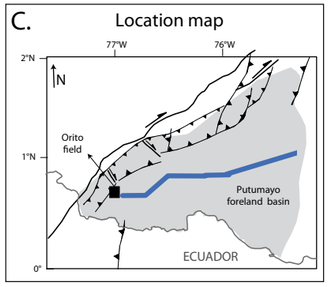

Figure 2.8 Regional 2D seismic profile showing the three main structural zones of the PFB. The seismic lines are migrated but the quality of the lines differs based on the parameters, age, and processin method; A) Un-interpreted regional seismic section in PFB; B) Interpreted regional seismic line. Note that the Pre-Cretaceous mega-sequence is unconformably overlain by upper Mesozoic formations. Older Triassic-Jurassic? normal faults in the present-day foredeep of the basin are reactivated during Cenozoic times. The Pre-Cretaceous basement seismic character is variable given its diversity of metamorphic, igneous and sedimentary rocks; C) Location map of seismic lines in A, B, and C

2.7.2. Structural thrust front

The Eastern Cordillera fold-thrust belt, in the western part of the PFB, is characterized by salients and reentrants in the thrust front (Fig. 2.3). Three seismic profiles from different areas along the thrust-front are shown in Figure 2.9, and include: 1) Orito thrust front area; 2) central thrust front area; and 3) Costayaco thrust front area.

The most southern area is the Orito thrust front which includes steeply dipping faults that are likely to be thick-skinned, and involving basement rocks (Fig. 2.9A). The seismic expression of the Orito thrust front area is represented by parallel and continuous seismic reflections of sequence II through IV that form a gentle anticline, associated with steeply dipping north-northwest-striking faults of fault family 3. This thrust front fault was identified in a 1-Km-wide deformed zone where the reflector continuity is lost. A series of back-thrusts of fault family 4 are also identified as related structures. They show a perceptible displacement at the sequence I top or sequence IV top which implies a Cretaceous and Eocene reactivation (Fig. 2.9A).

The central part of the Western structural zone includes faults of fault family 3 that are northwest-striking and have a low dip. Evidence foothills thrust front are shown in the Unicornio-1 (Fig. 2.9B) where basement rocks and younger sequences have been found at two different depths. Also, the seismic expression of the area displays parallel and relatively low-dipping reflectors related with sequence I to sequence IV which are disrupted by a 0.5 Km of a low-continuity zone that includes both parallel and horizontal reflectors corresponding to the fill of the PFB (Fig. 2.9B).

The Costayaco thrust front has smooth anticlines with northwest-trending fold axes, which are related to steeply-dipping backthrust (Fault family 4). The seismic expression shows clear parallel and continuous reflectors in sequence I to sequence IV, with specific areas where reflectors displacement is perceptible. This displacement is calculated around 150 ms for the back-thrust fault. The thrust front fault (Fault family 3) was defined in the other two southern areas but may be overprinted by Fault family 4 (Fig. 2.9B).

These three structural styles observed on Figure 2.9 imply strong along-strike variations in the amount of shortening at PFB and would be caused by the thick-skinned interaction between oblique convergence of the Nazca Plate, and basement discontinuities related to the Jurassic rift fabric of the basin or the Paleozoic folding fabric.

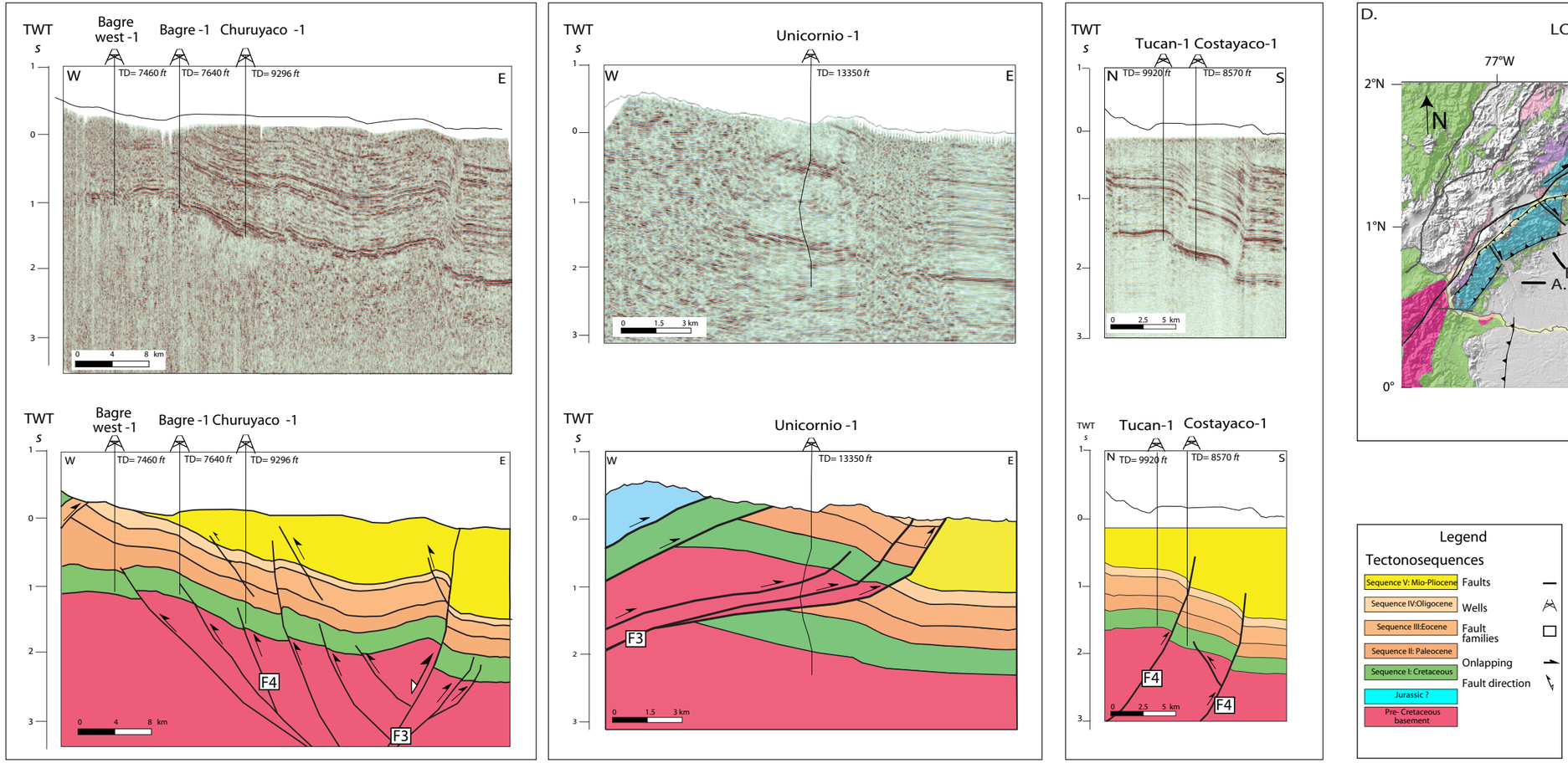

Figure 2.9 Thrust belt front structures at different locations; A) Orito thrust front area; B) Central thrust front area; C) Costayaco thrust front area; D) Location map including the main geological units and surface faults. The seismic lines were all migrated but the quality of the lines differs according to the parameters, age and processing methods.

2.7.3. Tectonosequences

A regional transect (Fig. 2.8), and a well-log cross section in the southern part of the PFB (Fig. 2.10) were integrated with structural maps and time thickness maps in order to illustrate five tectonosequences along with the hydrocarbon potential of the PFB. The structural maps are presented at a scale of 1:1100,000 with a contour interval of 400 ft. (122 m). in depth maps. The well correlation is composed of 8 wells with an east to west orientation. The wells have equal horizontal spacing and a vertical scaling of 1:150 with a stratigraphic datum at the center of the sequence 1 (Cretaceous).

- *Pre-Cretaceous basement*

Basement rocks in the hanging wall of the Eastern Cordillera thrust front (Fig. 2.8) exhume Andean basement, which was deformed by the Rio Negro-Jurena orogeny (1780-1550 Ma) (Cordani et al., 2010). Rocks beneath the PFB sedimentary record have been cored and show a variety of lithologies that include; such as, granitic (Bagre W1), metamorphic facies of schist and gneisses (Solita-1, Mandur-2, Caiman-3) (Ibañez-Mejia et al., 2011), and Triassic-Jurassic vulcanoclastic red-beds and lavas (Gavilan west-1) which, in turn, are filled half grabens related to the same extensional period (Fig. 2.8).

Seismic expression: The seismic expression of the PFB pre-Cretaceous basement varies by area of the PFB. The area corresponding to the West and Central structural zones includes the presence of strong deep reflections lying uncomformably beneath the Mesozoic deposits is observed. The continuity of those reflections is

subject to the acquisition parameters used, and the location of the pre-Cretaceous depocenter within the basin. The deepest and continuous reflections are found in the hanging wall of inverted antithetic normal faults of the families 1, 2 and 3, and are better preserved toward the north to the basin (Fig. 2.8). Strong, west-dipping reflections cutting vertically through seismic data mainly from 1.5 s to >3.0 s are a remarkable feature observed along this sector. Those reflections would represent the weakness zones that were reactivated and inverted during the Cretaceous.

The second area is located along the Eastern structural zone. The top of this igneous-metamorphic red beds unit is identified as the acoustic basement. This basement unit is characterized by a broad high amplitude reflection with relatively good continuity (Fig. 2.8); however the deeper seismic character is defined as chaotic, low-intensity reflections, in which strong dipping reflections are observed that can be interpreted as basement fabric discontinuities or igneous intrusions. Towards the east, marks left by erosive process over the crest of the structure are observed.

Well-log expression: No wells have reached the deepest basement sediments beneath the PFB, except the ones located at the eastern edge of the PFB that drilled tens of ft. into the crystalline section. For those wells, core data was extracted and provide evidence for a basement high in the area (Fig. 2.10).

TWT and depth structural maps: The basement structural depth map corresponds to the Jurassic-Cretaceous unconformity, and is represented in Figure 2.11A. Cenozoic or Cretaceous sediments pinch out against the unconformity surface depending of their position within the basin, which, in turn, represents a hiatus of more than 20 my. North-trending fault systems corresponding to the F1 and F2 fault

families have been mapped at pre-Cretaceous level along the Central structural zone. Those faults represent the inherited structures from the Triassic–Jurassic framework of horsts and grabens produced by regional extension. These N-S trending fault have an average fault throw of 20 ms, and reduce in flow from west to east.

NE-striking right-lateral strike-slip faults developed parallel to the thrust fault system; fault family 3 which occurs along the east margin of the Western structural zone. This transpressional system breaks the basement up into blocks, and gives the observed segmentation of the thrust front. The segmentation is characterized by an along strike variation in the location of the thrust front, which in turn is accompanied by a variable width of the folded area (Fig. 2.11A). The throw fault for this fault system in the southern sector has an average of 150 ms representing more than 600 ft. (183 m). (Fig. 2.8 – 2.9). In the northern sector, the fault system records a fault throw average of 80 ms, equivalent to more than 250 ft. (76 m) of throw.

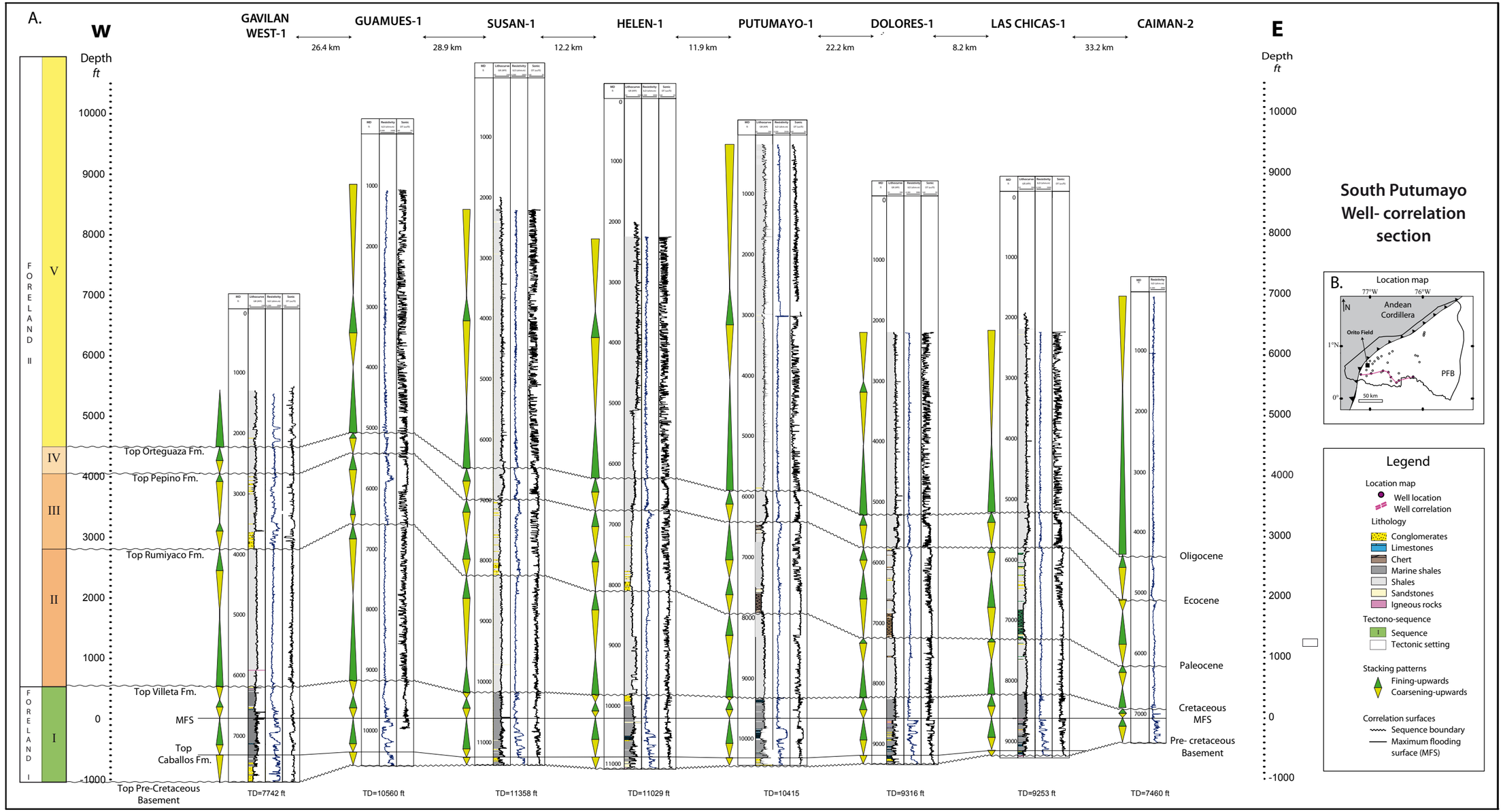

Figure 2.10 A) Well correlation at sequence tops in the PFB. Wedging can be seen in the PFB beginning in the Oligocene. The correlation is based on gamma-ray logs, resistivity, and sonic logs related to the asymmetrical foreland basin; B) Location map of wells.

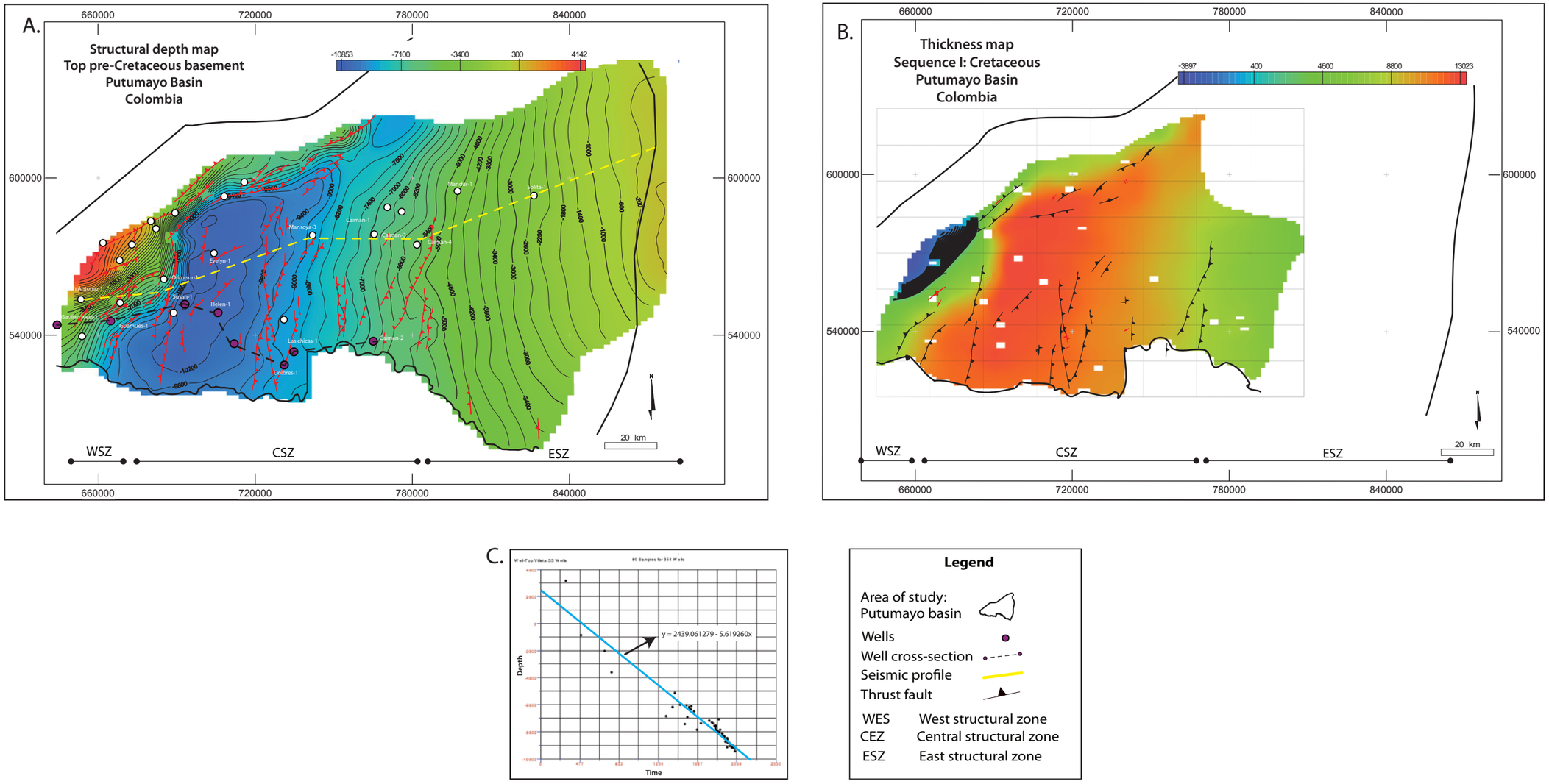

Figure 2.11 A) Pre- Cretaceous basement structural depth maps. Depth is measured in feets with the deeper values being the cooler colors and the shallower values being the warmer colors; B) Thickness map of sequence I (Cretaceous), from top pre-Cretaceous basement to top Cretaceous; C) Time vs. depth graph. Linear regression is applied to identify the relationship between both variables.

- *Sequence I : Cretaceous*

The Cretaceous sequence is divided in two sections. The basal section is composed mainly of fluvial sandstones (Caballos Fm.) deposited during the Early Cretaceous, and representing the most important hydrocarbon reservoir in the foothills area. The upper section includes a transgressive-regressive sequence of a shale-limestone-sandstone intercalations deposited during the Late Cretaceous. Those sandstones form the main reservoir for the foreland basin part of the PFB.

Seismic expression: The lower Cretaceous sequence is characterized at its base by a variable amplitude and low continuity reflector at the Western structural zone (Fig. 2.8). Along the Central structural zone, the basal seismic character is more continuous and uniform with a low impedance contrast. The basal reflectors are characterized by erosional surfaces pinching-out against the basement, which is easy to recognize in the northern lines (Fig. 2.8).

The upper Cretaceous sequence is characterized by a moderate to high amplitude and good continuity along the Western and Central structural zones (Fig. 2.8). Its basal reflectors show good impedance supporting the interpretation as a marker along the basin (Fig. 2.8). Those reflectors are pinching out against the basement towards the east of well Solita-1 (Fig. 2.10). The top reflector of the upper Cretaceous sequence has a low constant impedance and low continuity along the basin.

Well-log expression: the lower Cretaceous section is characterized by barrel-shaped sandstones, limestone and dolomite package intercalations. It has a varying

gross thickness more than 300 ft. to the west at Gavilan West-1 that thins out toward the east or is pinched out against the basement as, is observed in Las Chicas-1 well (Fig. 2.10). A major flooding event, accompanied by an increase of the shale/sand ratio in the middle of the sequence (Fig. 2.10), is observed in the eastern wells (GavilanWest-1 / Guamez-1). In Figure 2.10, thickness and facies changes caused by an irregular paleo-topography are evident at the base of the lower Cretaceous section.

The upper Cretaceous sequence is described as an intercalation of shale, limestone and small packages of sandstones. Based on well stacking pattern analysis, relatively complete third-order cycles with a maximum flooding surface has been identified along the basin within black shales of the upper Cretaceous (Villeta Formation). The sequence reaches its maximum thickness at the Guames-1 well (Fig. 2.10), and thins towards the east where it pinches out against the basement. The GR signature of this sequence is characterized by irregular high readings (>90 API units) in most of the shale sequence section. The sandstone packages generally exhibit a coarsening-upward log signature, with a gross thickness ranging from 40 ft. (12 m) to 10 ft. (3 m) (Fig. 2.10). The limestone packages are characterized by fairly high moderately uniform GR values.

TWT and depth structural maps: The top Cretaceous sequence map (Fig. 2.12A) exhibits the same features described for the Paleozoic map. The deepest section of the sequence is located at the center of the Central structural zone with values close to 9,100 ft. (2774 m). The fault pattern is the same as those described for the Paleozoic structure with the exception of some faults that never reached the top of

the sequence. The gross thickness map displays an 244 m. depocenter with a NE-SW trending region at the central structural zone (Fig. 2.11B).

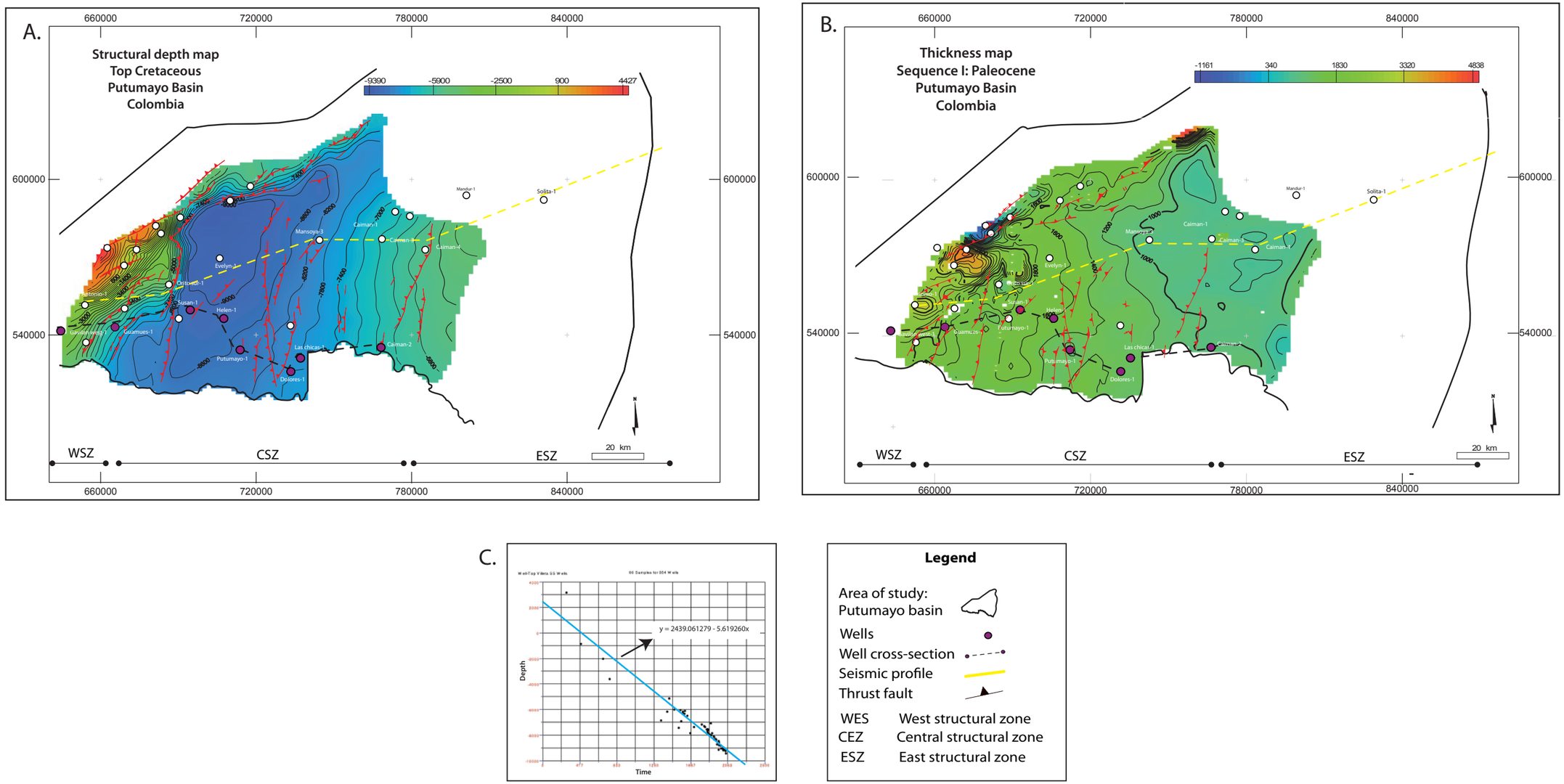

Figure 2.12 A) Top Cretaceous structural depth maps. Depth is measured in feets with the deeper values being the cooler colors and the shallower values being the warmer colors; B) Thickness map of sequence II (Paleocene), from top Cretaceous (Villeta Fm.) to top Paleocene (Rumiyaco Fm.); C) Time vs. depth graph. Linear regression is applied to identify the relationship between both variables.

- *Sequence II : Paleocene*

This sequence is important because it is interpreted as the main regional seal of the PFB due to its shale content (Fig. 2.10). It is approximately 2,300 ft. (700 m). thick in the western part and thinning to zero towards the east (Fig. 2.8-2.10)

Seismic expression: this sequence is characterized by a dull seismic response, moderate continuity, and low impedance contrast along the western zone (Fig. 2.8). The reflectors continuity decrease toward the west and upward, with a low impedance contrast. In the eastern structural zone, the reflectors shows an eastward continuity increase (>40 Km) where they pinch-out against the basement at east of the Solita-1 well (Fig. 2.8).

Well-log expression: The sequence is characterized by two fining upwards cycles with an intermediate coarsening-upwards cycle. The sequence shows high GR readings (>90 API units) except within thin sandstone packages of local continuity with medium GR values along the western and eastern areas of the Central structural zones (Fig. 2.8).

In the eastern area of the Central structural zone and Eastern structural zone, the sequence has medium-high GR readings (>70 API values) with intercalations of conglomerate and sandstones packages in the Dolores-1, and Las Chicas-1 wells (Fig. 2.10). The sequence reaches the maximum thickness at Guamuez-1 well and thinning to the east with a clear wedge shape (Fig. 2.10)

TWT and depth structural maps: The top Paleocene (sequence II) map (Fig. 2.13) exhibits the same features described by the Cretaceous sequence. Its areal

extension has been controlled by erosion of the Eocene unconformity, and the deepest section of the sequence is located parallel to the thrust front, which reaches values of 7,400 ft. (2256 m) in the area of Evelin-1 well (Fig. 2.13A).

The fault pattern is well defined towards the Western structural zone, reflecting a compressive regime, with less fault throw on the fault. Along the Central and Eastern zone, only a few faults reach the sequence top.

The gross thickness map shows a 1,600 ft. (489 m) depocenter, with Northeastern-Southwestern trending, at the central structural zone, implying a thicker zone. The sequence thins to pinch out to the eastern part of the basin (Fig. 2.12B).

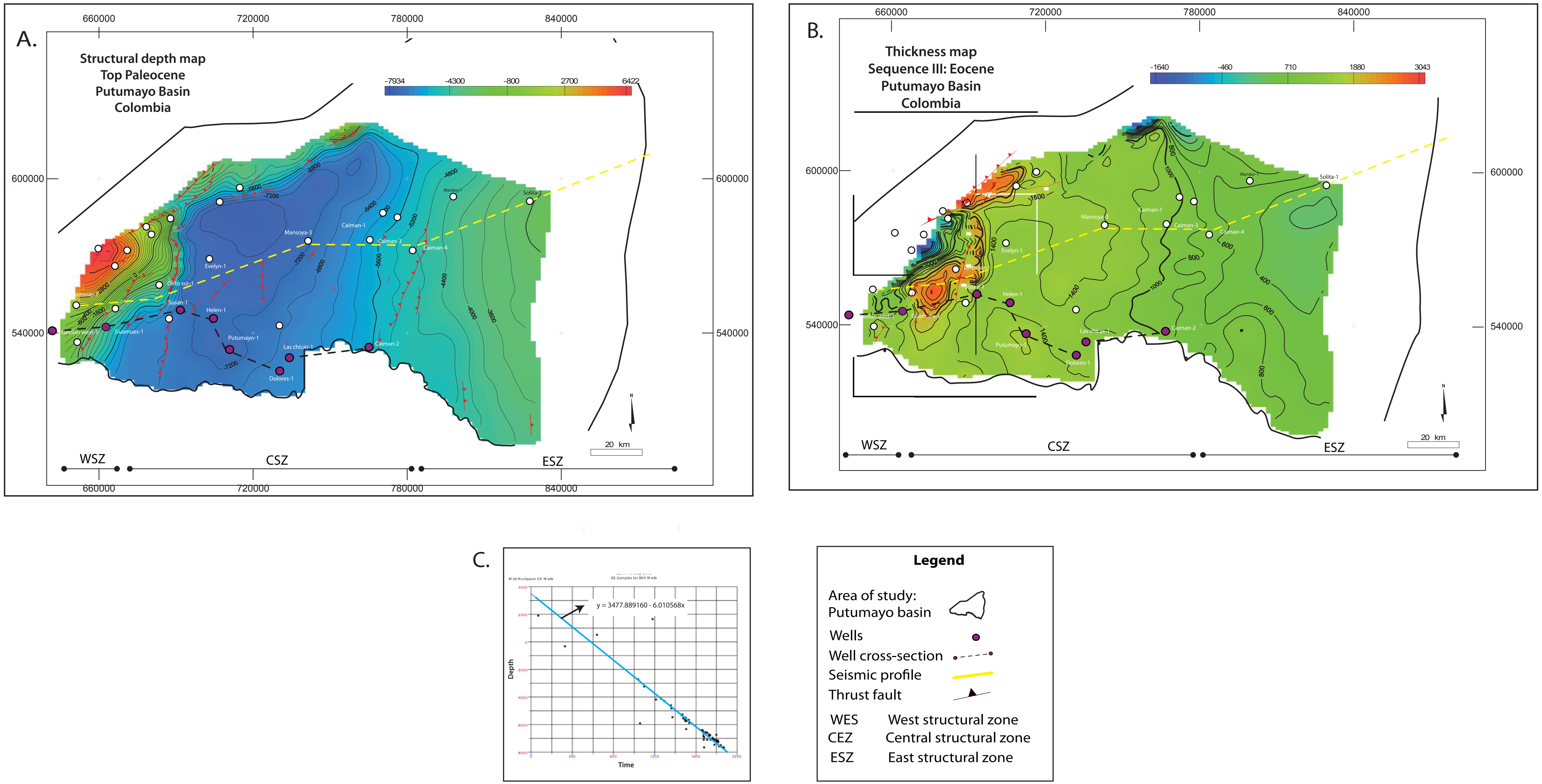

Figure 2.13 A) Top Paleocene structural depth maps. Depth is measured in feets with the deeper values being the cooler colors and the shallower values being the warmer colors; B) Thickness map of sequence III (Eocene), from top Paleocene (Rumiyaco Fm.) to top Eocene (Pepino Fm.); C) Time vs. depth graph. Linear regression is applied to identify the relationship between both variables.

- *Sequence III: Eocene*

The sequence consists of a siltstone package overlain at the base and top by two conglomeratic units.

Seismic expression: The seismic expression of the sequence III is characterized by a high amplitude and lateral continuity (>60 Km) corresponding to the conglomeratic packages along the three structural zones (Fig. 2.8). The continuity, and impedance contrast is reduced for the medium and base levels along the western structural zone. The sequence has a wedge-shape sequence and pinches-out against the basement at > 70 Km east of Solita-1 Well. It has a depocenter located in the west at Mansoya-1 well, and shows incised channels at the top of the sequence in the east, as well as the west area of the central structural zones (Fig. 2.8).

Well-log expression: The sequence is characterized by low GR readings (<60 API units) and high resistivity values for the sandstone and conglomeratic members (Fig. 2.10). These conglomeratic members are present along the three structural zones, and show an increase in the sand/shale radio toward the east, where the correlation of continuous chert packages is possible. The shaly member has serrate, medium to high GR readings (>70 API units) towards the west. In the eastern areas, the shaly member only appears present in the upper section of the sequence as is observed in the Caiman-2 well (Fig. 2.10).

TWT and depth structural maps: Figure 2.14 corresponds to the structure maps of the top of sequence III. It shows, essentially, the same general trend and features described in the deeper sequences. The formation is thinning towards the

east, pinching out against the basement east of the Solita-1 well. The thicker section is located parallel to the thrust front in the center of the basin, reaching values averaging -6000 ft. (-1829 m). In turn, the section shallows towards the north and south of the basin.

The gross thickness map shows a 1400 ft. (426 m). depocenter with NE-SW trending at the central structural zone, suggesting it is thicker zone with progressively reducing values towards the north and south to the basin (Fig. 2.13B).

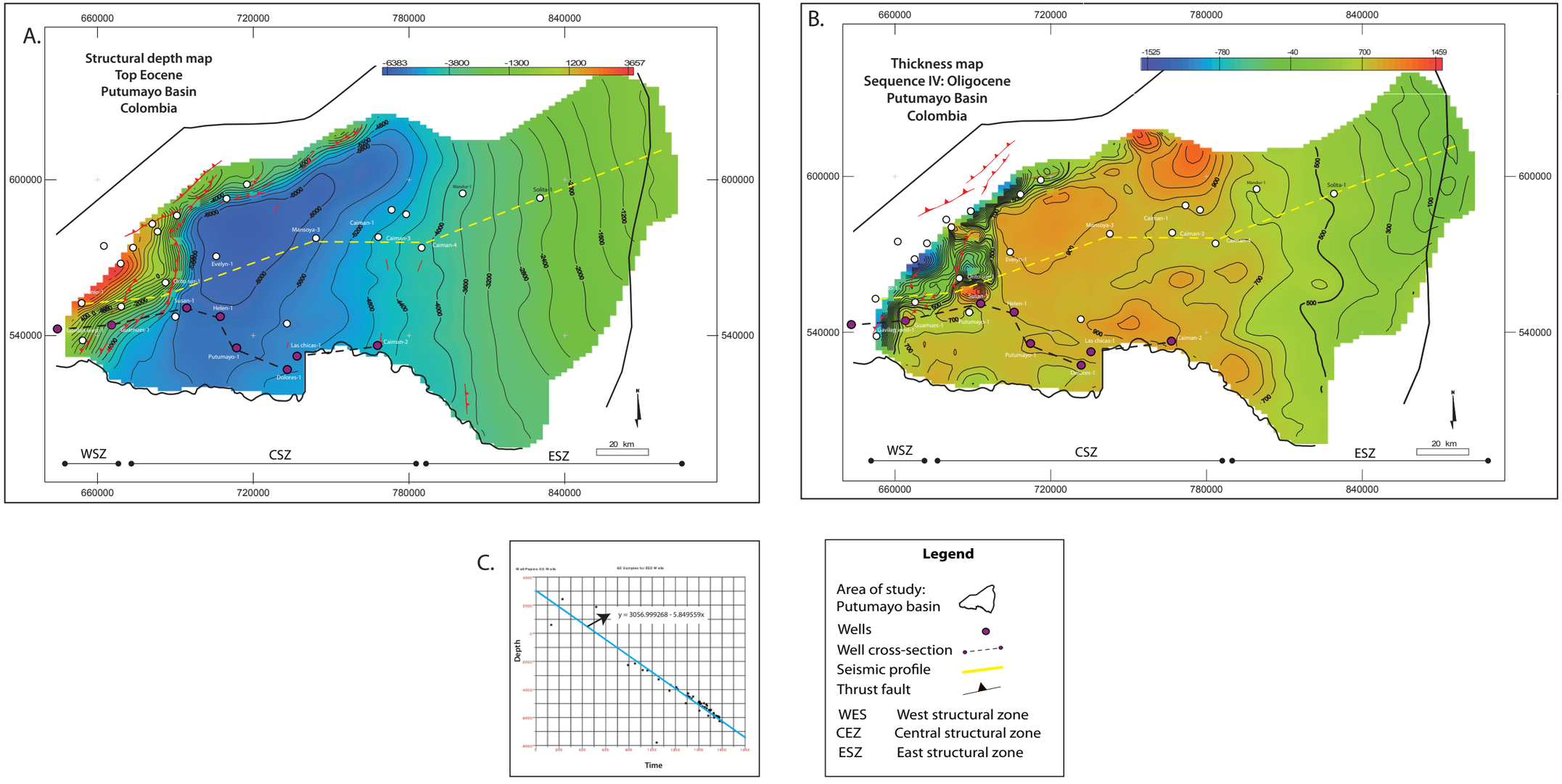

Figure 2.14 A) Top Eocene structural depth maps. Depth is measured in feets with the deeper values being the cooler colors and the shallower values being the shallower values being the warmer colors; B) Thickness map of sequence IV (Oligocene), from top Eocene (Pepino Fm.) to top Oligocene (Orteguaza Fm.); C) Time vs. depth graph. Linear regression is applied to identify the relationship between both variables.

- *Sequence IV: Oligocene*

Seismic expression: This sequence is characterized by a medium to high continuity and intermediate amplitude contrast at the top of the sequence and for the high sand/shale ratio members. The seismic expression for the shaly members has cloudy and low amplitude contrast (Fig. 2.8). The sequence does not express a marked wedge shape but continues toward the east beyond of the basin limits.

Well-log expression: The sequence is characterized by a high GR readings (>70 API values) at top and base, and a low to intermediate GR reading (<70 API values) at the middle (Fig. 2.10). The sequence has a slightly wedge shape with a sand/shale radio decreasing toward the east.

TWT and depth structural maps: Figure 2.15 corresponds to the structure maps of the top of Sequence IV. This shows essentially the same general trend and features described for the previous sequences. The formation is thinning towards the east, overcoming the depositional barrier represented by the Caquetá basement high. The thicker section is located parallel to the thrust front in the center of the basin, reaching values averaging 5000 ft. (1524 m) (Fig. 2.14B).

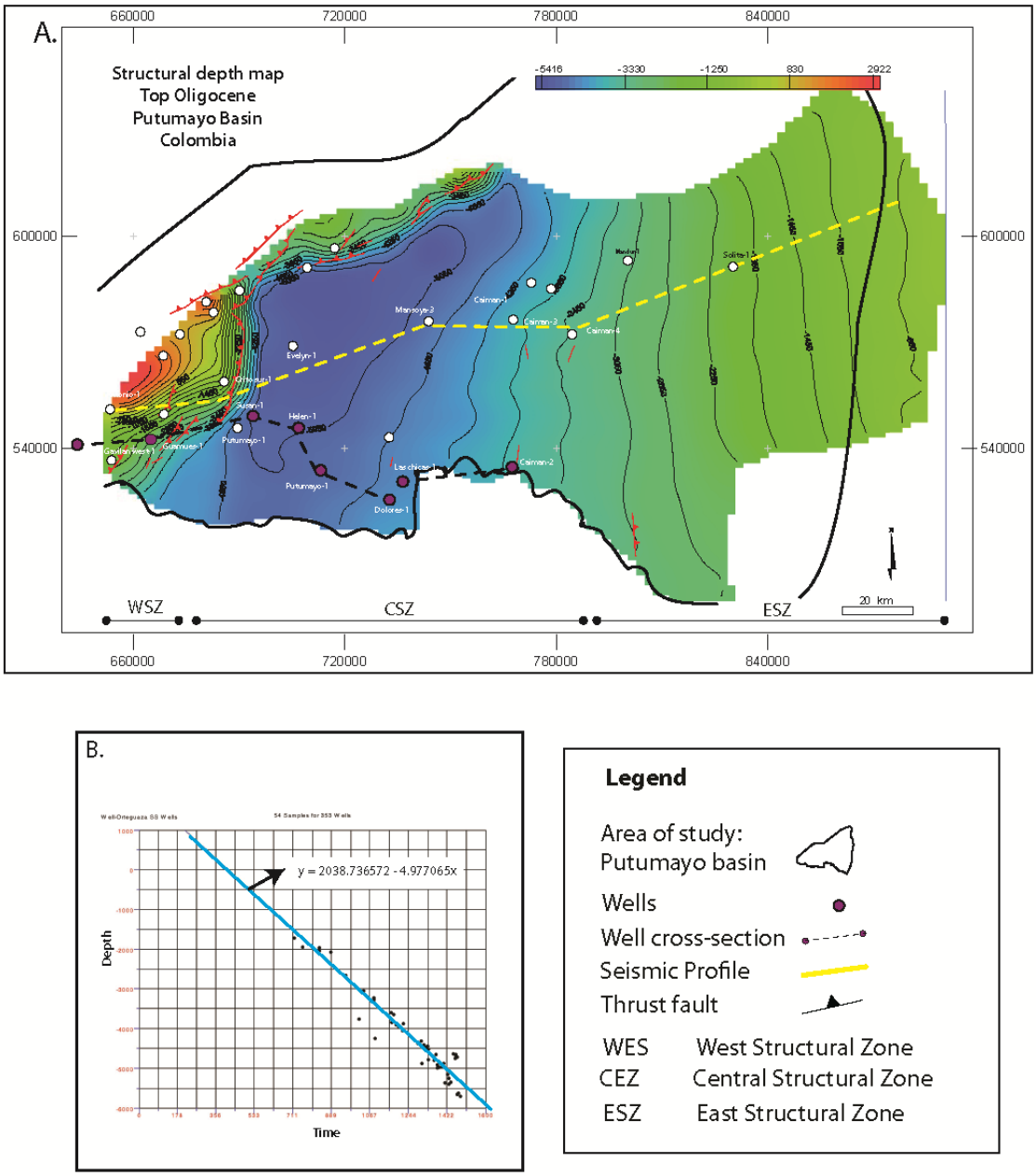

Fig. 2.15 A) Top Oligocene structural depth maps. Depth is measured in ft. with the deeper values being the cooler colors and the shallower values being the shallower values being the warmer colors; B) Time vs. depth graph. Linear regression is applied to identify the relationship between both variables.

2.8. DISCUSSION

2.8.1. Main structural features in PFB

Structures of the PFB were mapped using 3000 Km of seismic data tied to 32 wells (Fig. 2.6). Figure 2.16 summarizes in map view the main structural features, which includes: 1) an interpretation of strike-slip movement for the mountain front area with a restraining bend structure as the most important evidence; 2) a description, and location of the most important pre-Aptian depocenters implying a wide distribution of north-trending rifts; and 3) structural and sedimentary implications of the Caquetá arch for the eastern PFB.

- *Right-lateral strike-slip deformation*

Conjugate NW-SE right-lateral faults, folds, faults, and even oil fields mapped along the northern edge of the PFB show a sense of clockwise drag near the mountain front that is consistent with right-lateral shear driven by the active, right-lateral strike faults mapped by Velandia et al., (2005) along the Algeciras system fault (Fig. 2.16). Together these faults form a continuous, active faulting zone, with 5 Km right-lateral offset, between accreted terrains and more stable and South American plate.

It is located approximately 30 Km to the west of the study area, bounding the southeastern side of the Upper Magdalena basin (UMV) and striking parallel to the mountain range (Fig. 2.16). This system continues to the south into the La Sofia system fault, in Ecuador, which has an average offset between 7.5 to 10.5 Km

(Jimenez, 1997) (Fig. 2.3A). In this Ecuadorian area the Sofia strike-slip fault system has an ESE-WNW trending and north-south transpressional structures (Ego et al., 1996).

Associated northeastern-southwestern major dextral-slip movements in PFB and Oriente basin are a kinematic consequence of the large-scale motion of the obliquely plate convergence showed in the GPS vectors across the plate boundary (Fig. 1.1) in which the lateral displacement of these features contributes to the recent deformation of the Andes in southern Colombia and northern Ecuador.

- *Deformation of the PFB mountain front*

The gravity map shows a prominent gravity low in Putumayo foothills (Fig. 2.4) that can be correlated with the narrow but continuous, inverted Triassic-Jurassic rift interpretation of Sarmiento-Rojas et al., (2006) for the northern Andes. This interpretation proposes that the mountain front fault is a relatively straight inverted normal fault which separates Triassic sedimentary rocks from the undeformed sediments of the PFB (Fig. 2.3A); however thrusts in the Orito and Costayaco front areas are not continuous along the entire mountain front as in the Llanos basin to the northeast (Fig. 2.9). These areas exhibit well-developed anticline structures of deformed Cenozoic rocks (Fig.2.9A) and back thrusts (Fig. 2.9B), associated with the main mountain thrust front (Family 3) located 50 Km east of the general trend (Fig. 2.16).

Structural and seismic data suggest that these Cenozoic structural highs can be interpreted as two restraining bends (Fig. 2.16). Restraining bends are defined as offset rhomboidal areas where bounding strike-slip faults are stepping-over, and in which the slip transfers, between overstepping, and creates separate and sub-parallel strike-slip faults (Wilcox et al., 1981) (Fig. 2.16). In this example, a reactivation of right-lateral shear along Algeciras fault, which is the mountain front fault, at some point during the Pliocene (Velandia et al., 2005) has produced an asperity or restraining bend (Fig. 2.16). Other examples, has been described in the Tranverse Ranges of southern California (Yeats and Berryman, 1987), Hispaniola (Mann et al., 1984) and the southern Alps of New Zealand (Yeats and Berryman, 1987). All these bends, including the PFB restraining bend, result in major deflections (15-30º) of a principal strike-slip fault zone of their associated plate boundary zone and resulting in a crustal shortening an topographic uplift of the area (Mann et al., 1984) (Fig. 2.16).

- *Implication of north-south-striking pre-Aptian structures*

The gravity map in Figure 2.4 shows large north-trending arches along the eastern edge of the PFB and the Oriente basin of Ecuador alternating with thick and narrow through basins, which are likely filled with pre-Aptian sediments, including Jurassic red-beds, and the Paleozoic sequence. The Jurassic volcano-sedimentary sequence was developed in a discontinuous way and preserved in rifts associated with extensional structures of Jurassic age and overlain by the largely undeformed fill of the PFB (Fig. 2.8).

The pre-Aptian basins and structures are oblique to, and truncated by the Andean mountain front rather than being parallel to it, as observed in other areas of the Llanos basin to the northeast (Fig. 2.16). This trend might be controlled by regional lineaments defined seismically in the basement (Fig. 2.8) that could possibly represent planes of metamorphic foliation, pre-existing fractures, or dikes (Rosello et al., 2006). The discontinuities are mainly identified to the west, and could be planes of weakness where normal faults were developed during the Jurassic and reactivated as thrust faults in Cenozoic times (Baby et al., 1997).

North-trending, pre-Aptian structures have important implications for hydrocarbon exploration, not only because they reveal the location of associated pre-Aptian basins that can be interpreted as potential kitchen for the Paleozoic organic shales that might occur in the PFB, but also because represent a risk in hydrocarbon preservation due to its continual reactivation since the Jurassic.

- *Caquetá arch: Eastern boundary*

The Caquetá arch forms a prominent north-trending arch on the gravity map (Fig. 2.4); it also has a seismic expression in an area of chaotic reflection in the eastern part of the PFB (Fig. 2.8). Structurally, this basement high only exhibits a few slightly inverted normal faults near its crest (Fig. 2.8). In addition, steeply dipping reflections are observed, and can be interpreted as basement fabric discontinuities or younger igneous intrusions related with the Guyana shield. This shield outcrops towards the east of the study area (Fig. 1.1) in which, diabase dikes and sills are described in southeastern Venezuela (Briceño and Shucbert, 1990).

The subsurface history of the Caquetá arch can be correlated, towards the south, with the Guárico high in Ecuador (Fig. 2.4). The arch is described as a collection of foreland basement involved uplifts related with the Panama arc subduction during the Late Cretaceous-Paleocene and the continuous subduction of Nazca plate (Jaques, 2003). These structural and timing observations are showing that the Guárico and the Caquetá basement highs are considered as the eastern PFB boundary, which can be interpreted as paleo-geographic barriers, at least from the Paleocene and have prevented hydrocarbons from migrating northwards into the PFB.

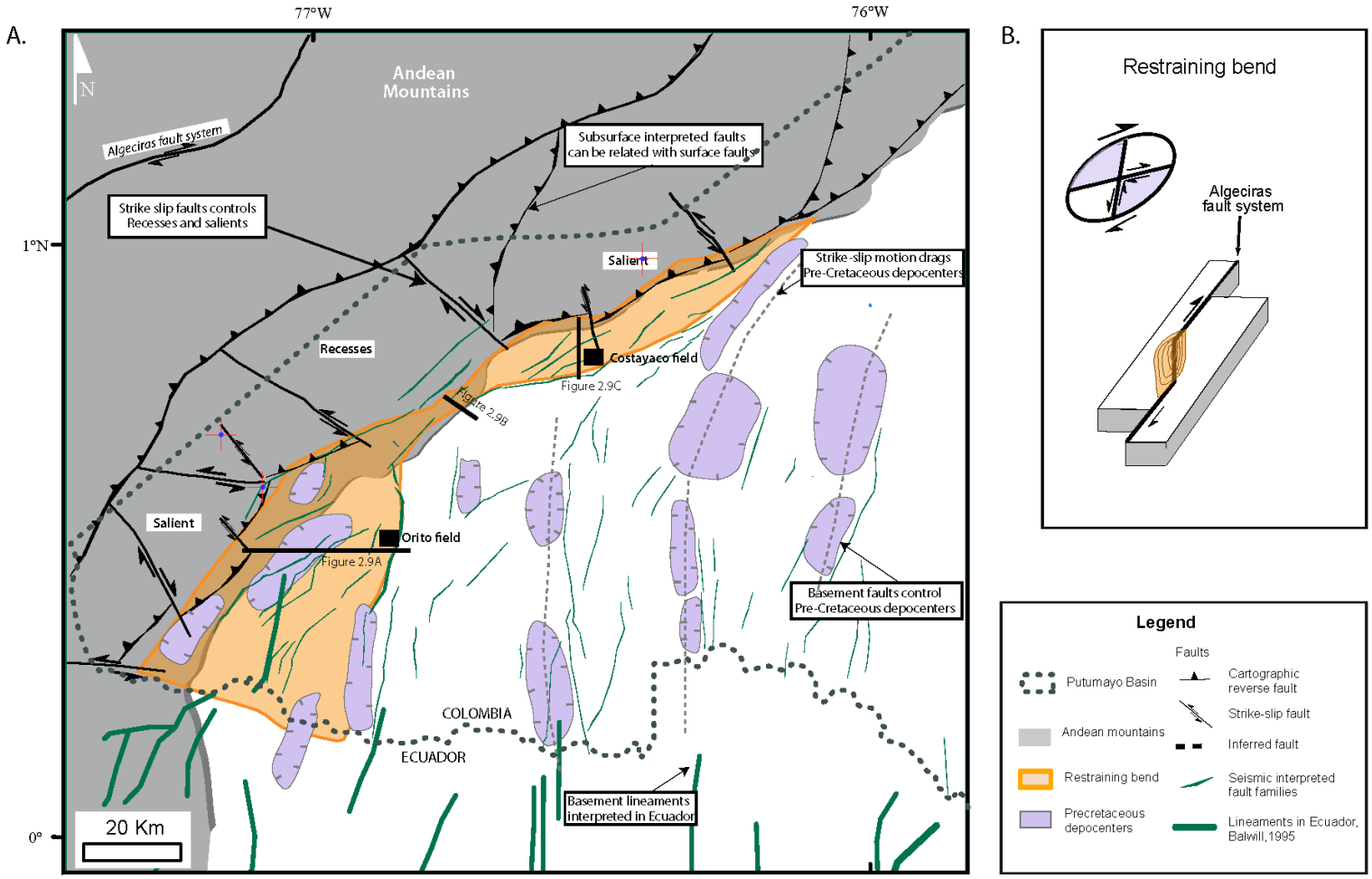

Figure 2.16 A) The mountain front is interpreted as two left-stepping restraining bends produced by right-lateral shear along the mountain front fault (Velandia et al., 2005). The oil fields at the foreland area are mainly controlled by pre-Cretaceous, N-S-striking normal faults (F1) and by inversion structures related to oblique compression during Cenozoic times; B) Restraining bend model and the infinitesimal strain ellipse associated with a strike-slip showing areas of compression and extension (modified from Wilcox et al., 1981)

2.8.2. Summary of basin evolution and paleogeography

Basin evolution and paleogeographic maps are presented based on 2D seismic data, and well-log observations for the PFB. The proposed evolution compromises several sequences since the Early Cretaceous using plate reconstructions as basemaps (Mann et al., 2010), and showing interpreted environments and possible paleo-flow directions (Fig. 2.17). Also, a 1D burial history of two different wells are shown in order to analyze erosion periods and subsidence rates (Fig. 2.19)

These maps and the burial history correspond to geological input information needed for the flexural modeling proposed for the second chapter of this thesis; which includes the distance from the subduction zone, the geographical location of the tectonic load, the interpreted sequence pinch-out and the general geometrical arrangement of the basin for this time.

- *Early Cretaceous (Sequence I)*

Post-rift thermal subsidence in the Eastern Cordillera caused an eastward shift of sedimentation, beyond the margin of the Jura-Triassic rift, into the area of the PFB (Casero et al., 1997) (Fig. 2.18). The stratigraphy consists on shoreface, and fluvial incised valley facies, with marine episodes, onlapping unconformably towards the east to the pre-Cretaceous sedimentary rocks (Fig. 2.10). Based on this, the interpreted paleogeography involves fluvial/ lithoral environments, with the main uplifted area towards the east and the paleo-currents flowing from east to west (Fig. 2. 17A).

- *Upper Cretaceous (Sequence I)*

During the Late Cretaceous the Caquetá high became a paleogeographic barrier, in which the Llanos and the Putumayo basins were differentiated (Casero et al., 1997). This sequence consists in an intercalation of carbonate, shales, and marine sandstones which overlay slightly unconformable on the lower Cretaceous sequence (Fig. 2.10). It is interpreted as shallow marine areas with fluvial incised valleys, carbonate mud shelf and carbonate shelf facies (Fig. 2.17B). These environmental conditions can be related with open marine conditions.

The NS-trending faults (Fault family 4) have been reactivated (Fig. 2.18) associated with uplift of the Palo-Central Cordillera, in which the Putumayo basin together with the Upper Magdalena Valley (UMV) are interpreted as foreland basins (Gomez, 2005). Regional reconstructions show that the paleo-Central Cordillera has been uplifted as the magmatic arc, and the subduction zone occurs at 1000 Km (Mann et al., 2010).

- *Paleocene (Sequence II)*

The Paleocene sequence is represented by interbedded siltstones, and claystones overlying unconformably on the lower Cretaceous sequence (Fig. 2.10). The thickness represents a sedimentary wedge displaying variations from 300 ft. (91 m) in the western part to 50 ft. (15 m) to the east (Fig. 2.13). The shaly facies change towards the north to fluvial sandstones. This sequence does not have continuity

towards the east, and north inferring that the paleo-currents might come from the north (Fig. 2.17). The sediments supply might come from the Caquetá high which is interpreted as a positive zone (Fig. 2.17).

- *Eocene (Sequence III)*

In this period a strong compressional tectonic phase uplifted the Garzón massif in eastern boundary of the Cordillera (Casero et al., 1997). Evidences of sub-horizontal shortening in the Putumayo can be seen in the reactivation of the faults family 3 and fault family 4.

Fluvial conglomerates and sandstones facies are showing a regional transgression followed by intense erosion (Fig. 2.18). The geometrical distribution of these facies (Fig. 2.17), and the presence of chert in well logs (Fig. 2.10) are showing a shift of the sediment supply source from the east to the uplifted the paleo-Eastern cordillera, in which the paleo-currents have been interpreted as flowing from the northeast to the southwest (Fig. 2.17).

- *Oligocene (Sequence IV)*

This sequence consisting of fine-grained rocks associated with continental and transitional facies (Portilla, 1991), lays unconformably over the Eocene sequence. It has a wedge geometrical arrangement showing the foreland basin tectonic setting (Fig. 2.8).

- *Miocene-Pliocene (Sequence V)*

A thick and monotonous sequence of interbedded sandstones and shales was deposited in continental environments (Fig. 2.10). This sequence forms a sedimentary wedge thickening to the west. The accommodation space was a result of the continental crust flexure together with trans-tensional and transpressional event.

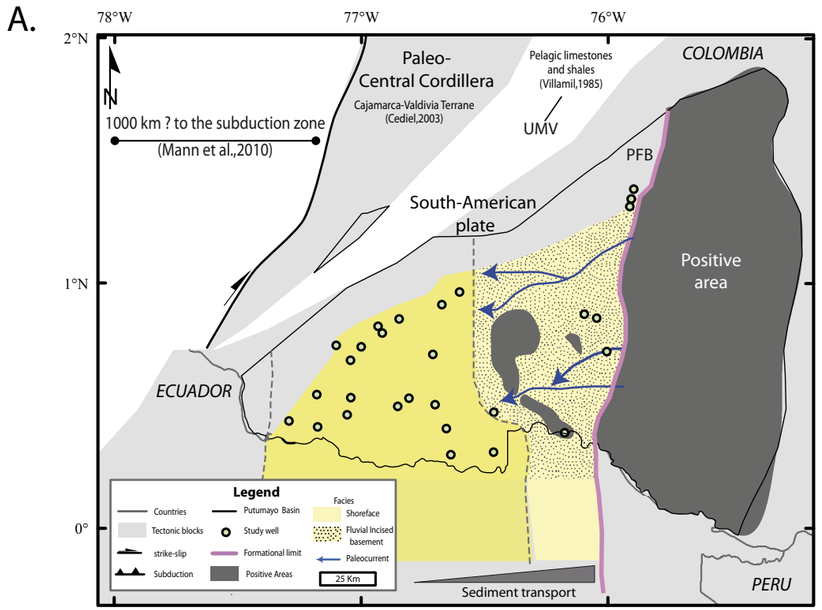

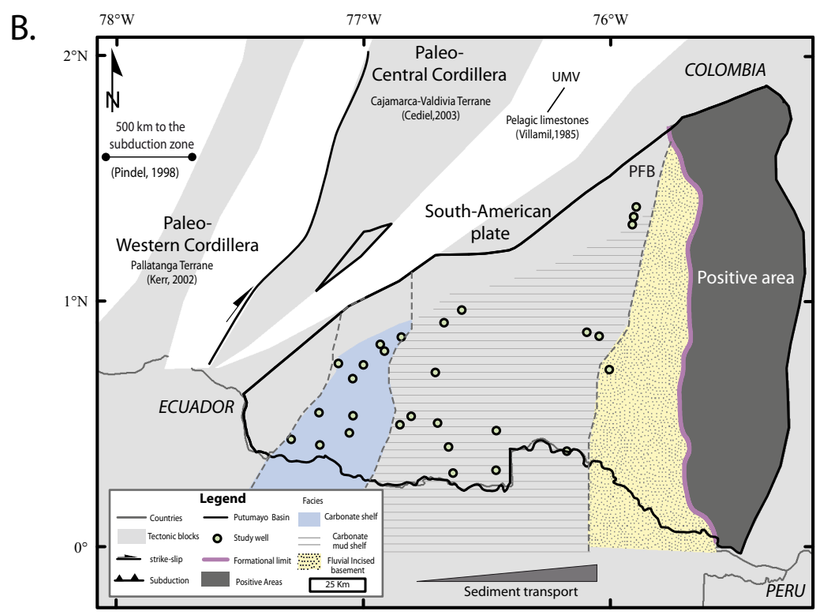

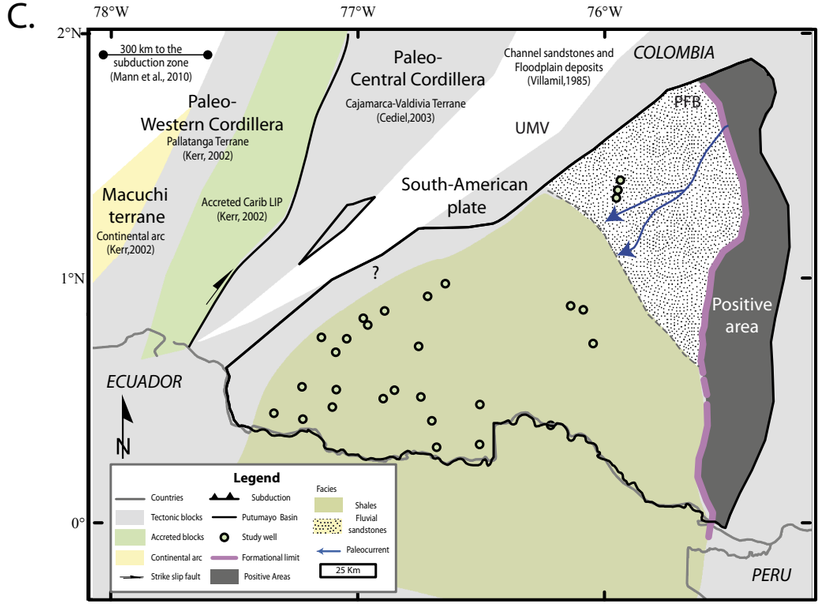

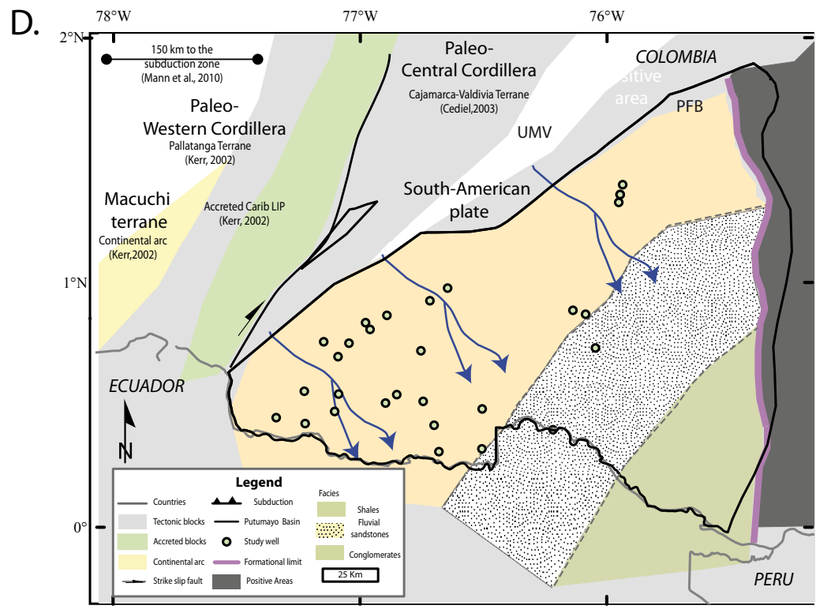

Figure 2.17 Paleogeographic maps overlain on tectonic reconstructions of basement blocks and showing paleo-flow directions, and hinge-lines for: A) Lower Cretaceous (Sequence I); B) Upper Cretaceous (Sequence I); C) Paleocene (Sequence II); D) Eocene (Sequence III). White spaces represent areas of future shortening related with the uplift of the Andes mountain (tectonic reconstructions are taken from Mann et al., 2010). Paleogeography in the Upper Magdalena valley (UMV) is taken from Villamil, (1985)

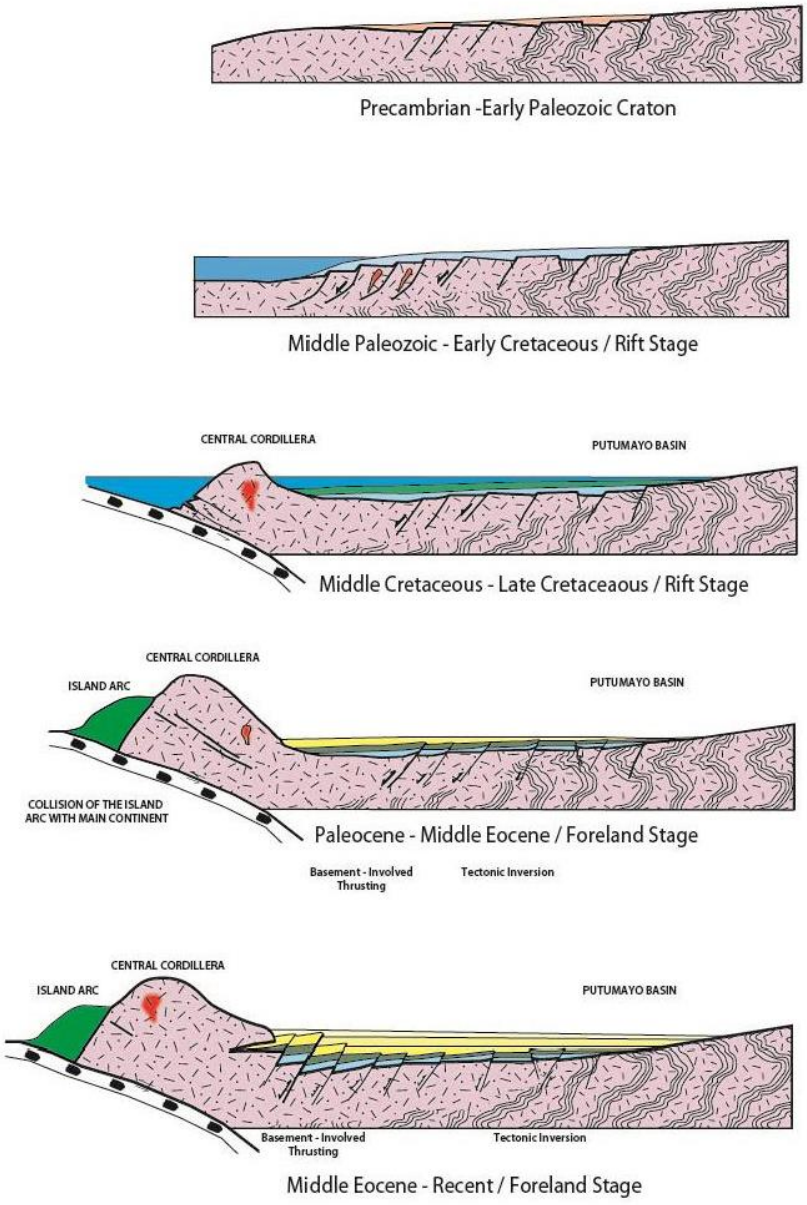

Fig. 2.18 Synthesis of the geological evolution of sedimentary sequences in the Putumayo foreland basin. Each tectonosequence is thought to be developed in a similar process because Nazca plate has been subducting since the Precambrian. Modified from Cordoba et al., (1997).

2.8.3. Implications for hydrocarbon exploration

The cumulative production of 310 MBOE (Million Barrels of Oil Equivalent) to December 2005 (ANH, 2012), the remaining potential of 90 MBOE, and the existing production facilities and the OTA pipeline with a transportation capacity of 90,000 BPD (ANH, 2012) (Fig. 2.1), guarantee the production of new reserves in the foreland Putumayo basin. Furthermore, the high exploration potential makes the PFB economically attractive because these statistics also demonstrates the occurrence of at least one active petroleum systems.

Discoveries in the PFB show three petroleum systems: Villeta-Caballos, Villeta-Villeta, and Villeta-Pepino (Gonçalves et al., 2002); in which the main source rock is restricted to the Late Cretaceous hydrocarbon generation facies and the reservoir rocks are related with the Cretaceous marine and continental sandstones together with the Paleocene fluvial sandstones.

- *Source rock*

The main source rock is the Late Cretaceous sequence, related with intervals at the lower Aptian-Albian, and Cenomanian-Turonian of the Villeta Formation (Gonçalves et al., 2002). The structural map at top of this sequence (Fig. 2.12) is showing that a potential Cretaceous source kitchen would be at the Miocene to present kitchen towards the Eastern Cordillera due to their depths of 10,000 ft. (3048 m), and 3964 m. are near to the typical oil –window depths. Regional source rock richness shows an increase of TOC% values in intervals related with the regional

maximum flooding surface in the Late Cretaceous (Gonçalves et al., 2002) (Fig. 2.10).

- *Reservoir rock*

Main reservoir rocks correspond to massive sandstones of the Cretaceous sequence (Fig. 2.10); which include: the Caballos Formation (Albian-Albian) and the Villeta Formation (Albian-Coniacian). Secondary reservoirs are conglomerates present in the Eocene sequence (the Pepino Formation). Based on the well-log correlation (Fig. 2.10); the Early Cretaceous (the Caballos Formation) reservoirs correspond to sands deposited in fluvial deltaic environment, with average porosity of 12% and a variable sand/shale ratio; while the upper Cretaceous reservoir (the Villeta Formation) correspond to sands associate to a marine platform, and with average porosity of 16%.

- *Trap*

Plays associated with Eastern Cordillera uplift: the hydrocarbon accumulation in the Putumayo foothills are trapped in well-formed asymmetric anticlines associated with Cenozoic low-angle thrust faults (fault family 3) (Fig. 2.19). The main oil field associated with this play concept is the Orito field. The structural deformation, and the trap quality of the play associated with the Eastern Cordillera uplift decreases its prospectivity towards the west.

Plays associated with inverted rift structures: the rifts are relatively minor features with fault throws that are less than 50 ms two way time; however, small asymmetrical folds of the upper Cretaceous-Paleocene rocks are formed above these faults (fault family 2). Oil fields as Nancy-Burdine, and Acae-San Miguel in the Central structural zone are examples of accumulations in small folds and basement faults. These structures are relatively similar and might be correlated to the major scale of the inverted rifts in the Ecuador. The map view in Fig. 2.19 shows that some inverted rift trends are laterally extensive and can be traced from the northern Ecuador into the central part of the PFB

Plays associated with stratigraphic traps: the play concept in the Eastern structural zone is related with the onlapping of the Cretaceous since the Oligocene sequences towards the Caquetá basement high. This change in lateral facies between the porous sedimentary rocks, and the impermeable basement can create stratigraphic traps (Fig. 2.19). The quality of reservoirs in the Cretaceous sequence might be good towards the east because of the fluvial incised valleys interpreted in the paleogeography map; however the Cenozoic sequences are expected to have a great variability due to the change of source rock to the west (Fig. 2.19).

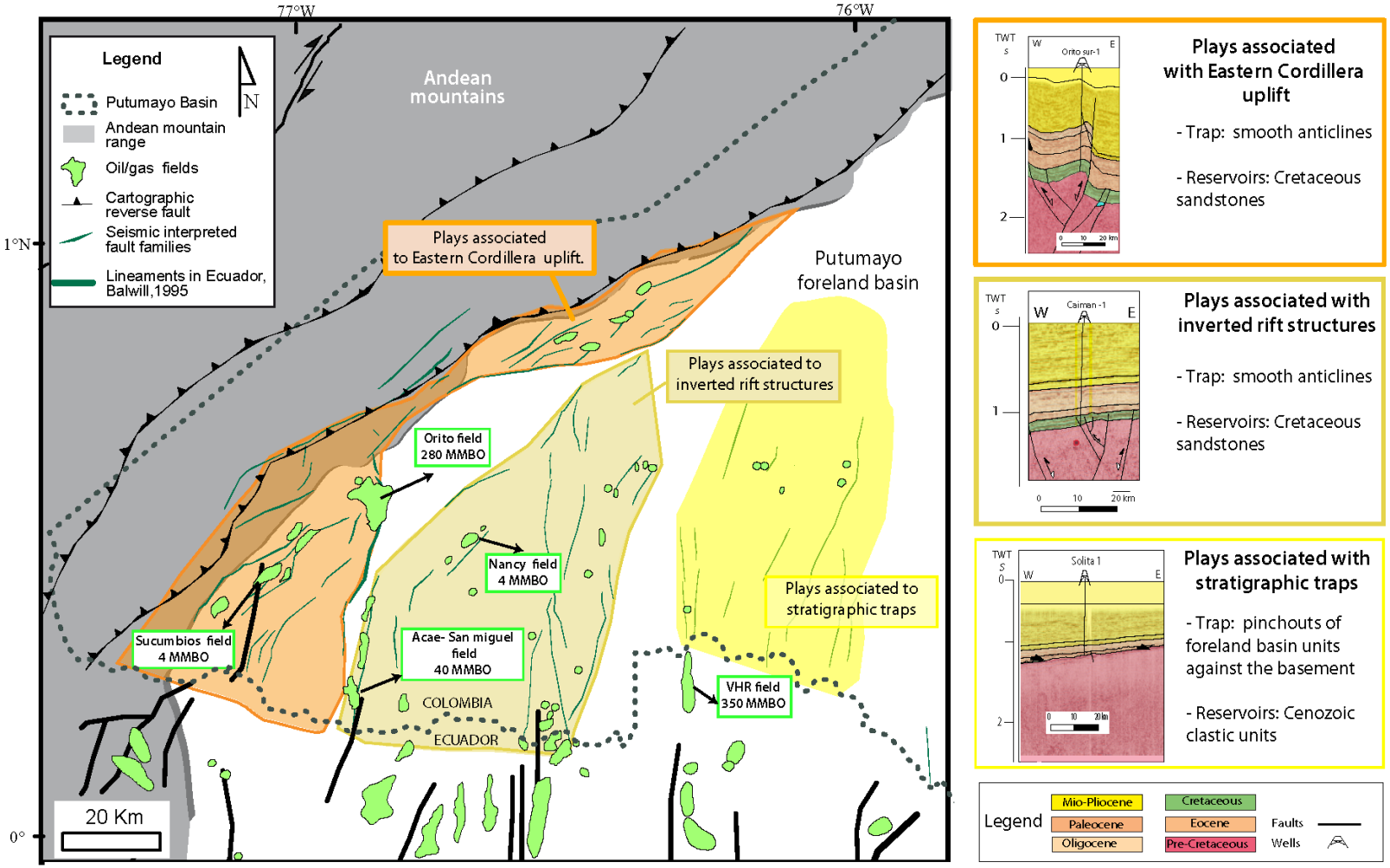

Figure 2.19 Play concept map for the PFB; A) map view of the Play concepts showing the major trap structures; B) plays associated with Eastern Cordillera uplift; C) plays associated with inverted rift structures; D) plays associated with stratigraphic traps.

2.9. CONCLUSION

The geodynamics and tectonosequences of the PFB were identified based on seismic interpretation and well correlation. They reveal that the present-day configuration of the PFB is the result of different deformational stages. Four major deformation events can be recognized in the PFB: 1) The regional pre-Cretaceous north-south trending structures related to the Caquetá arch; 2) the structural features of the north-east, south-west Mesozoic extension; 3) structures produced by the Andean convergence during the Late Cretaceous to the present that tend to be imposed progressively toward the foreland developing inversions on the pre-existent normal faults; and 4) the Cenozoic right-strike-slip motion.

Each particular structural feature characterized a structural zone. The Western structural zone is typified by imbricate over thrust, and east-dipping back-thrust faults. The Central structural zone identified by buried the pre–Cenozoic rift structures and the Eastern structural zone is a relatively undeformed area delimited by the Caquetá arch.

The interpreted tectonosequences, divided by regional unconformities are: the Cretaceous (sequence I), the Paleocene (sequence II), the Eocene (sequence III) the Oligocene (sequence IV), and the Miocene (sequence V). The sequence I (Cretaceous) consists of marine sediments deposited during a general transgressive period. The uplift of the central Cordillera and the Western Cordillera formed the Cretaceous-Paleocene foreland basin in which the sequence II is deposited in the distal areas of the basin. The sequence III (Eocene) registers a second phase of foreland basin due to the uplift of the

Eastern Cordillera, showing a main change in the source of sediments to the Andes; then during the Oligocene, the thick sequence IV is showing an overfilled foreland basin. The sequence V is showing the last pulse of the Andean orogeny in which the Orito trap probably formed.

CHAPTER 3: 3D FLEXURAL MODELING OF THE PUTUMAYO FORELAND BASIN

3. 3D FLEXURAL MODELING OF THE PUTUMAYO FORELAND BASIN

3.1. INTRODUCTION

A foreland basin can be modeled as a result of lithospheric bending resulting from the combined effect of tectonic, and sedimentary loads (Cardozo and Jordan, 2001). The Oriente-Putumayo-Llanos foreland basin, located in Colombia, is one example of a foreland basin formed by flexure of the lithosphere beneath the thrusted load of the Andean Mountains that flanks the basins on their western edge (Fig. 3.1).

The scope of this chapter is to identifying and model the lithospheric flexural deflection at Putumayo basin in southern Colombia, and to determine the best possible modeling parameters to fit the overall structure and geologic history of the basin that was described in Chapter 2 of this thesis. The model will show the location and geometry of the forebulge through time which I can compare with observations from Chapter 2.

I used a forward 3D flexural model based on a Matlab code (Cardozo, 2009) to quantify the flexure of the lithosphere caused by the load of the Andean Mountains and sediment that was deposited in or near the basin. Key parameters in the model needed to quantify the amount of deflection of the lithosphere that need to be constrained as much as possible by observations of the actual PFB include: basinal area, flexural rigidity of the lithosphere, Young's modulus, Poisson's Ratio, load of sedimentary fill, mesh size, effective elastic thickness of the lithosphere, basement

geometry, rigidity value, and composition and distribution of the tectonic load. The geometry of the PFB sedimentary infill is dependent not only on the tectonic evolution of the basin but also on the rheological behavior of the lithosphere during the flexure (Cardozo, 2009).

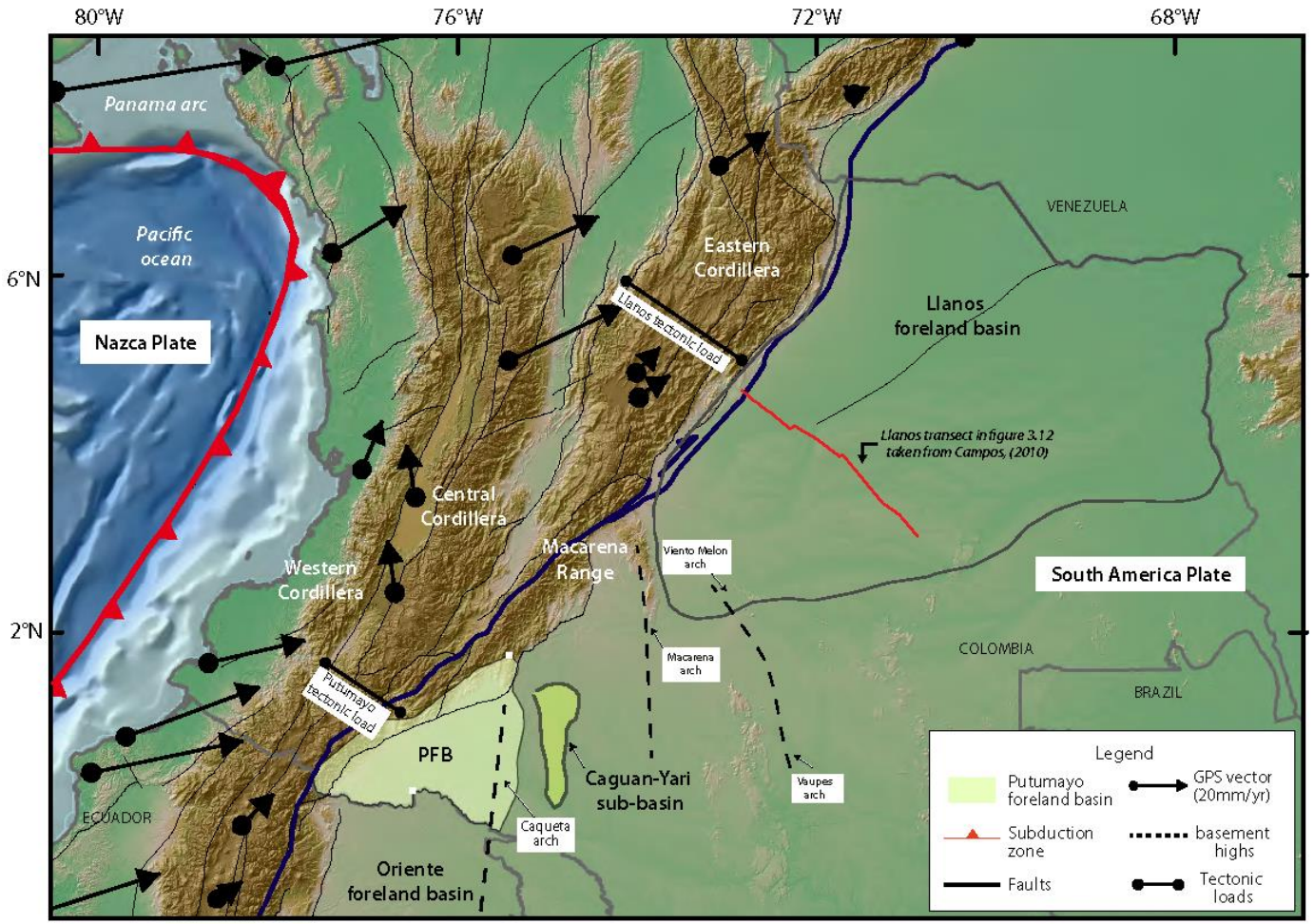

Figure 3.1 Map of northern South America showing the location of the Oriente-Putumayo-Llanos foreland basins of Colombia and major arches and basement highs separating these basins. GPS data is from Trenkamp et al. (2002).

3.2. PREVIOUS WORKS

Several previous basin modeling studies have estimated the effective elastic thickness (Te) of foreland basins along the Andean Mountains of the western South America using gravity and topographic data, including Stewart and Watts (1997), Tassara et al. (2007) and Perez-Gussinye et al. (2007). Based on these previous studies, calculated effective thickness values ranging from 5 Km, for the Andes, to 85 Km for the cratonic area of the South American plate. The calculated (Te) values are important for the analysis of long-term tectonic process, for understanding the thermo-mechanical properties of the lithosphere (Watts and Burov, 2003), and for modeling the orogenic and surface processes in foreland basins (Garcia-Castellanos, 2002).

Previous calculations of the flexure of the lithosphere of the PFB and Llanos basins in Colombia have been carried out by Cardozo (1997), Campos (2010), Sarmiento-Rojas (2001), Londono (2004), and Londono et al. (2012). Cardozo, (1997) developed a finite element model using orogenic and sedimentary load information from geologic and paleogeographic observations, and was able to calculate a T_e value of 70 Km for the Llanos foreland basin. Sarmiento-Rojas (2001) used a finite difference technique to model flexural effects of the Cordillera Oriental in the Late Magdalena and Llanos basin for the Mesozoic, Paleocene, and Neogene times.

Studies by Londono (2004), and Londono et al. (2012) used 2D flexural modeling using chronostratigraphic units defined for the PFB. Changes in the lithospheric strength and in the distribution of the supra-crustal load through

Cenozoic times produced an average value of T_e of 35 Km under PFB where the flexure and subsidence is caused mainly by sedimentary load. Campos (2011) determined changes in the loading magnitude of the Cenozoic Llanos foreland basin using six chronostratigraphic units he defined from interpretations of seismic data and assuming that the basins deformed as a continuous beam of variable elastic thickness.

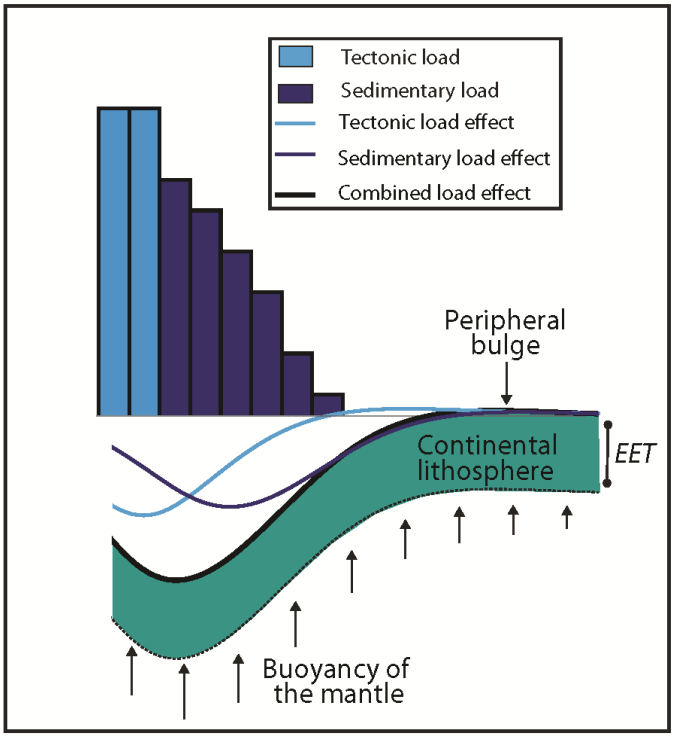

Figure 3.2 Model of the deflection of a continuous plate under a distributed sedimentary load from foreland basin sediments and tectonic load from an orogenic belt (modified from Allen and Allen, 2005). The arrows show the buoyancy effect of the lower mantle beneath the lithosphere

3.3. FLEXURAL MODEL AND SENSITIVITY PARAMETERS

An important characteristic of the lithosphere is its capacity to acquire strength as it is cooling. This characteristic has significant implications in the behavior of the lithosphere when is subjected to stress. A cooler and stronger lithosphere is important to understand its capacity to support the loads of sedimentary basins or large igneous provinces and influence its style of deformation at convergent plate boundaries when it is flexed or bent (Turcotte and Schubert, 2002) (Fig. 3.2)

The bending of the plate depends of the elastic properties of the lithosphere and is expressed by the general equation for the defection of the plate defined as;

$$D\frac{d^4w}{dx^4} + P\frac{d^2w}{dx^2} = V(x) \qquad \textit{Equation 1.}$$

with w = w(x) the deflection, i.e., the vertical displacement of the plate, D the flexural rigidity, and P a horizontal force. (Allen and Allen, 2005)

Flexural rigidity D, where large values of D corresponds a stiff plate, depends on elastic parameters as well as the thickness of the plate (*Equation 2*):

$$D = \frac{Eh^3}{12(1-\nu^2)} \qquad \textit{Equation 2.}$$

with E the Young's modulus, ν the Poisson's ratio, and h the elastic thickness. From *equation 2* and making some assumptions and calculations, it is possible to define the effective thickness of the plate.

The concept of effective elastic thickness (T_e) or flexural rigidity is defined as the strong part of the lithosphere that is able to support a load and where both the brittle and ductile layers of the lithosphere contribute to its strength. The T_e lower limit of is identified along the 600ºC isotherm along the oceanic lithosphere (Burov et al., 1995), but it is not well defined for continental crust due to the non-geological or physical correlation (Burov et al., 1995). The behavior of the lithosphere can by modeled as the deflection of a thin elastic infinite plate over and inviscid fluid (Turcotte and Schubert, 2002); which is equivalent to the mantle restoration force that returns the deflected lithosphere to its original configuration (Turcotte and Schubert, 2002).

The T_e value depends of the thermal gradient, composition, as well as the geological evolution, and tectonic configuration of the area. Relatively weak zones that had experienced different tectonic settings and/or magmatic activity, and major sutures are characterized by the occurrence of relatively lower T_e values. On the other hand, stable cratonic provinces are strong enough to inhibit tectonism, support sedimentary load exhibit high T_e values (Perez-Gussinye et al. 2007). It is agreed by the different authors that have published T_e value estimations for South America (Stewart &Watts 1997, Tassara et al. 2007, Perez-Gussinye et al. 2007, Sacek et al. 2009) a value increase from the Andean margin toward the interior of the plate.

The accommodation space and the stratigraphy of the sedimentary record in a foreland basin are closely linked to several factors including: 1) strength of the flexed plate (Te); 2) thrust system migration; and 3) geometry and distribution of the load (erosion and deposition) (DeCelles and Giles, 1996). The recognition of the four-component in the modern foreland basin system may hold the key to reconstructing the time-space structural development on the foreland basin systems (Horton and DeCelles, 1997) as well as their implications in the petroleum system. An additional factor that controls the subsidence in the basin is viscous coupling between the base of the continental plate and downward circulating mantle-wedge material that is entrained by the subducting slab.

The flexural response for a broken plate is observed in the figure 3.2. The deflection caused by the tectonic load is expected to be close to the load due its geometry and structure. The shortening and thickening of the wedge, or extension and forward propagation of the wedge affected the shape deflection of the lithosphere. The deflection caused by sedimentary load is expected to be localized far to the load with a height for the forebulge with less magnitude that produced by the tectonic load.

3.4. CASE STUDY: PUTUMAYO FORELAND BASIN

The Putumayo foreland basin (PFB) is located in the southern part of Colombia, South America resulting from the interaction between the Nazca plate and the South American plate (Fig. 3.1). It is bounded on the west by the Colombian Andes, a Cenozoic fold and thrust belt of Mesozoic sedimentary rocks. Towards the east, the Guyana shield and the Caquetá arch, together with north-south-trending basement arch series, separates the Caquetá basement arch divides the PFB from Caguán-Yarí sub-basin and the Llanos basin (Fig. 3.1).

- *Tectonic load: Colombian Andes*

The Colombian Andes, identified as the main tectonic load of the area, is generally divided in three Cordilleras: the Western Cordillera, the Central Cordillera, and the Eastern Cordillera; however towards the south these three branches are located close enough that are simply identified as the Andean mountains (Fig. 3.1). According to the GPS vectors measurements by Trenkamp et al. (2002) this area shows a transpressive component which is clearly identified with a series of right-strike-slip faults in the PFB thrust front (Fig. 3.1).

- *Foreland basin geometrical arrangement*

In general, the foreland basins consist of four discrete zones, referred to as: the wedge-top, foredeep, forebulge, and back-bulge (DeCelles and Giles, 1996) (Fig.

3.3). In the PFB the wedge-top corresponds to the Orito thrust front area which compromises an area of 20 Km affected by active thrusting, and the right-lateral-strike-slip movements. This tectonic regime implies a significant displacement of the thrust front location through the basin.

The foredeep corresponds in the PFB to the Central structural zone. It is identified as the deepest zone of the basin reaching at least 11000 ft. of sedimentary column, next to the Andean mountains, onlapping and thinning-out to zero towards the forebulge area which corresponds to the Eastern structural zone. It is expected to found the forebulge in the Caquetá structural high, and the back-bulge might correspond to the Caguán-Yarí sub-basin which onlaps to the Guyana shield (Fig. 3.3).

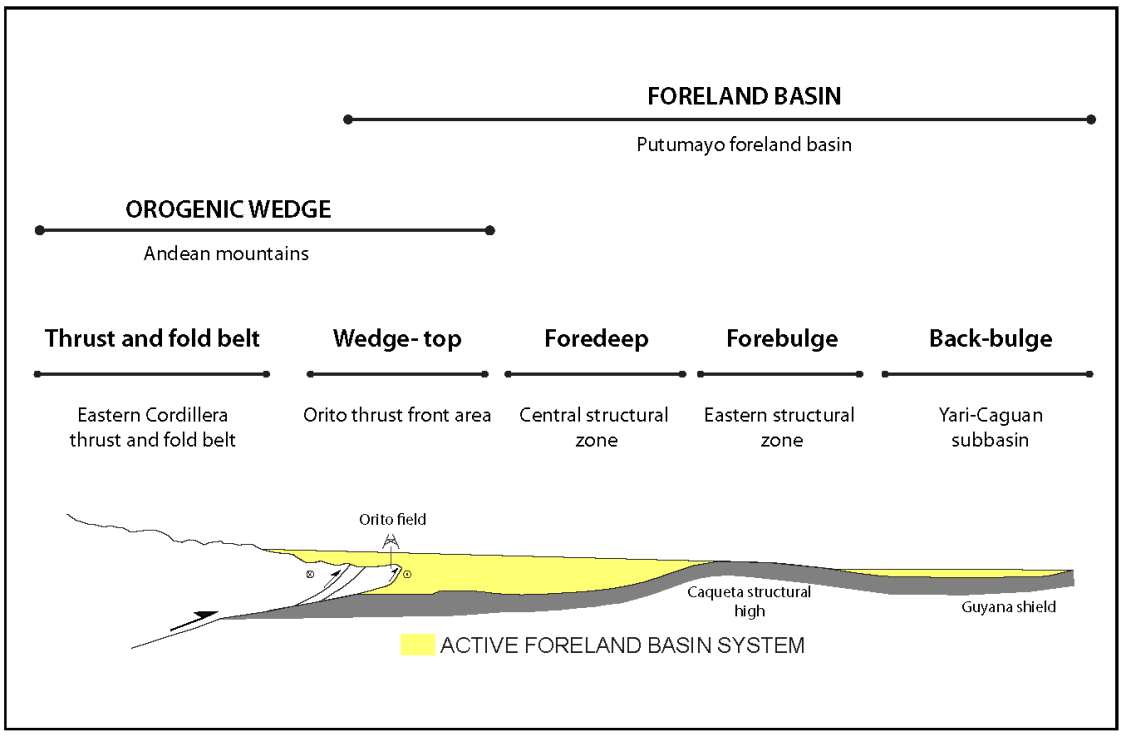

Fig. 3.3: Squematic cross-section of the foreland basin systems and fold and fold-thrust belt showing the wedge-top, foredeep, forebulge, and back-bulge depozones shown at approximately true scale (DeCelles and Giles, 1996)

3.5. METHODOLOGY

We use as input, the depth maps of the studied sequences obtained from the 2D seismic interpretation, plate reconstruction, the tectonic evolution of Caribbean (Mann et al., 2010), regional and local studies performed in PFB (Jimenez, 2007; Portilla, 2001; Pindell, 1998), estimated values of elastic thickness proposed for PFB (Londono, 2012; Tassara et al., 2007), anomaly Bouguer GEOSAT gravity map, and well information to predict sedimentary thicknesses, and basin geometries.

The FLEX3D Matlab code from Cardozo (2009) was used to model the flexural deflection of the lithosphere on PFB. This Matlab code is based on the equation 3.83 of Ventsel and Krauthammer (2001) for thin plates, and shells solution by centered finite differences. The input for the model is: *.txt* files for the modeled loads and T_e values lithosphere values for the study area. In order to establish the T_e value for the lithosphere under PFB since Cretaceous to Oligocene, and present day, two different models setup were carried out.

3.5.1. Flexure of the plate for present day

The currently morphological and geological configuration of the PFB, and the adjacent Eastern cordillera were modeled with the objective to estimate the T_e value for the lithosphere under the PFB, and predict their forebulge location.

Based in previous regional effective elastic thickness (T_e) values range obtained by Londono et al. (2012), five scenarios of constant T_e for different values as 15, 20, 25, 30, 35 Km were evaluated for PFB. In addition, a variable T_e values configuration proposed by Tassara et al. (2007) was tested.

- *Definition of main input modeling*

Load: The Andean mountain range is identified as the tectonic load for the PFB at present day. The topography values of the Cordillera located at west to the study area were obtained from the digital elevation model of Colombia (DEM). This tectonic load was modeled as rectangular blocks of average density and high (Table 3.1). The approximate load location, and density are taken as an average value from the geologic and gravity map while the high of the blocks are read from topographic contours (Fig. 3.4).

With a transverse longitude of 64 Km and an orientation of North-northwestern, the Eastern Cordillera makes width to the north. It is compose by a Precambrian and Paleozoic basement, covered by a thin deformed sequence of Mesozoic and Cenozoic sedimentary rocks due to the Andean tectonic phase (10.5 Ma) (Taboada et al., 2000)

The western limit of the Cordillera is given by the Romeral fault system which interpreted as a paleo-suture and marks the edge of the continental crust (Fig. 3.4). The eastern limit is given by compositional rock and topographic changes, moving from steep to flat topography.

Plate configuration: The T_e values, used for the 360,000 Km^2 modeled lithospheric plate varies from 15 to 35 km, with a step increment of five km. The geo-mechanical constants used in the different modeled plates are described in the Table 3.1

Once the deflection is obtained, the surface and corresponding different profiles were extracted and mapped in convenient way that allowed compare those with the basement depth map profile obtained from seismic interpretation. The selected profiles are distributed along the basin perpendicularly to the thrust front compression trend, and compared against the seismic basement profile obtained from seismic interpretation.

It is possible to say that the T_e value of the modeled surface deflection that more closely matched the seismic depth basement surface, give us the today lithospheric elastic parameters under PFB.

PUTUMAYO FORELAND BASIN	
Parameter	**Value**
Mesh size (m)	5,000 m
Poisson's ratio	0.25
Gravitational Force	9.81 ms-1
Mantle Density	3300 kg/m3
Density of Fill Material	2450 kg/m3
Load density	2700 kg/m3
Young's Modulus (Gpa)	70

Table. 3.1 General mathematical parameters used in this study for modeling.

3.5.2. Flexure of the lithosphere through the time in PFB.

The flexural evolution of PFB from the Cretaceous to the Oligocene is obtained analyzing the sedimentary and tectonic loads for each period. The workflow (Londono et al., 2012) used to model the flexure of the lithosphere consists in seven steps described as follows: (Fig. 3.5).

- *Porosity-depth curves*

The first step for perform the flexural model for PFB is to determine the porosity-depth curves for the basin. There are recognized porosity-depth trends obtained from several basins worldwide, which the simplest is the linear trend expressed as:

$$\emptyset = \emptyset_0 - ay$$

Equation 3

where $\emptyset_0$ is the initial porosity, and a represent the porosity depth coefficient with the inconvenience that negative porosity values are obtained as depth increased (Allen and Allen, 2005).

Another porosity-depth relationship is the negative exponential (Athy, 1930) is given by

$$\emptyset = \emptyset_0 e^{-cy}$$

Equation 4

where *c* is a coefficient determining the slope of the $\emptyset$ depth curve, *y* is the depth, and $\emptyset_0$ is the porosity at the surface, which produces an asymptotic low porosity with increasing depth

For this work, the Althy's porosity-depth relationship was used, and their coefficients where obtained cross-plotting porosity values against depth for the well of the basin (Fig. 3.6).

Among the parameters that influence the porosity-depth relationship are: pre-burial mineralogy, texture, pressure, temperature gradients, age, and timing of petroleum migration (Ramm, 1992, Magara, 1980). The most important factor that causes porosity loss is mechanical compaction. It is caused by reorientation and physical deformation of the grains but their effect is decreased by the presence of very high pore pressure formations (Ramm, 1992).

In order to obtain the porosity values for the different analyzed sequences, the log curve data of 25 (wells) consisted in digital LAS were analyzed. The neutron and density logs are normally present along the sequence I. For this reason, the average porosity values for this sequence were obtained applying the following script:

$$PHIAVE = (PHID + PHIN)/2$$

Equation 4

where *PHIAVE* is the average porosity, *PHID* is porosity values derived from density, and *PHIN* is porosity values derived from neutron tool. In wells without Density derived porosity curve *PHID*, it was generated using the following equation:

$$PHID = (RHOM - RHOB) / (RHOM - RHOF)$$

Equation 5

where $RHOM$ is the average density of the matrix, $RHOB$ is bulk density measured by the tool, and $RHOF$ is the fluid density, that is water for our case. For this work, values of 1.00 gm/cc for the bulk density fluid, and 2.650 for sandstone matrix density where used. Due to the lithology heterogeneity of the sequence, in special the high present of clay minerals a correction in the calculated values were performed in order to avoid pitfalls in the porosity determination.

For sequences II, III, and IV, the sonic log was the only porosity log available and the porosity values were calculated using the Wyllie time-average equation (Wyllie, et al., 1956) that relates sonic velocities with the porosity of a rock, and is expressed follows:

$$\frac{1}{V} = \frac{\emptyset}{V_f} + \frac{1 - \emptyset}{V_{ma}}$$

Equation 6

where, ϕ is the total porosity, V is the tool-measured compressional velocity (*Vp*); *Vfl* is the velocity (compressional) of the interstitial fluid, *Vma* is velocity of the matrix material, and ∅ is porosity. The above equation is rewritten in terms of interval travel-times as:

$$\Delta t = \emptyset \Delta t_f + (1 - \emptyset) \Delta t_m$$

Equation 7

where, Δt is the measured interval travel-time.

- *Decompaction of the defined tectonosequences*

The rock volume loss through the time due to porosity reduction is removed from the selected tectonosequences using the porosity-depth relationship, and the depth coefficient c-factor obtained in the previous step. The thickness of the decompacted sequence represents the accommodation space of the basin for this time period, in which the tectonic and sedimentary loads deflected the lithosphere. For decompaction process, the 3D move software was used and an Airy isostatic rebound was taking in account during the decompaction of the sequence.

- *Thickness maps of decompacted tectonosequences*

Thickness maps for each tectonosequence between the basement, and the top the selected sequence were analyzed, and decompacted. This thickness volume represents the input to calculate the deflection caused by sedimentary load in the basin. The obtained decompacted thickness maps were modeled as rectangular blocks of 25 Km^2 of base, and average density of 2700 Kg/m using the Petrel® software.

- *Flexural deformation due to sedimentary load*

A compute flexural deformation caused by sedimentary load was calculated using the FLEX3DV Matlab script (Cardozo, 2009) with the parameters estipulate in the Table 3.1 and a constant T_e value of 30 Km. The obtained deflection values were exported from the Matlab software in .txt files and then displayed in a convenient way into the petrel software.

- *Subsidence related to tectonic load*

The deformation obtained due to the sedimentary load is subtracted from the decompacted thickness of the analyzed sequence; as a result, the deflection caused by tectonic load is calculated. If the difference is positive, its represents the accommodation space created by the thrust wedge load. On the other hand, if the difference is negative, its means that no tectonic loading occurred during the frame time sequence.

- *Load location through time*

In order localize in the accurately the tectonic load for PFB through the time, the paleogeographic maps in the Fig. 2.17 were used. For the sequence I, the tectonic load was located at an average distance of 38 km to the west from line that represents the present day location of the border of the basin. For the sequence II and III the tectonic load was located at 28 and 5 km respectively.

- *Flexural deformation related to tectonic load*

Calculated the flexural deformation caused by tectonic load was preform using the flex3dv Matlab script (Cardozo, 2009) with the parameters estipulate in the Table 3.1 and a constant T_e value of 30 Km. The obtained deflection values were plotted in order to compare their variations along the selected profiles.

A. Andean Mountain range topographic surface

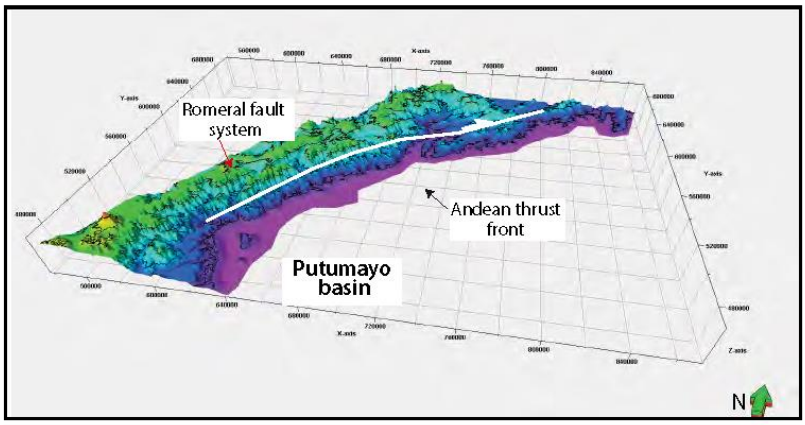

B. 3D grid from Petrel

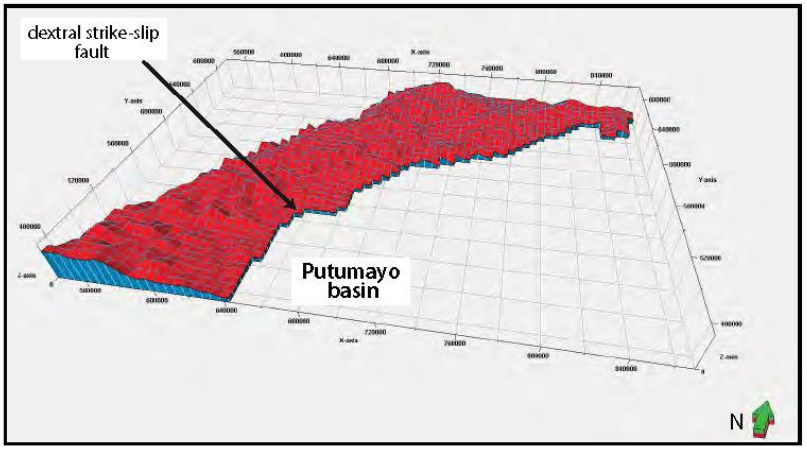

C. 3D model from Matlab script (Allmendinger et al., 2012)

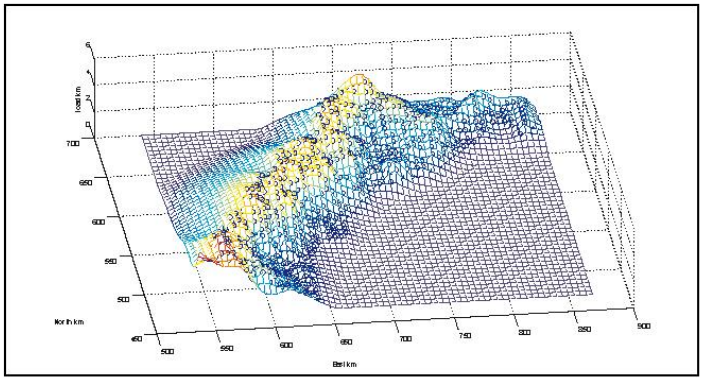

Fig. 3.4 The Andean mountain range is identified as the tectonic load of the PFB; A) topographic surface with contours every 500-m between the Andean trust front and the Romeral fault system; B) Tectonic load is modeled as rectangular blocks of average high, and density; C) 3D grid from Matlab script (Cardozo, 2009).

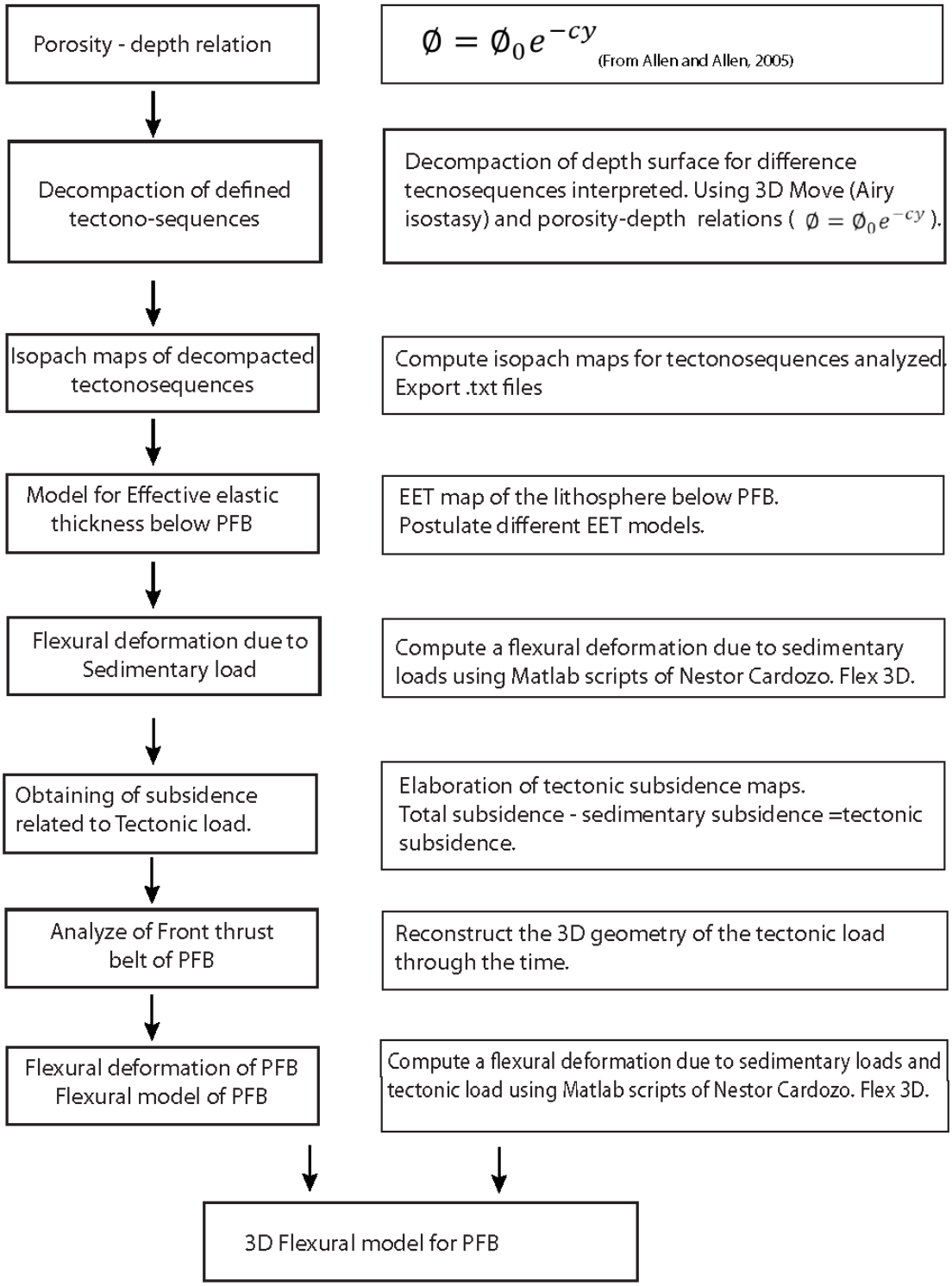

Fig. 3.5: Work-flow summary for the 3D modeling, after Londono et al. (2012)

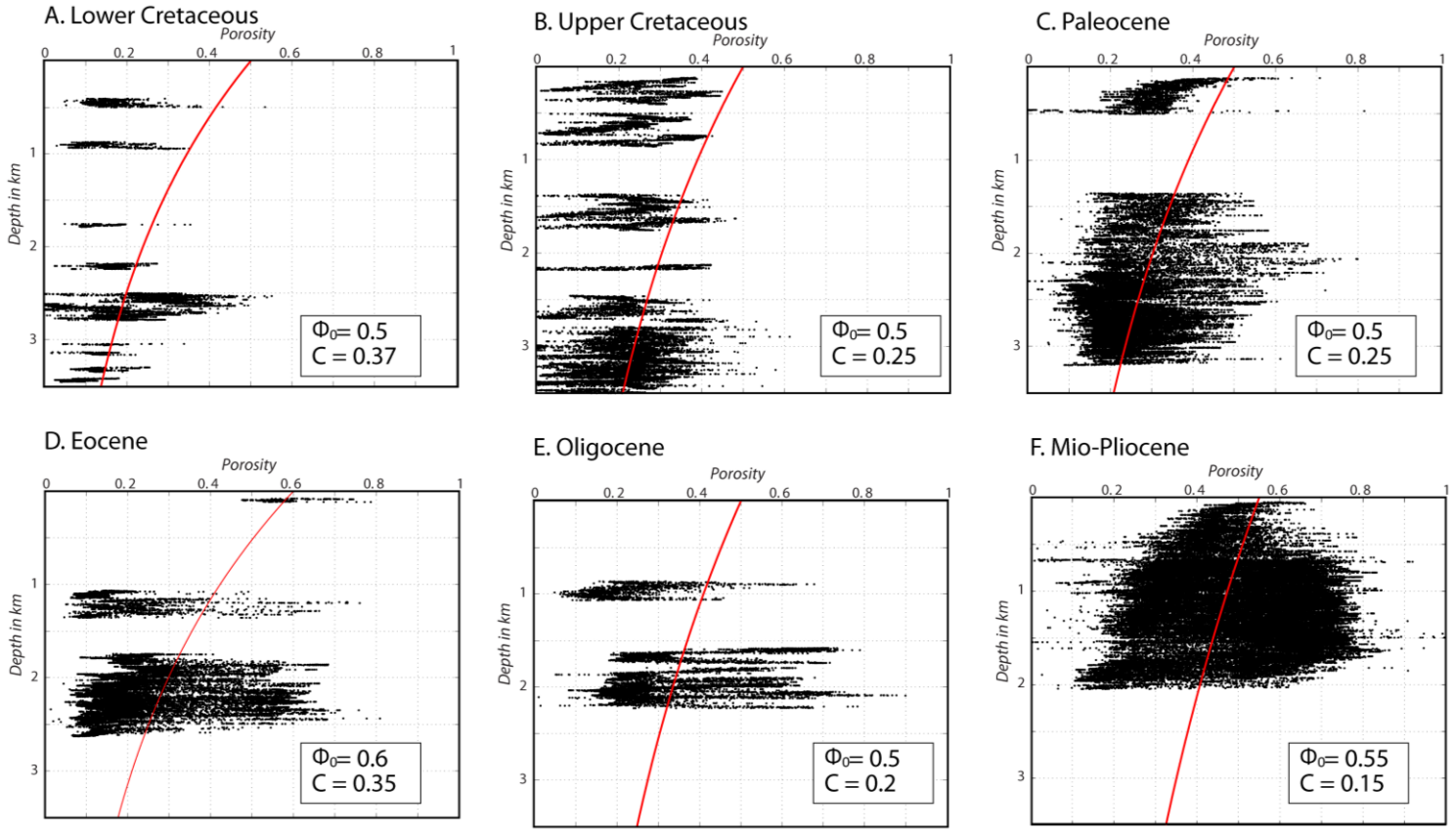

Figure 3.6 Porosity trends, showing the mathematical regression and the values for porosity at surface and the constant C. A) Lower Cretaceous; B) Upper Cretaceous; C) Paleocene; D) Eocene; E) Oligocene; F) Mio-Pliocene.

3.6. 3D FLEXURAL MODELING OF THE PUTUMAYO FORELAND BASIN

3.6.1. Present-day lithosphere deformation: Profiles and deflection

The results gathered from the 3D model of the flexural code for PFB demonstrated that as the rigidity of the lithosphere increases, the depth of deflection decreases. For example, the lithosphere with T_e value of 15 Km resulted in over 6,700 m. of lithospheric deflection while a lithosphere with a T_e value of 35 Km resulted in only about 9,000 ft. (2,700 m) of deflection (Fig. 3.7 C Section SW-NE 1). Results from 3D model along the different selected profiles (Fig. 3.7 C) illustrated similar conclusions as the depth of deflection went from approximately 7,000 m. to less than 3,000 m. (fig. 3). The height of the forebulge for the different models ranges from 150 m. to 30 m. in which the highest values correspond to the low T_e value for the plate (Fig. 3.7).The distance from the eastern border line of the load to the highest point of the forebulge (Fig.s 3.7, 3.8), varies from 260 Km to 360Km where the closest line correspond to 15 Km value of T_e. The forebulge location obtained from the deflection of the Tassara et al. (2007) T_e values crosses through forebulge lines location correspond to the values of 30 and 35 Km of T_e in a NE direction.

A.

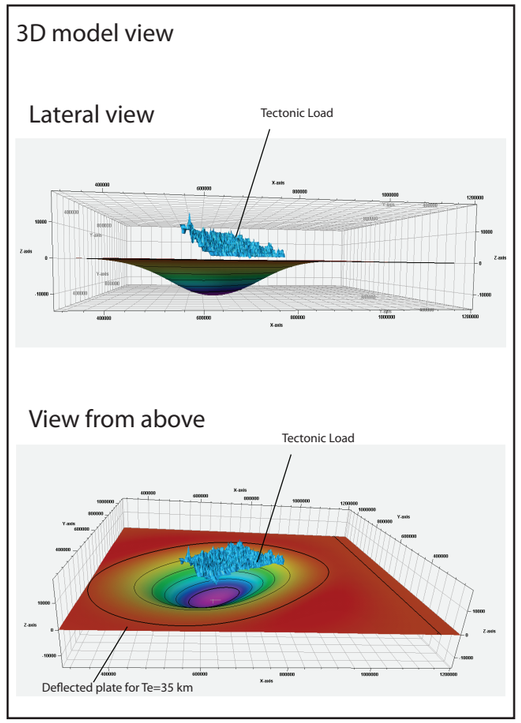

B.

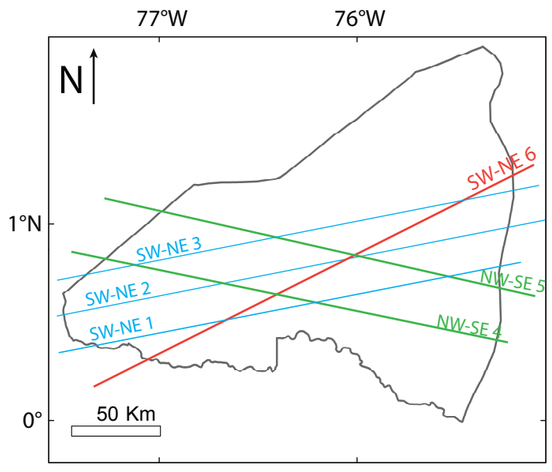

C.

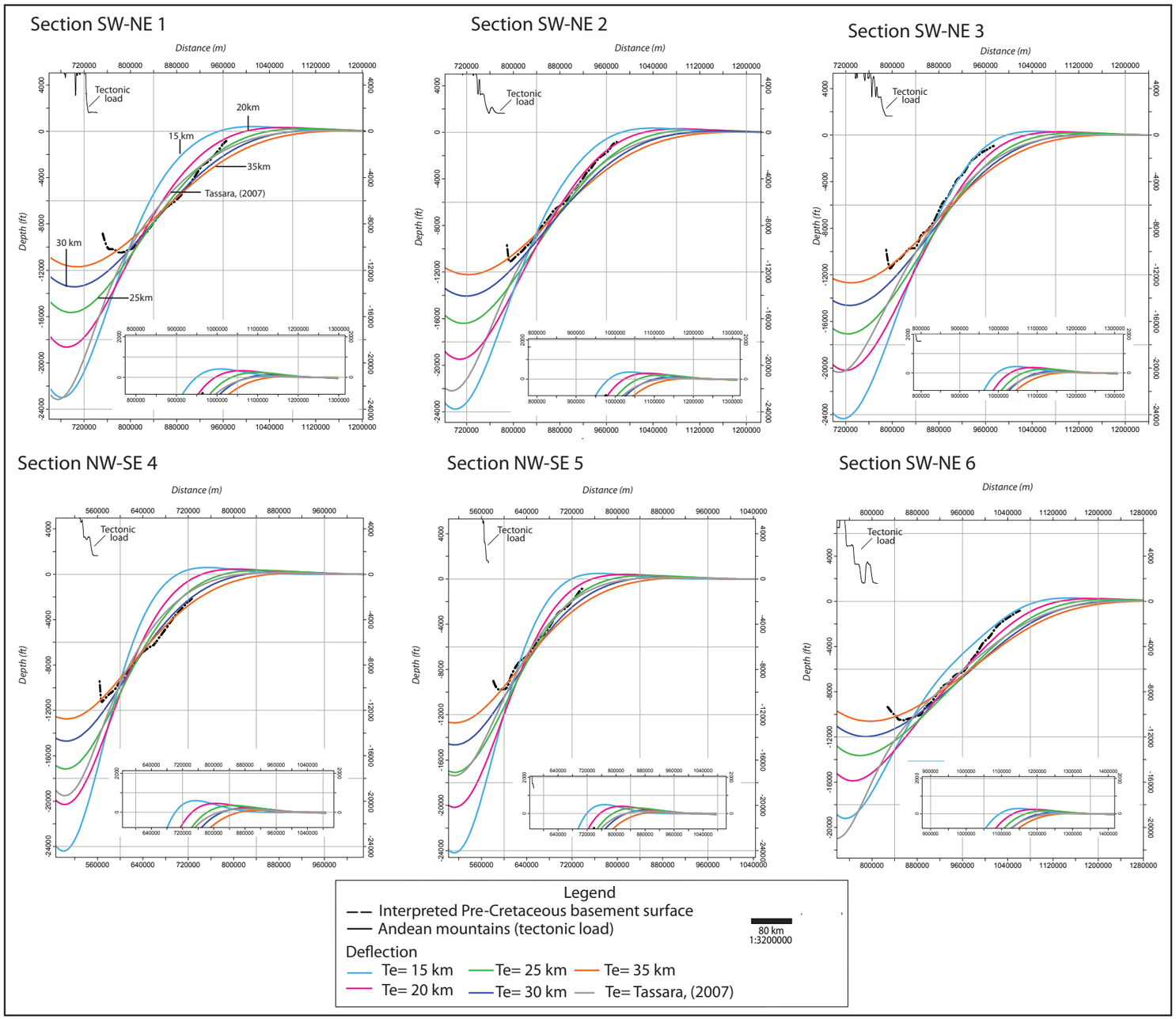

Figure 3.7: 3D flexure of the lithosphere under the PFB and the Andean Montain range as the tectonic load, for different Te (Te= 15 km, Te=20 km, Te=25 km, Te=30 km, Te=35km and Te= Tassara,(2007). A) 3D Model; B) Location map of regional sections; C) Comparison of different regional section.

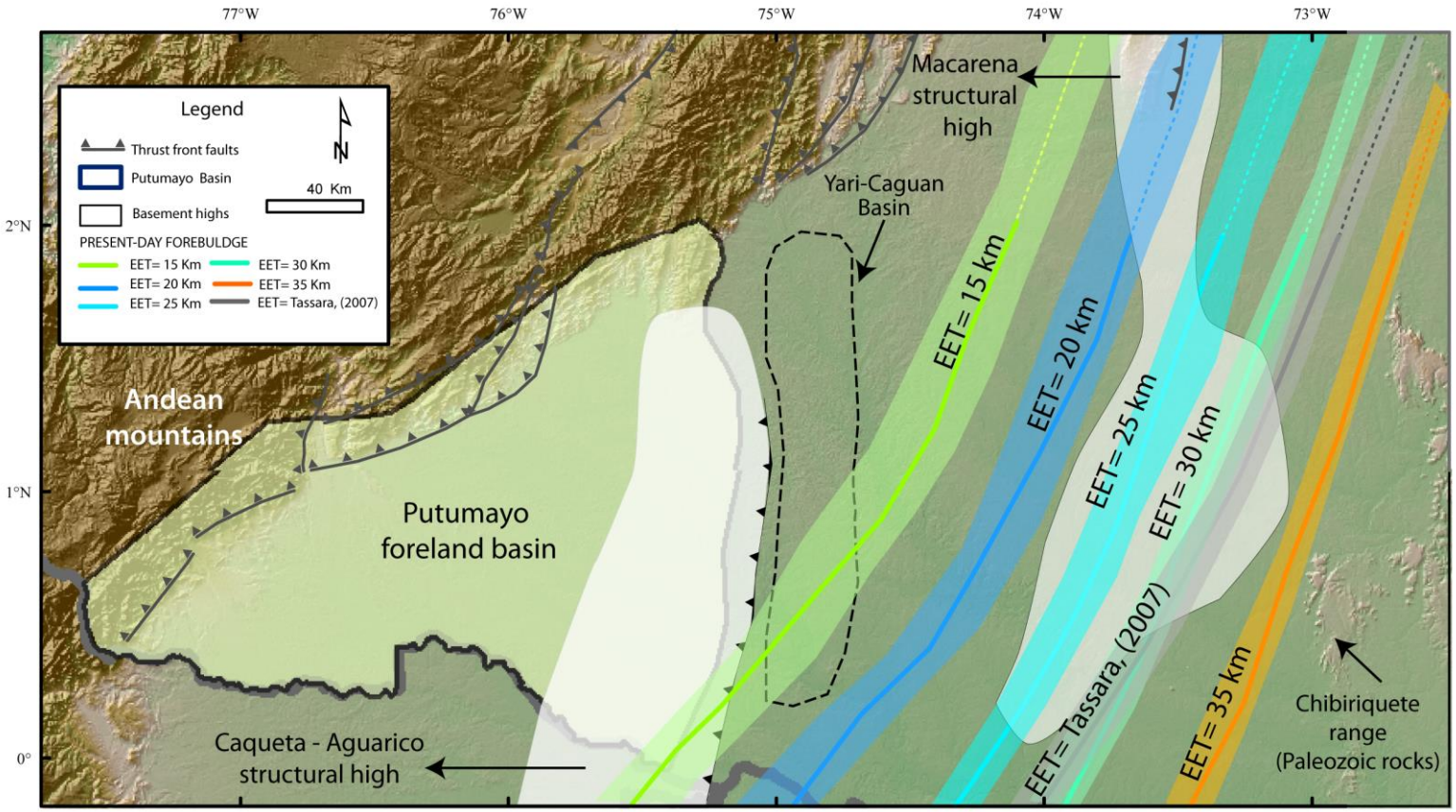

Figure 3.8 Map view of the present-day forebulge location for different values of EET.

3.6.2. Cretaceous-Oligocene lithosphere flexure

- *Cretaceous-Oligocene sedimentary load*

The deflection obtained from the sedimentary load through the time reflects that by the period of the sequence IV (Oligocene) was reached the maximum lithospheric deflection values ranging between 1,800 ft. (548 m) to 1,000 ft. (304 m) (Fig. 3.9). The lower deflection value for this sequence is reached northward of the basin.

A decrease in the sedimentary deflection is observed as far the sequence becomes older, for which the sequence I (Cretaceous) reach their highest deflection in the section NW-SE-4 (Fig. 3.9). The sequences II and III have intermediate deflection values and continue with the tendency of reach the minimum deflection values toward to north of the basin.

The forebulge height due to by the sedimentary loads (Fig. 3.9) for the modeled sequences ranges between 60 ft. (20 m) to 10 ft. (3 m), and their map distribution are represented in the Fig. 3.9. The distance from the eastern border line of the load to the highest point of the forebulge is located at 160 Km, for the sequence IV, and 190 Km for the sequence I.

A.

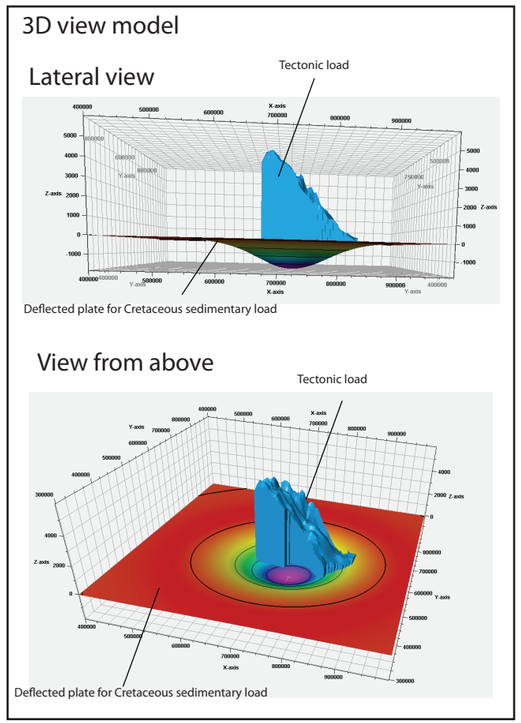

B.

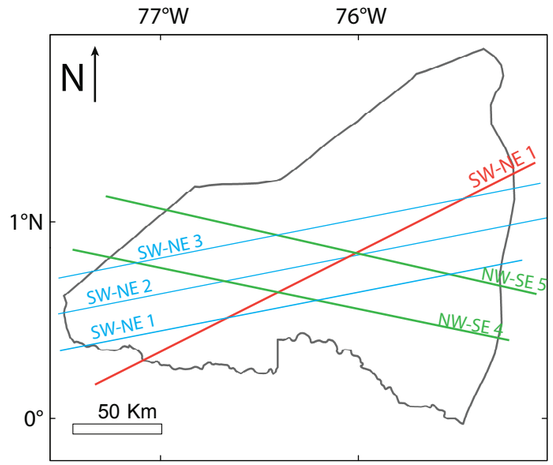

C.

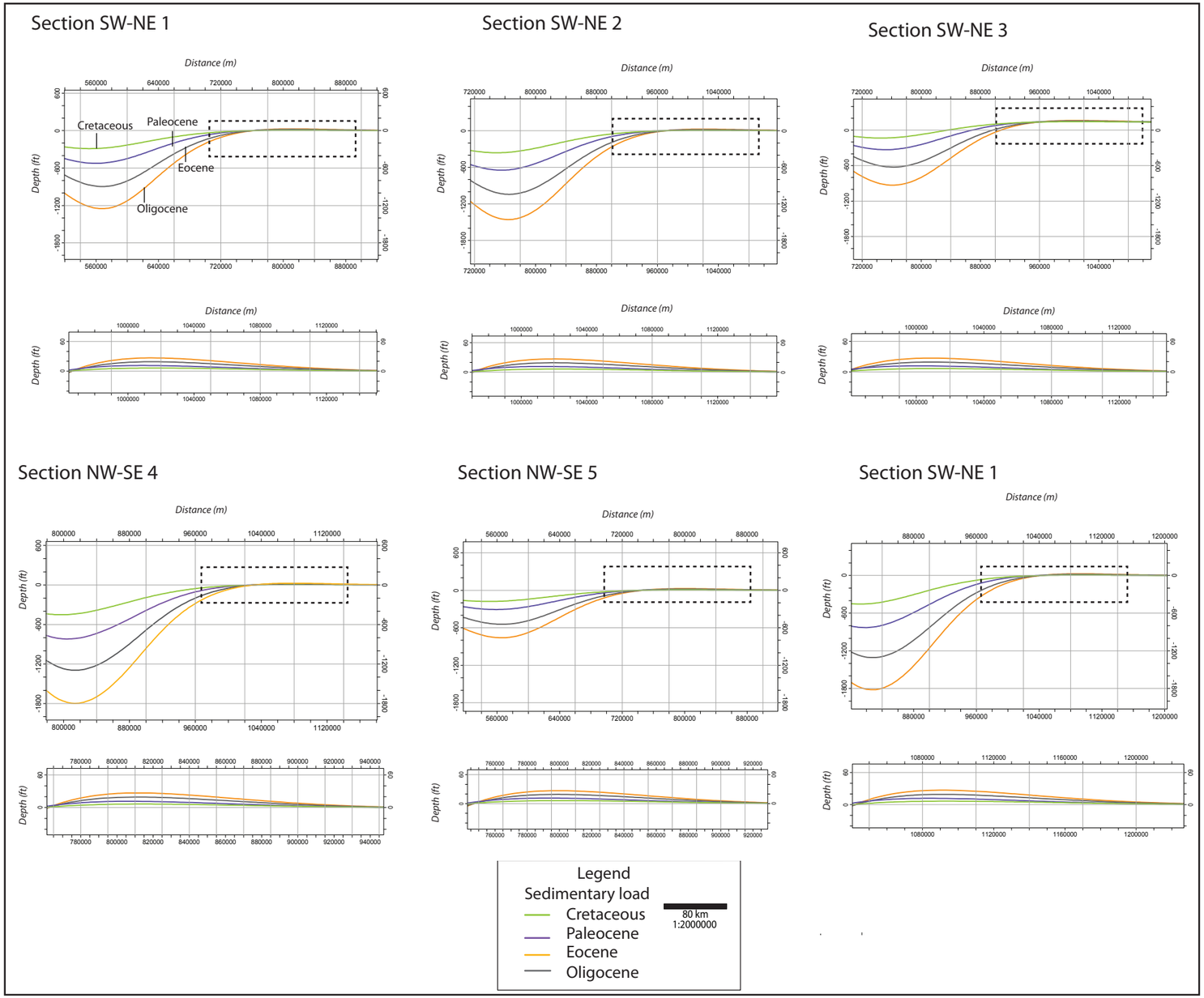

Figure 3.9: 3D flexure of the lithosphere under the PFB for 4 main tectonosequence as main sedimentary load using Te=30 km. A) 3D Model, examples of lateral and above view of the tectonic load and the deflected plate for Cretaceous period; B) Location map of regional sections; C) Comparison of different regional section.

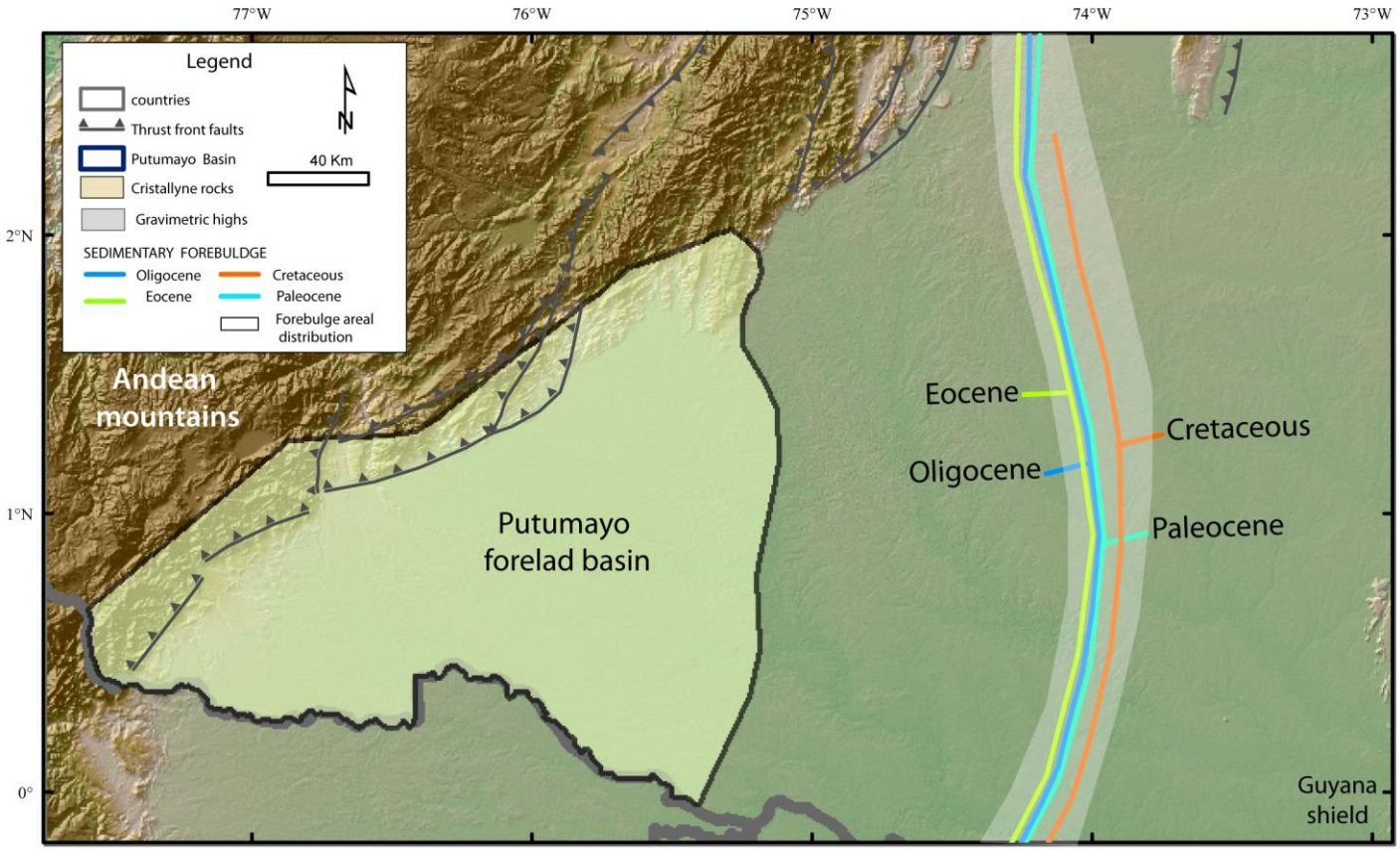

Figure 3.10 Map view of the sedimentary forebulge location for different epochs.

- *Cretaceous- Oligocene tectonic load*

After the subtraction of the deflection caused by sedimentary load to the decompacted thickness (Fig. 3.11A), the sequences I, II, and III demonstrated have tectonic contribution for the deflection of the basin. The sequence I and II reached deflection values from 600 ft. (183 m) to 400 ft. (122 m); while the sequence III expresses values between 100 ft. (30 m) to 50 ft. (17 m). The height of the forebulge for the analyzed sequences have no values upper to 50 ft. (17 m) along the different selected transects. The Fig. 3.12 shows the location of the tectonic forebulge which are closest to the basin that the forebulge generated for sedimentary load.

A.

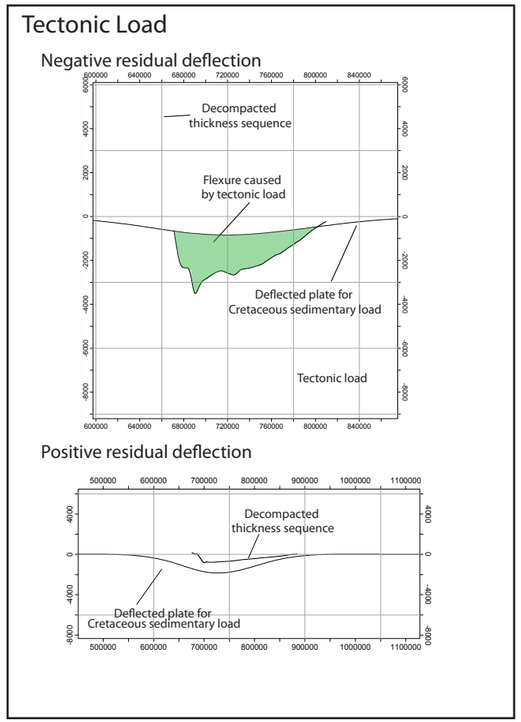

B.

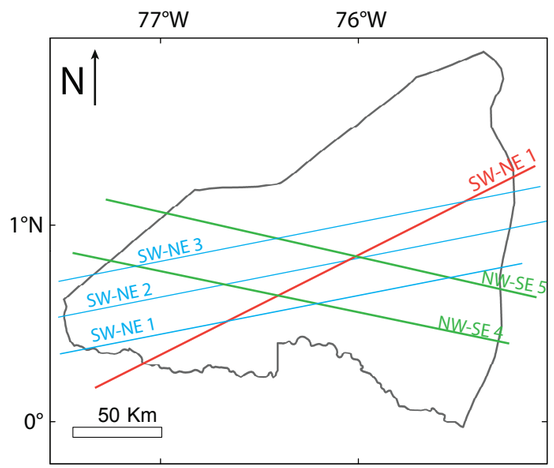

C.

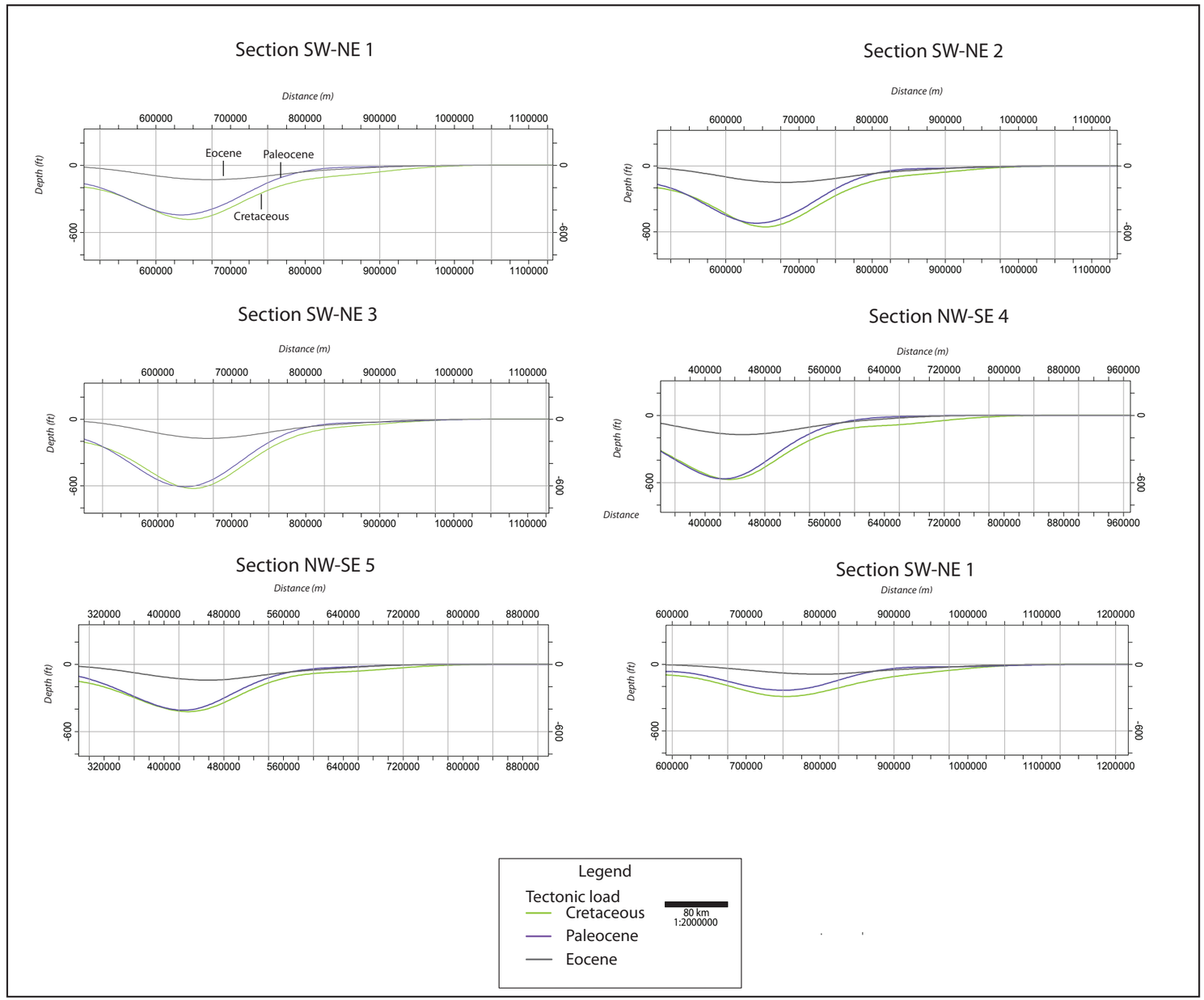

Figure 3.11: 3D flexure of the lithosphere under the Tectonic load for 3 main tectonosequence as main load using Te=30 km. A) 2D model examples of the residual deflection for positive and negative values; B) Location map of regional sections; C) Comparision of different regional section.

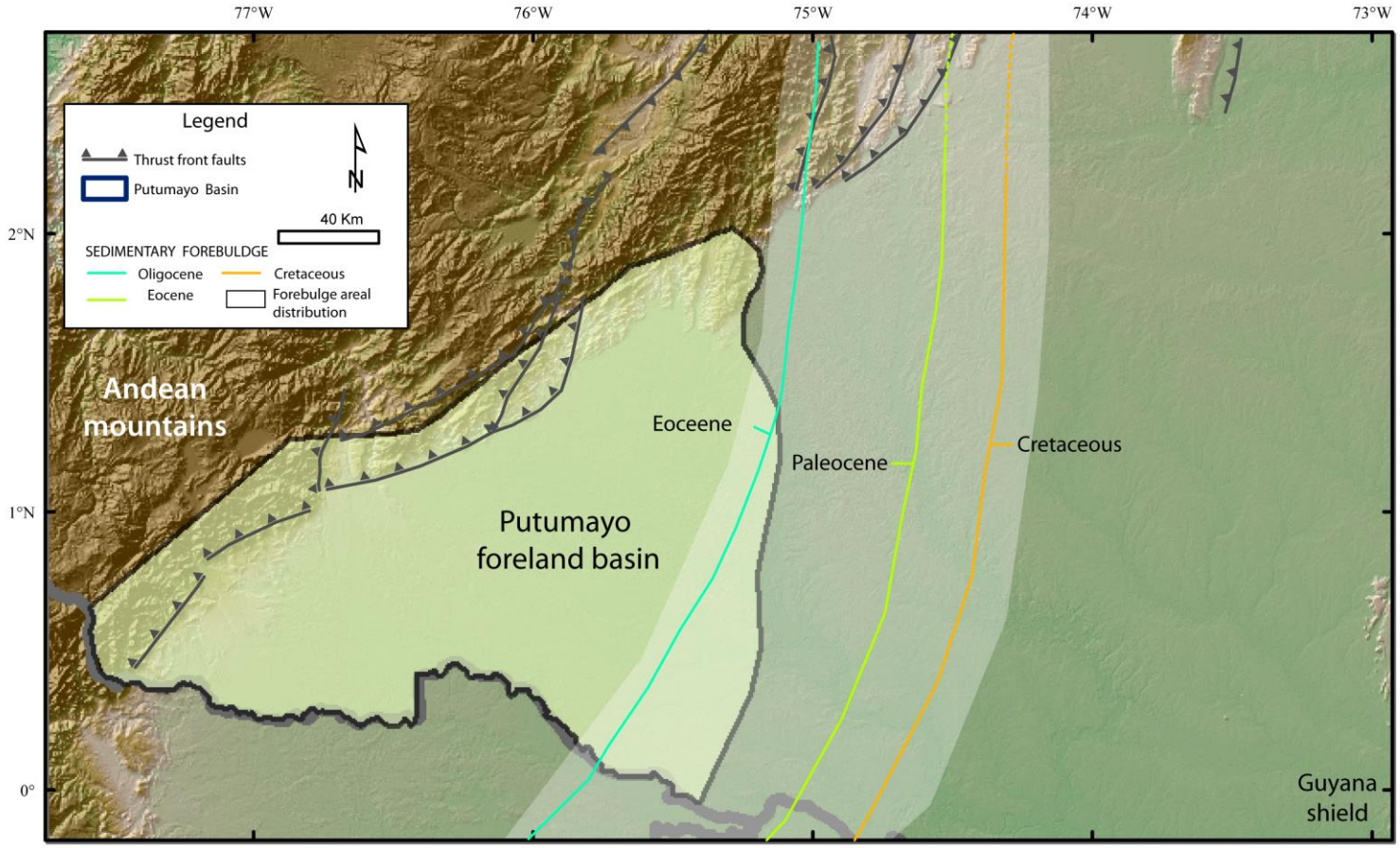

Figure 3.12 Map view of the tectonic forebulge location for different epochs.

3.7. DISCUSSION

3.7.1. Pre-existing weaknesses of the crust bellow the PFB, and their relationship with the forebulge development

The proposed present-day tectonic forebulge of the PFB, based on the flexural profile shown in Figure 3.11, is located 300 Km to the west from the Andean mountains (Fig. 3.12). This distance is greater than the average 250-km width of the basin which involves a forebulge offset due to basement tectonics, and pre-existing crust breaks or weaknesses that control the location of the forebulge (Fig. 3.13A). The geological interpretation of the flexural modeling requires that the Andean Mountains acts as the main tectonic load located at the west, and leads the creation of the accommodation space in the area adjacent to the fold-thrust belt. The present-day forebulge, which is interpreted as the Caquetá basement arch, does not coincide with the location predicted by flexural modeling (Fig. 3.13B).

The Caquetá arch, composed of dense igneous and metamorphic rocks of the Guyana shield, is interpreted as a positive topographic feature until the Late Cretaceous (Fig. 2.13C). The fact that the Caquetá arch is located further west than the predicted location of the forebulge from flexural modeling, implies that a pre-existing weakness implies an important role of the basement rocks controlling the sedimentary filling of the PFB. The basin can be interpreted as a broken foreland basin with the forebulge formed parallel to the Caquetá arch. Strecker et al. (2011) has discussed this type of foreland basin with are spatially limited (Fig. 3.13C).

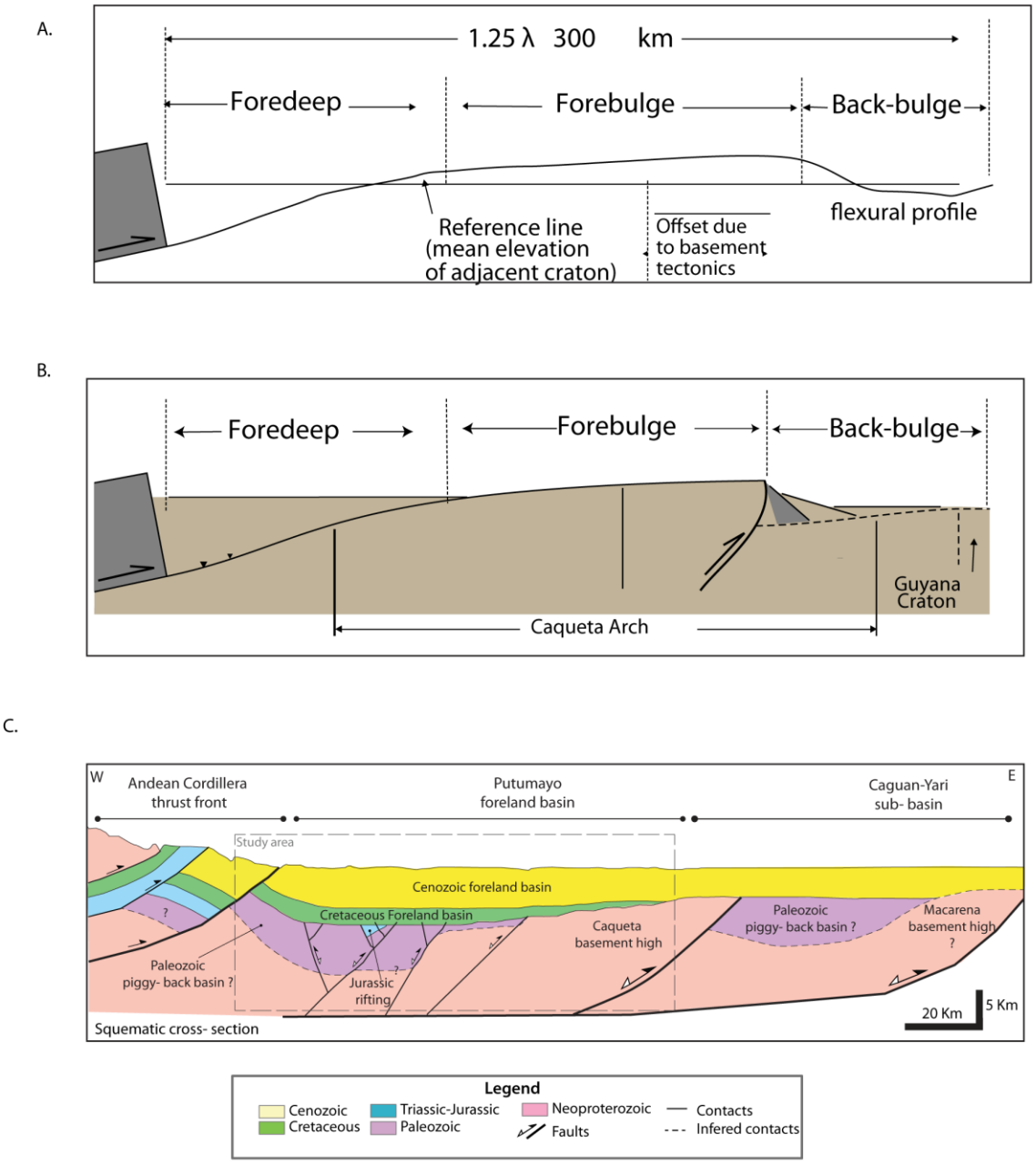

Figure 3.13: Present-day forebulge interpretation. A) 3D flexural modeling result. The model predicts that the modern forebulge does not coincide with the Caquetá arch; B) Geological interpretation; C) Regional structural profile. The zone of maximum flexure has been located along the western area of the Central structural zone since Oligocene. I interpret the forebulge of the PFB to be fault-bounded along its eastern edge and to include a half-graben represented by the Caguán-Yarí basin.

3.7.2. Evolutionary model

Londono (2004) and Londono et al. (2012) built a conceptual model of three main stages for sedimentary sequences within foreland basins: 1) thrusting deflects the plate and creates accommodation space; 2) the sedimentary fill enlarges, and deepens the deflection by subsidence; and 3) the river system reaches an equilibrium stage, and an unconformity develops (Fig. 3.14). In the Putumayo basin, tectonosequences provide evidence for at least two tectonic pulses since the Late Cretaceous- Paleocene (Fig. 3.15).

During the Late Cretaceous, a tectonic load creates the accommodation space in the basin during the initial foreland basin phase (Fig. 3.15). This agrees with predictions from the Mann et al. (2010) regional plate reconstruction in which the Cajamarca-Valdivia terrane (Cediel et al., 2003) initiated collision with the South America plate from southern Colombia and migrated to northward (Fig. 2.17A)

The Paleocene sequence shows a subsidence increase that I relate to increased flexure of the PFB, uplift of the Central Cordillera, and accretion of the Western Cordillera (Fig. 3.15). This age of this uplift is earlier than the Eocene age reported by Nie et al. (2010) based on detrital zircons from the Llanos basin. The difference agrees with the Mann et al. (2010) reconstructions in which these events started in the south and continuously progressed towards the north.

During the Eocene the subsidence of the PFB creates more accommodation space than the effect of the tectonic load because the foreland basin is in a relatively

quiescent tectonic stage and the sedimentary fill enlarges and deepens the deflection (Fig. 3.15).

The Oligocene is interpreted as the overfilled stage of the PFB, in which the sedimentary load effect reaches equilibrium (Fig. 3.11).

During the Eocene the subsidence of the sedimentary column creates more accommodation space than the tectonic load because the foreland basin is in a relative quiet tectonic stage and the sediments enlarge and deepen the deflection (Fig. 3.11).

The Oligocene is interpreted as an overfilling stage of the foreland basin, in which the sediments reaches an equilibrium that can be observed in the flexural modeling as a major sediment load contribution than the tectonic load (Fig. 3.11).

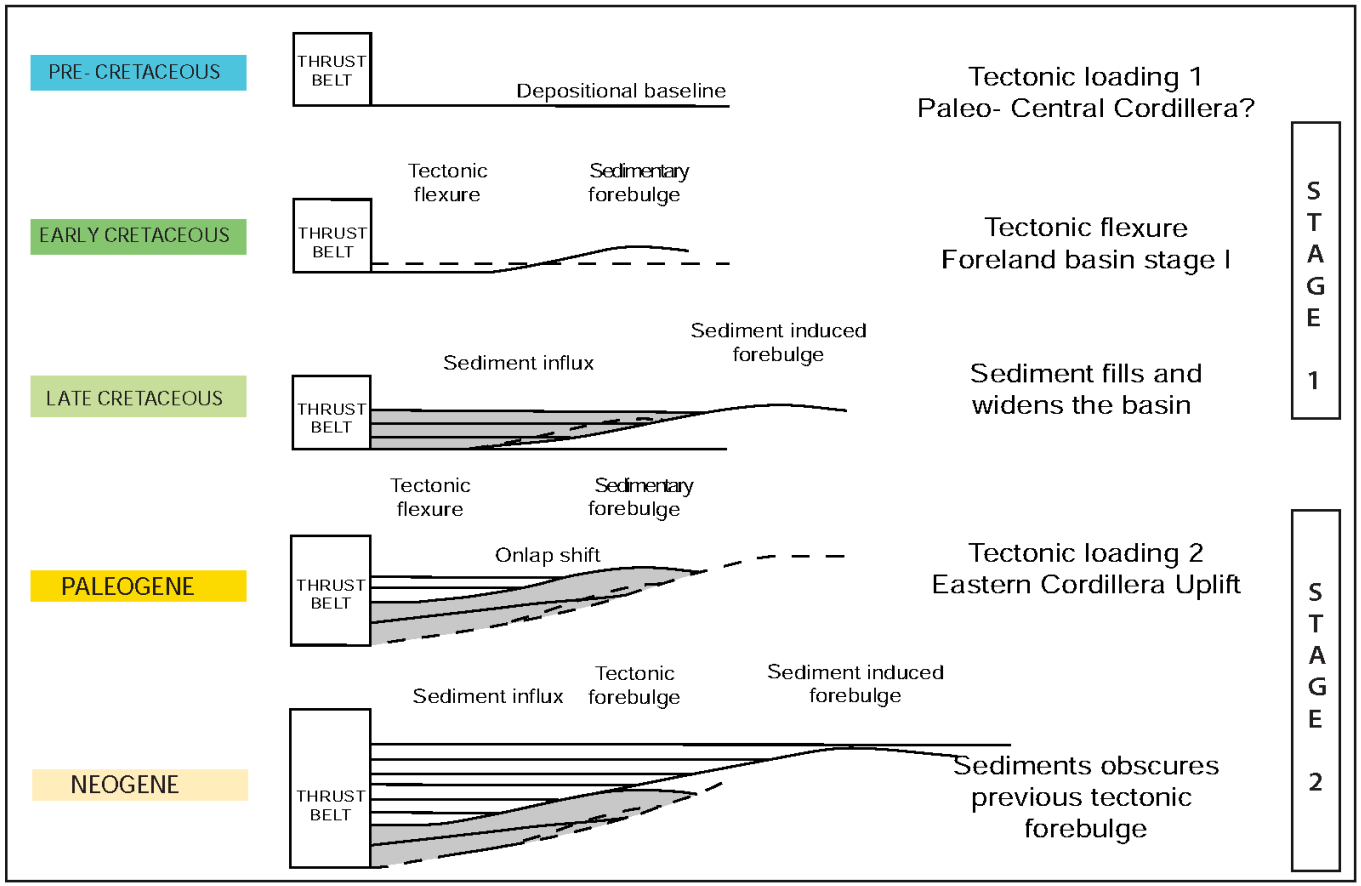

Figure 3.14 Simplified geologic evolution since the Late Cretaceous of the PFB (modified from Londoño, 2012). Two main foreland stages related with the uplift of the paleo-Cordillera Central and the Eastern Cordillera were identified. The thicker part of the PFB is adjacent to the thrust belt and contains up to 3 km of Paleocene to recent clastic sedimentary rocks of non-marine origin, which can be interpreted as overburden rocks overlying Cretaceous source rocks.

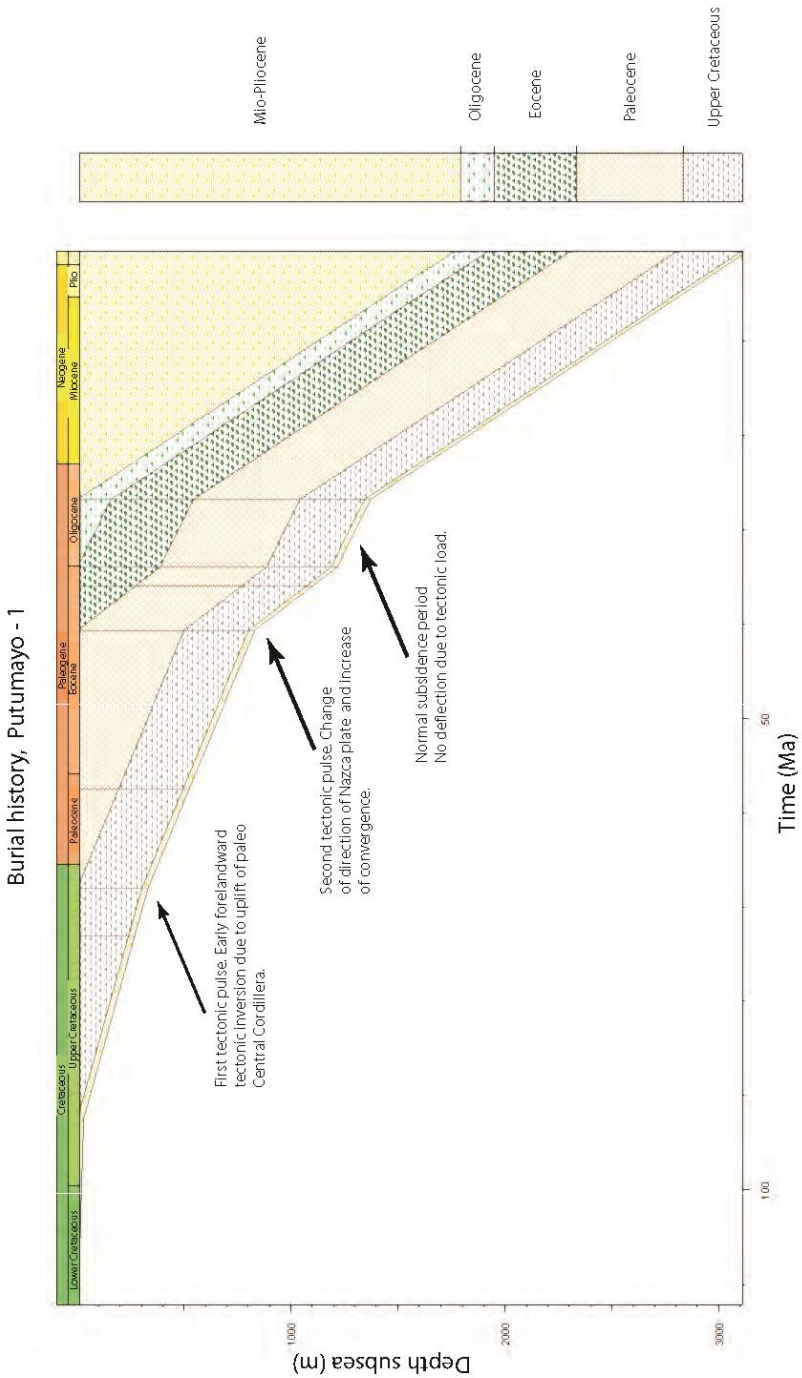

Figure 3.15 Burial history plot for Putumayo -1 well located in the foredeep of the PFB. The subsidence curve, shows two main tectonic pulses at Late Cretaceous-Paleocene and Eocene times.

3.7.3. Model uncertainty and constraints

- *Uncertainty due to location and distribution of the tectonic load through the time*

The error added to the model due to the estimation on the location and distribution of the tectonic load was calculated in about 30%. The error amount was estimated due to the modeling of the loads with the same volume but distributed in different areal extension. For the PFB case, the tectonic forebulge location is expected to be close to the tectonic load, whereby the area where are located should to be extended to the west of the stated location.

- *Te values for lithosphere under PFB*

The value of the T_e for the PFB ranges from 25 to 35 Km as shown by the profiles in the Fig. 3.7. This variation is attributed to the location of the basin on a transition zone between a flat to steeper-dipping subducting slab, along with the presence of Carnegie ridge in the same location. Moreover, the extensional and compressional events that affected the PFB may have generated zones of weakness in the basement of the PFB that would reduce the T_e value of its underlying lithosphere.

3.7.4. Implications for hydrocarbon exploration

The flexural modeling shows two main tectonic pulses resulting in two major subsidence phases affecting the PFB during the Late Cretaceous-Paleocene, and the Eocene (Fig. 3.15). In these two phases the tectonic and sedimentary load generates the accommodation space needed to provide overburden for hydrocarbon maturation.

The main source rock in the area is identified as the Early Cretaceous marine shale, and carbonate which generates hydrocarbons in two migration pulses (Goncalves et al., 2002). The first pulse occurs in the Oligocene and fills traps in the foreland area and the second pulse occurs in the Late Miocene (Goncalves et al., 2002). Filling of foreland traps means that the pre-Andean traps are required to account for the existence of these accumulations in the foreland area. The updip boundary of for both oil migration events is the Caquetá arch that forms an important paleogeograhic boundary (Fig. 2.17). The second migration may have led to updip migration that bypasses the Caquetá arch but a lack of traps in the updip area may have meant that these hydrocarbons were note preserved.

3.7.5. Comparison between the Llanos and Putumayo forelands basin

There are several major differences between the Llanos foreland basin which lacks significant, underlying zones of weakness in its basement and the PFB which contains numerous reactivated zones of weakness (Fig. 3.15). Although both basins formed primarily as the result of crustal-scale flexure, the PFB contains a reactivated high-angle, Paleozoic? structures which act as a major control in the cross sectional structure of the basin (Fig. 3.15). Other differences in the two foreland basins include:

- *Width of the foreland basin:* the Llanos basin is a wider foreland basin of around 800 Km, while the Putumayo basin has a width of 205 km (Fig. 3.16C).
- *Maximum sedimentary thickness of the foreland basin*: The sedimentary thickness in the Llanos basin reaches at least 3 km (Campos, 2011), while the PFB is 2.5 Km
- *Tectonic load average width*: The Eastern Cordillera is much wider adjacent to the Llanos foreland basin (200 Km) than it is adjacent to the PFB (65 Km).
- *Tectonic load maximum thickness*: The highest elevation in the Eastern Cordillera reaches about 5000 m in the northern area near the Llanos basin, whereas the highest value near the PFB is 4500 m.
- *Direction of transportation*: The GPS vectors show a more orthogonal convergence in the Llanos basin instead of the strike-slip convergence toward the south, as in the Putumayo basin, (Trenkamp, 2002) (Fig. 3.1).

- *Shortening:* Shortening in the Llanos basin is the approximately 60 Km (Horton et al., 2010), while in the Putumayo basin shortening only reaches 9 Km (Jimenez 1997).
- *Present-day forebulge location*. The sedimentary forebulge in the Llanos basin is located around 800 Km from the tectonic load, while for the Putumayo basin is located 330 Km from the tectonic load.

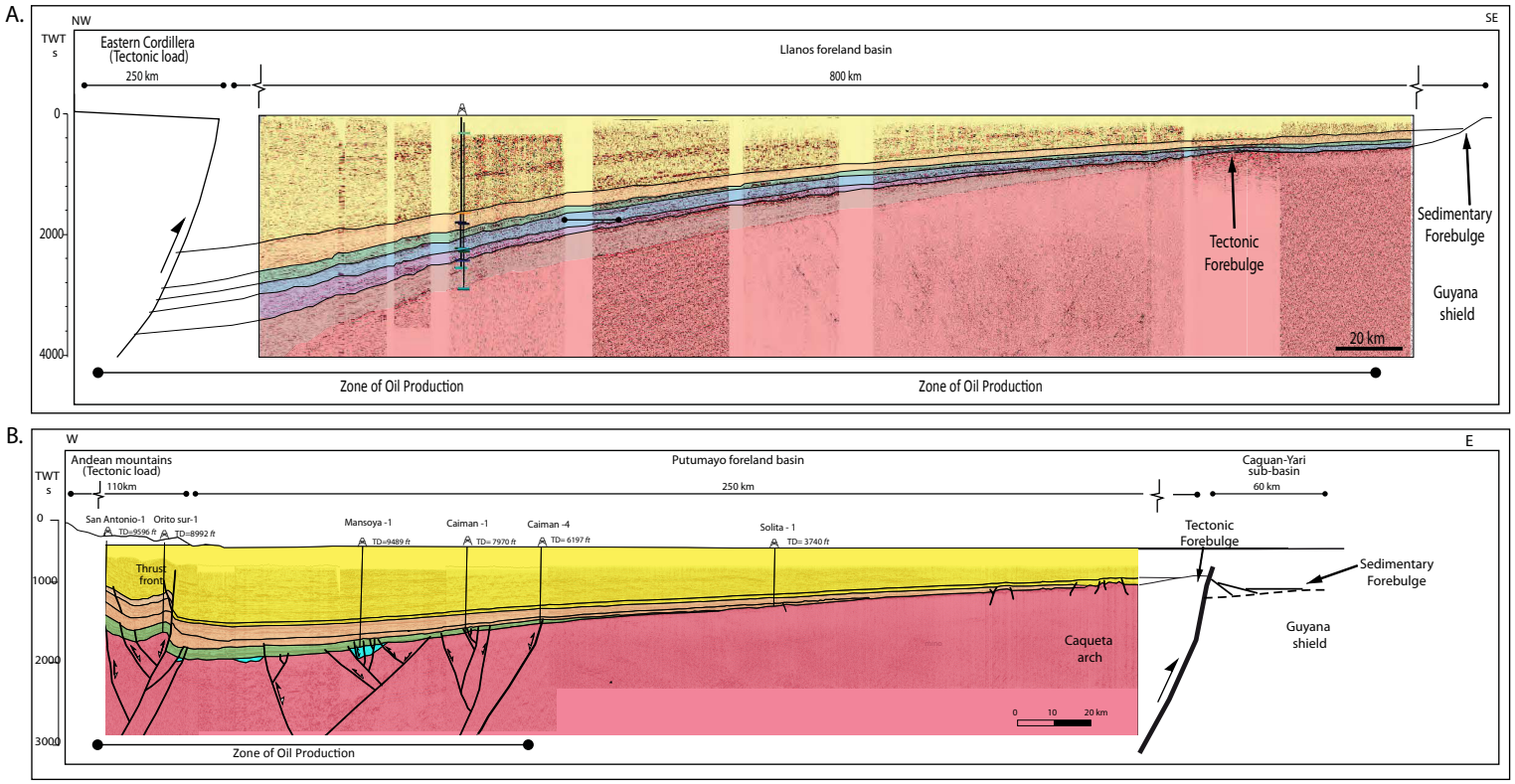

Characteristics		Basin	
		Llanos basin	Putumayo basin
Basin	Average width	800 Km	205 Km
	Maximum thicKness	4Km	3.3 Km
Tecotonic Load (Andean mountains)	Average Width	250 Km	110 Km
	Maximum thicKness (measured from the sea level)	3.3 Km	3.5 Km
	Direction of load transport	Orthogonal convergence	StriKe-slip convergence
	Shortening	60 Km	9 Km
Relative location of the Forebulge at present-day	Sedimentary	800 Km	300 Km
	Tectonic	150 Km	100 Km

Figure 3.16 Comparison between the Llanos basin and the Putumayo basin, Colombia; A) Regional 2D seismic profile showing the geometrical arrangement of Llanos basin, and interpreted location of the tectonic load and forebulge of the basin (from Campos, 2011); B) Regional 2D seismic profile showing the geometrical arrangement of Putumayo basin and interpreted location of the tectonic load and forebulge of the basin; C) Summary of the basinal sizes, size of tectonic loads, and main characteristics of the forebulge for both basins; D) Location map of both foreland basins.

3.8. CONCLUSION

Flexural modeling reveals that the observed asymmetric, cross-sectional geometry of the Cretaceous-Oligocene in the Putumayo basin was a result of the uplift of the Andean Mountains (tectonic load), the wide sedimentary column filling the basin (sedimentary load), and the plate configuration (T_e). The subsidence history of the basin was reproduced with an elastic semi-infinite plate in which the elastic thickness values (T_e) ranging from 25 to 35 Km, are the estimations that adjust with the basement configuration.

The mechanical models used in this work predicted that the forebulge at present-day is located 300 Km to the east of the Eastern Cordillera, and exceeds the longitudinal area of the basin, implying a broken foreland basin, in which the basement configuration of the PFB has conditioned the developed and flexure of the lithosphere under PFB. The crystalline basement is associated with igneous and metamorphic rocks of the Guyana shield and is interpreted as a positive topography feature until the Late Cretaceous. The presence of the basement highs limited the hydrocarbon migration restricting the distribution of the oil field areas to the foredeep section of the PFB due to the paleo-barrier character of the basement high (Caquetá arch).

For the analyzed sequences, the sedimentary load is mainly responsible for the flexure of the underlying plate, as well as the topographic expression of the sedimentary bulges which are no higher than 50 m, and are not distinguishable at the seismic scale used within this work. The maximum deflection of the plate for the

analyzed sequences was reached in the sequence IV in which, the sedimentary load was the main factor that caused deflection. The sequences I-II-II had sedimentary and tectonic input.

REFERENCES

Allen P.A, and Allen A.J, 2005, Basin Analysis. Principles and Applications, Blackwell Publishing, Oxford, 549 p.

Athy, L.F., 1930, Density, porosity, and compaction of sedimentary rocks: American Association of Petroleum Geologists (AAPG) Bulletin, v. 14, p. 1-24.

Baby, P., Rivadeneira, M., Barragán, R., and Christophoul, F., 2013, Thick-skinned tectonics in the Oriente foreland basin of Ecuador: Geological Society, London, Special Publications, v. 377, p. 1-20.

Baby, P., Rivadeneira, M., Da Vila, C., Galarraga M., Rosero, J., and Vega, J., 1997, Estilo tectónico y etapas de deformación de la parte norte de la cuenca Oriente ecuatoriana: Asociación Colombiana de Geólogos y Geofísicos del Petróleo (ACGGP), p. 288-302.

Balkwill, H., Rodriguez, G., Paredes, F., Almeida, J., Tankard, A., Suárez S, R., and Welsink, H., 1995, Northern part of Oriente basin, Ecuador: reflection seismic expression of structures: American Association of Petroleum Geologists Bulletin (AAPG), v.84, no.5, p. 559-571.

Barrett, S.F, and Isaacson, P.E, 1988, Devonian paleogeography of South America, *in* N.J. McMillan, A.F Embry, and D.J Glass, eds, Devonian of the worls: Canadian Society of Petroleum Geologist Memoir (CSPG), v. 14, no.1, p. 655-667.

Bayona, G., Cortés, M., Jaramillo, C., Ojeda, G., Aristizabal, J. J., and Reyes-Harker, A., 2008, An integrated analysis of an orogen--sedimentary basin pair: Latest Cretaceous--Cenozoic evolution of the linked Eastern Cordillera orogen and the Llanos foreland basin of Colombia: Geological Society of America Bulletin, v. 120, no. 9/10, p. 1171-1197.

BEICIP-ECOPETROL, 1988, Evaluación regional geológica y geofísica de la Cuenca del Putumayo: Bogotá, Ecopetrol, 170 p.

Belotti, H., Silvestro, J., Conforto, G., Pozo, M., Erlicher, J., Rodriguez, J., and Rossello, E., 2003. Recognition of Tectonic Events in the Conformation of Structural Traps in the Eastern Oriente Basin, Ecuador, poster presented in American Association of Petroleum Geologists (AAPG) Convention, Salt Lake City,Utah, 2003.

Briceño, H. O., and Schubert, C., 1990, Geomorphology of the Gran Sabana, Guayana Shield, southeastern Venezuela: Geomorphology, v. 3, no. 2, p. 125-141.

Burov, E.B., and Diament, M., 1995, The effective elastic thickness (Te) of continental lithosphere: What does it really mean?: J. Geophys. Res., v. 100, p. 3905-3927.

Bourdon, E., Eissen, J.-P., Gutscher, M.-A., Monzier, M., Hall, M. L., and Cotten, J., 2003, Magmatic response to early aseismic ridge subduction: the Ecuadorian margin case (South America): Earth and Planetary Science Letters, v. 205, no. 3–4, p. 123-138.

Campbell, C. J., and Bürgl, H., 1965, Section Through the Eastern Cordillera of Colombia, South America: Geological Society of America Bulletin, v. 76, no. 5, p. 567-590.

Campos, H., 2011, Tectonostratigraphic and subsidence history of the northern Llanos foreland basin of Colombia, 2011. M.S. Thesis. The University of Texas at Austin, 126p.

Cardozo, N., 1997, Thermomechanical Modeling of the Llanos Basin Colombia, South America: Master's Thesis, Ohio University, 60p.

Cardozo, N., and Jordan, T., 2001, Causes of spatially variable tectonic subsidence in the Miocene Bermejo Foreland Basin, Argentina: Basin Research, v. 13, p. 335-357.

Cardozo, N., 2009, flex3dv [Script], retrieved January 2013, from http://homepage mac. com/nfcd/work/programs. html

Casero, P., J. Salel, and Rossato, A., 1997, Multidisciplinary correlative evidences for polyphase geological evolution of the Foot-hills of the Cordillera Oriental, VI Symposio Bolivariano 'Exploración Petrolera en las Cuencas Subandinas' Memorias, Volume I: Cartagena, Colombia, p. 100-118.

Cediel, F., Shaw, R. P., Cáceres, C., and Bartolini, C., 2003, Tectonic assembly of the Northern Andean Block. *in* C. Bartolini, R. T. Buffler & J. Blickwede, eds., The Circum-Gulf of Mexico and the Caribbean: Hydrocarbon Habitats, Basin Formation, and Plate Tectonics, p. 815–848.

Chinn, D. S., and Isacks, B. L., 1983, Accurate source depths and focal mechanisms of shallow earthquakes in western South America and in the New Hebrides Island Arc: Tectonics, v. 2, no. 6, p. 529-563.

Colletta, B., Hebrard, F., Letouzey, J., Werner, P., and Rudkiewicz, J., 1990, Tectonic Style and Crustal Structure of the Eastern Cordillera (Colombia) from a Balanced Cross-section *in* J. Letouzey, eds., Petroleum and Tectonics in Mobile belts: Paris, Editions Technip, p. 81-100.

Cooper, M., Addison, F., Alvarez, R., Coral, M., Graham, R. H., Hayward, A., Howe, S., Martinez, J., Naar, J., and Peñas, R., 1995, Basin development and tectonic history of the Llanos Basin, Eastern Cordillera, and middle Magdalena Valley, Colombia: American Association of Petroleum Geologists (AAPG) Bulletin, v. 79, no. 10, p. 1421-1443.

Cordani, U. G., Fraga, L. M., Reis, N., Tassinari, C. C. G., and Brito-Neves, B. B., 2010, On the origin and tectonic significance of the intra-plate events of Grenvillian-type age in South America: A discussion: Journal of South American Earth Sciences, v. 29, no. 1, p. 143-159.

Córdoba, F., Buchelli, F., Moros, J., Calderón, W., Guerrero, C., Kairuz, E., and Magoon, L., 1997, Proyecto evaluación regional Cuenca del Putumayo—Definición de los sistemas petrolíferos: Ecopetrol, Internal report, Bogotá, 140 p.

Cortes, M., B. Colletta, and J. Angelier, 2006, Structure and tectonics of the central segment of the Eastern Cordillera of Colombia: Journal of South American Earth Sciences, v. 21, p. 437-465

Daly, M. C., 1989, Correlations between Nazca/Farallon Plate kinematics and forearc basin evolution in Ecuador: Tectonics, v. 8, no. 4, p. 769-790.

DeCelles, P.G., and Giles, K.A., 1996, Foreland basin systems: Basin Research, v. 8, no.2 p. 105-123.

Dumont, J. F., Santana, E., and Vilema, W., 2005, Morphologic evidence of active motion of the Zambapala Fault, Gulf of Guayaquil (Ecuador): Geomorphology, v. 65, no. 3–4, p. 223-239.

Duque-Caro, H., 1990, The Choco block in the northwestern corner of South America: Structural, tectonostratigraphic, and paleogeographic implications: Journal of South American Earth Sciences, v. 3, no. 1, p. 71-84.

Garcia-Castellanos, D., 2002, Interplay between lithospheric flexure and river transport in foreland basins: Basin Research, v. 14, p. 89-104.

Ego, F., Sébrier, M., Carey-Gailhardis, E., and Beate, B., 1996, Do the Billecocha normal faults (Ecuador) reveal extension due to lithospheric body forces in the northern Andes?: Tectonophysics, v. 265, no. 3–4, p. 255-273.

Escalona, A., and Mann, P., 2006, Sequence-stratigraphic analysis of Eocene clastic foreland basin deposits in central Lake Maracaibo using high-resolution well correlation and 3-D seismic data: American Association of Petroleum Geologists (AAPG), Bulletin, v. 90, no. 4, p. 581-623.

Gómez, E., Jordan, T. E., Allmendinger, R. W., and Cardozo, N., 2005, Development of the Colombian foreland-basin system as a consequence of diachronous exhumation of the northern Andes: Geological Society of America Bulletin, v. 117, no. 9-10, p. 1272-1292.

Gómez Tapias, J., Nivia Guevara, A., Montes Ramírez, N., Jiménez Mejía, D., Tejada Avella, M., Sepúlveda Ospina, M., Osorio Naranjo, J., Gaona Narváez, T., Diederix, H., and Uribe Pena, H., 2007, Mapa Geológico de Colombia (1: 1,000,000), Instituto Colombiano de Geología y Minería, Bogotá.

Gonçalves, F.T.T., Mora, C.A., Córdoba, F., Kairuz, E.C., and Giraldo, B.N., 2002, Petroleum generation and migration in the Putumayo Basin, Colombia: insights from an organic geochemistry and basin modeling study in the foothills: Marine and Petroleum Geology, v. 19, p. 711-725.

Gutscher, M. A., Malavieille, J., Lallemand, S., and Collot, J. Y., 1999, Tectonic segmentation of the North Andean margin: impact of the Carnegie Ridge collision: Earth and Planetary Science Letters, v. 168, no. 3–4, p. 255-270.

Higley, D. K., 2001, The Putumayo-Oriente-Maranon Province of Colombia, Ecuador and Peru: Mesozoic-Cenozoic and Paleozoic Petroleum Systems, US Department of the Interior, US Geological Survey, v. 63, Denver. 110 p.

Horton, B.K., and DeCelles, P.G., 1997, The modern foreland basin system adjacent to the Central Andes: Geology, v. 25, p. 895-898.

Horton, B. K., Saylor, J. E., Nie, J., Mora, A., Parra, M., Reyes-Harker, A., and Stockli, D. F, 2010, Linking sedimentation in the northern Andes to basement configuration, Mesozoic extension, and Cenozoic shortening: Evidence from detrital zircon U-Pb ages, Eastern Cordillera, Colombia. Geological Society of America Bulletin, v. 122, no. 9-10, p. 1423-1442.

Ibanez-Mejia, M., Ruiz, J., Valencia, V. A., Cardona, A., Gehrels, G. E., and Mora, A. R., 2011, The Putumayo Orogen of Amazonia and its implications for Rodinia reconstructions: New U–Pb geochronological insights into the Proterozoic tectonic evolution of northwestern South America: Precambrian Research, v. 191, no. 1–2, p. 58-77.

Isaacson, P., and Sablock, P., 1988, Devonian system in Bolivia, Peru and northern Chile *in* N.J. McMillan, A.F Embry, and D.J Glass, eds, Devonian of the worls: Canadian Society of Petroleum Geologist Memoir (CSPG), v. 14, no.1, p. 719-728.

Jacques, J., 2003, A tectonostratigraphic synthesis of the Sub-Andean basins: implications for the geotectonic segmentation of the Andean Belt: Journal of the Geological Society, v. 160, no. 5, p. 687-701.

Jacques, J., 2003, A tectonostratigraphic synthesis of the Sub-Andean basins: inferences on the position of South American intraplate accommodation zones and their control on South Atlantic opening: Journal of the Geological Society, v. 160, no. 5, p. 703-717.

James, D. E., and Murcia, L. A., 1984, Crustal contamination in northern Andean volcanics: Journal of the Geological Society, v. 141, no. 5, p. 823-830.

Jimenez, J.C., 1997, Structural Styles of the Andean Foothills, Putumayo Basin, Colombia: Master's thesis, University of Texas at Austin, 74 p.

Londono, J., and Lorenzo, J. M., 2004, Geodynamics of continental plate collision during late tertiary foreland basin evolution in the Timor Sea: constraints from foreland sequences, elastic flexure and normal faulting: Tectonophysics, v. 392, no. 1–4, p. 37-54.

Londono, J., Lorenzo, J. M., Ramirez, V, 2012, Lithospheric flexure and related base-sea level stratigraphic cycles in continental foreland basins: An example from the Putumayo Basin, Northern Andes *in* D. Gao, ed., Tectonics and Sedimentation: Implications for Petroleum Systems: American Association of Petroleum Geologists (AAPG) Memoir 100, p.357-375

Magara, K., 1980, Comparison of porosity-depth relationships of shale and sandstone: Journal of Petroleum Geology, v. 3, p. 175-185.

Mann, P., and Burke, K., 1984, Neotectonics of the Caribbean: Reviews of Geophysics, v. 22, no. 4, p. 309-362.

Mann, P., Burke, K., and Matumoto, T., 1984, Neotectonics of Hispaniola: Plate motion, sedimentation, and seismicity at a restraining bend: Earth and Planetary Science Letters, v. 70, no. 2, p. 311-324.

Mann, P., and Escalona, A., 2010, Caribbean basins, tectonics and hydrocarbons (CBTH) phase II- Atlas volume, University of Texas, Jackson School of Geoscience, Institute of Geophysics and University of Stavanger, Norway, Department of Petroleum Engineering: Austin, Texas, 83 p.

Moreno-Lopez, M. C., 2012, Evolution of the southern Llanos basin, Colombia: Master's thesis, University of Stavanger, Norway, 88 p.

National Hydrocarbons Agency, 2012, Indicadores Diciembre 2012: Bogota, ANH (National Hydrocarbon Agency).

Nie, J., Horton, B.K., Mora, A., Saylor, J.E., Housh, T.B., Rubiano, J., and Naranjo, J., 2010, Tracking exhumation of Andean ranges bounding the Middle Magdalena Valley basin, Colombia: Geology, v. 38, p. 451-454

Pardo Casas, F., and Molnar, P., 1987, Relative motion of the Nazca (Farallon) and South American plates since Late Cretaceous time: Tectonics, v. 6, no. 3, p. 233-248.

Pennington, W. D., 1981, Subduction of the Eastern Panama Basin and seismotectonics of northwestern South America: Journal of Geophysical Research: Solid Earth, v. 86, no. B11, p. 10753-10770.

Pérez-Gussinyé, M., Lowry, A.R., and Watts, A.B., 2007, Effective elastic thickness of South America and its implications for intracontinental deformation: Geochem. Geophys. Geosyst., v. 8, no.5.

PetroEcuador, 2010, El Petroleo en Ecuador, Petroecuador, Quito, 133 p.

Pindell, J.L.T., K. D., and Kennan, L., 1998, Putumayo basin, Colombia: Bogota, Ecopetrol, Internal report, p. 40.

Portilla, C.O., 1991, The Putumayo fold-belt, Colombia, South America: structural interpretation and hydrocarbon potential, degree of Master of Science thesis, University of South Carolina, 87 p.

Ramm, M., 1992, Porosity-depth trends in reservoir sandstones: theoretical models related to Jurassic sandstones offshore Norway: Marine and Petroleum Geology, v. 9, p. 553-567.

Ramos, V. A., 2009, Anatomy and global context of the Andes: Main geologic features and the Andean orogenic cycle in S. M Kay, V. A, Ramos, and W. R, Dickinson, eds., Backbone of the Americas: Shallow subduction, plateau uplift, and ridge and terrene collision, Geological Society of America Mem 204, p. 67-83

Rigo de Righi, M., and Bloomer, G., 1975, Oil and gas developments in the Upper Amazon Basin—Colombia, Ecuador, and Peru, *in* Proceedings of the 9th World Petroleum Congress, Volume 3, p. 181-192.

Rossello, E., Nevistic, V., Covellone, G., Bordarampa, C., Salvay, R., Pina, L., Araque, L., and Giraudo, R., 2006, The Pre-Aptian records of the Putumayo Basin (Colombia): New frontier opportunities for HC exploration in a mature basin?, in Proceedings 9th Simposio Bolivariano-Exploracion Petrolera en las Cuencas Subandinas, p. 1-5.

Sacek, V., and Ussami, N., 2009, Reappraisal of the effective elastic thickness for the sub-Andes using 3-D finite element flexural modelling, gravity and geological constraints: Geophysical Journal International, v. 179, p. 778-786.

Sarmiento, L., 2001, Mesozoic rifting and Cenozoic basin inversion history of the Eastern Cordillera, Colombian Andes inferences from tectonic models PhD. Dissertation: Vrije Universiteit, 295 p.

Sarmiento-Rojas, L. F., Van Wess, J. D., and Cloetingh, S., 2006, Mesozoic transtensional basin history of the Eastern Cordillera, Colombian Andes: Inferences from tectonic models: Journal of South American Earth Sciences, v. 21, no. 4, p. 383-411.

Schmitz, M., 1994, A balanced model of the southern Central Andes: Tectonics, v. 13, no. 2, p. 484-492.

Stewart, J., and Watts, A.B., 1997, Gravity anomalies and spatial variations of flexural rigidity at mountain ranges: J. Geophys. Res., v. 102, p. 5327-5352.

Strecker, M.R., Hilley, G.E., Bookhagen, B., and Sobel, E.R., 2011, Structural, geomorphic, and depositional characteristics of contiguous and broken foreland basins: Examples from the eastern flanks of the Central Andes in Bolivia and NW Argentina: *in* C. Busby, and Azor-Pérez, A, eds., Tectonics of Sedimentary Basins: Recent Advances, p. 508-521.

Taboada, A., Rivera, L.A., Fuenzalida, A., Cisternas, A., Philip, H., Bijwaard, H., Olaya, J., and Rivera, C., 2000, Geodynamics of the northern Andes: Subductions and intracontinental deformation (Colombia): Tectonics, v. 19, p. 787-813.

Tassara, A., Swain, C., Hackney, R., and Kirby, J., 2007, Elastic thickness structure of South America estimated using wavelets and satellite-derived gravity data: Earth and Planetary Science Letters, v. 253, p. 17-36.

Trenkamp, R., Kellogg, J.N., Freymueller, J.T., and Mora, H.P., 2002, Wide plate margin deformation, southern Central America and northwestern South America, CASA GPS observations: Journal of South American Earth Sciences, v. 15, p. 157-171.

Turcotte, D.L., and Schubert, G., 2002, Geodynamics: Applications of Continuum Physics to Geological Problems, Cambridge University Press, 455. p.

Vargas, C. A., and Mann, P., 2013, Tearing and Breaking Off of Subducted Slabs as the Result of Collision of the Panama Arc-indenter with Northwestern South America. Bulletin of the Seismological Society of America, 103, no.3, p. 2025-2046.

Velandia, F., Acosta, J., Terraza, R., and Villegas, H., 2005, The current tectonic motion of the Northern Andes along the Algeciras Fault System in SW Colombia: Tectonophysics, v. 399, no. 1–4, p. 313-329.

Ventsel, E., and Krauthammer, T., 2001, Thin Plates and Shells: Theory, Analysis, and Applications, CRC press, 440 p.

Watts, A.B., and Burov, E.B., 2003, Lithospheric strength and its relationship to the elastic and seismogenic layer thickness: Earth and Planetary Science Letters, v. 213, p. 113-131.

Wilcox, R. E., Harding, T. t., and Seely, D., 1981, Basic wrench tectonics: American Association of Petroleum Geologists (AAPG) Bulletin, 57, no.1, p. 74-96.

Villamil, T., 1999, Campanian–Miocene tectonostratigraphy, depocenter evolution and basin development of Colombia and western Venezuela: Palaeogeography, Palaeoclimatology, Palaeoecology, v. 153, p. 239-275.

Williams, K. E., 1995, Tectonic subsidence analysis and Paleozoic paleogeography of Gondwana: American Association of Petroleum Geologists (AAPG) Memoir, 79, p. 79-89.

Wyllie, M.R.J., Gregory, A.R., and Gardner, L.W., 1956, Elastic wave velocities in heterogeneous and porous media: Geophysics, v. 21, p. 41-70.

Yeats, R. S., and Berryman, K. R., 1987, South Island, New Zealand, and transverse ranges, California: A seismotectonic comparison: Tectonics, v. 6, no. 3, p. 1- 3